Evaluating Flow Separation Model Fidelity for Stall in Piloted Flight Simulation

Rasa Vaznelytė

TU Delft

Evaluating Flow Separation Model Fidelity for Stall in Piloted Flight Simulation

Thesis report

by

Rasa Vaznelytė

to obtain the degree of Master of Science
at the Delft University of Technology

Thesis committee:

Chair:	Dr. ir. C.C. de Visser
Supervisor:	Dr. ir. D.M. Pool
External examiner:	Dr. A. Bombelli
Additional member:	ir. M.L. Fiechter
Place:	Faculty of Aerospace Engineering, Delft
Project Duration:	January, 2025 - February, 2026
Student number:	5019214

An electronic version of this thesis is available at `https://repository.tudelft.nl/`.

Faculty of Aerospace Engineering · Delft University of Technology

Cover: Original work by the author, where a photograph was used as a reference from CBP [1].

Preface

So the time flies and my 6.5 year long journey at Delft University of Technology comes to an end. These years have been hectic, full of ups and downs, tears and joys. With this thesis, I close this chapter of my life. I would therefore would like to express my gratitude to everyone involved.

During this thesis, I was provided an opportunity to have an invaluable array of hands-on experience. From helping out putting tufts on the aircraft wings and participating in Pietro's flight test, to implementing Joey's stall model in the SIMONA Research Simulator and performing experiments. One memorable moment I want to share is running the aircraft model for the first time in the simulator with motion. It was a little scary, but unforgettable experience. While there was a lot of uncertainty on how it will behave, it was also the moment when countless of weeks of non-stop coding became a tangible object, that can be moved and controlled. I am therefore thankful to everyone involved in the Stall Modeling Task Force for this opportunity — I would not trade my thesis topic for anything else. I am happy to gain knowledge in this field and bring a humble contribution to the Stall Task Force research towards safer aviation.

I would like to thank my supervisor Daan Pool, who patiently guided me through the research process and the writing of this thesis. Thank you for believing in me, pushing me to achieve more. For seeing me as a potential future researcher and investing your time and experience. I sincerely appreciate it. I would also like to thank Coen de Visser who was also involved in the research and providing invaluable input and support during the stall meetings.

I want to express my gratitude to Hans Mulder for generously dedicating his time to participate in the research of this thesis and beyond. From testing stall models and providing feedback in the flight simulator, to unforgettable stall flight test experience.

I would also like to thank Menno and Fred for their extensive knowledge of the aircraft, welcoming me around the hangar, and helping out to find answers to many aircraft and procedure related questions.

I would further like to thank Olaf, Ferdinand, and René for the support with the DUECA code implementation and for helping ensure the experiments ran smoothly on the SIMONA simulator.

The experience during this year would not have been as nice if it was not for the friends surrounding me. The fun and conversations during coffee breaks were refreshing and uplifting. Besides the fun, it was also a learning experience with lots of knowledge exchange. Thank you for keeping me sane and motivated to achieve higher, and for making the overall thesis experience special! In addition, I would also like to thank Aida, Elias, Aeva and Isabelle for being great friends and sticking around from the very first days of university.

I would also like to thank my partner-in-crime Baturay, who was always there for me during this thesis and beyond, offering support during the most stressful moments and sharing in the joy of the more exciting ones.

One thing for certain is that I wouldn't be here wrapping up my thesis if it was not for my parents' support. I therefore want to express my deepest gratitude to my Mom and Dad. For all their sacrifices made to allow me to study abroad. I want to thank my Mom for spending countless evenings helping me out during the early years of my Bachelors, and my Dad giving valuable life advice. Ačiū.

R. Vaznelytė

Delft, February, 2026

Contents

Nomenclature

List of Symbols

$\bar{c}$	Mean aerodynamic chord (MAC) [m]
a_1	Flow separation abruptness parameter [-]
b	Wingspan [m]
C_D	Aircraft drag coefficient [-]
C_L	Aircraft lift coefficient [-]
C_m	Pitch moment coefficient [-]
C_T	Thrust coefficient [-]
C_{L_α}	Lift curve slope [-]
$C_{L_{\max}}$	Maximum aircraft lift coefficient [-]
C_{m_0}	Zero-lift moment coefficient [-]
C_{m_q}	Pitch damping coefficient [-]
$I_{(xx,yy,zz,xz)}$	Moments of inertia [kg·m^2]
$K_{\{q,x,z\}}$	Pitch, heave, and surge gain [-]
m	Empty mass [kg]
q	Pitch rate [rad/s]
S	Wing area [m^2]
V_∞	Free stream air velocity [m/s]
X	Non-dimensional flow separation point (model M1) [-]
X_w	Non-dimensional flow separation point of wing remainder (model M2) [-]
$x_{c.g.}$	Aircraft center of gravity [m]
X_{ss}	Non-dimensional flow separation point from stall strip (model M2) [-]

AoA	Angle-of-attack
DUECA	Delft University Environment for Communication and Activation
EASA	European Union Aviation Safety Agency
FSTD	Flight Simulation Training Device
FTIS	Flight Test Instrumentation System
IATA	International Air Transport Association
ICAO	International Civil Aviation Organization
JND	Just-Noticeable Difference
LOC-I	Loss of Control in Flight
MAC	Mean Aerodynamic Chord
MSE	Mean Square Error
PIO	Pilot Induced Oscillations
SIMONA	International Research Institute for Simulation, Motion and Navigation
SNLS	Separable Nonlinear Least squares
SPS	Stall Protection System
SRS	SIMONA Research Simulator
SWS	Stall Warning System
UPRT	Upset Prevention and Recovery Training

List of Figures

List of Tables

Part I

Literature Review & Research Definition

1

General Introduction

Loss of Control in Flight (LOC-I) has been the leading category of fatal accidents for over 50 years [2]. According to IATA, between 2009 and 2018, 94% of accidents in this category involved human fatalities, making most of them catastrophic events [3]. The number of these accidents has been reducing with the implementation of new technology, such as flight envelope protection systems, but the fatality statistics remain high [4]. This means that while not being very common, LOC-I still remains one of the deadliest threats in the aviation safety domain.

In response to these statistics, the mandatory Upset Prevention and Recovery Training (UPRT) was introduced in 2019 by ICAO [5]. Currently, this training heavily relies on practice flights conducted in the real aircraft. To utilize current flight simulation training devices (FSTDs) and strengthen UPRT, many fidelity enhancements must be made to avoid negative training [6]. One of these is the expansion of model fidelity into a post-stall region [7].

While the introduction of full-flight simulators to UPRT training is a promising addition, there are no well defined regulations on the accuracy of the stall simulation it self. Research has been done to explore this issue; Schroeder et al. [8] examined how pilots perceive stall models generated using different resources, while Grant et al. [9] explored whether changing fidelity parameters of existing aircraft model was noticed by the pilots flying the simulation. In both experiments, it was observed that pilots were not as sensitive to these changes, but there was no clear conclusion on whether these changes can affect the quality of stall recovery training.

To explore this further, the stall research group from Delft University of Technology has conducted research into developing stall models based on the Cessna Citation II. These models were then used in the human-in-the-loop experiments using the SIMONA Research Simulator (SRS) to quantify the Just noticeable difference (JND) margins in flow separation model fidelity. At the moment, the JND research has been only performed on one model by Van Ingen et al. [10], which is modeled using a single Kirchhoff's flow separation state to describe the non-linear dynamics of the stall. However, since then, the stall model has received new updates and improvements [11, 12, 13, 14].

The most recent stall modeling addition by Herbold [14] uses two flow separation states: the first one modeling the flow separation effects of the stall-strip on the inboard part of the wing, and the second modeling the flow separation effects for the remainder of the wing. This model has shown a significant improvement in model fit to flight experiment data. In addition, the existence of these two distinct flow separation regions has been verified with tufted-wing stall experiments, performed by Deligios [15]. This new breakthrough has drawn a lot of interest on how the new way of looking at the wing stall model would perform in full-flight simulation.

Therefore, the focus of this thesis is the implementation of the two-state flow separation model by Herbold [14] and the assessment of its fidelity compared to the previously implemented single-state flow separation model developed by Van Ingen et al. [10]. This is accomplished by conducting pilot-in-the-loop tests using the SIMONA Research Simulator, where an experienced test pilot performs quasi-steady stall maneuvers. The test pilot's feedback and experiment log data are used to assess the fidelity and differences between the two stall models.

The outline for the report is as follows. **Part I** presents the literature study and defines the initial research scope. The **Part II** contains the scientific article and the main results of this thesis, detailing the

pilot-in-the-loop tests conducted to compare the selected stall models and their outcomes. After that the **Part III** reintroduces the research questions with an updated scope, to better reflect the refined goals of this research and the findings presented in the scientific article. This is followed up by additional results that were found prior to the piloted simulation tests. Finally, the updated research questions are answered in **Part IV** and recommendations are provided for further research.

2

Literature Review

2.1. Introduction to Aerodynamic Stall

Aerodynamic stall is a phenomenon, which occurs when airflow separates from a lifting surface, resulting in a loss of lift and an increase of drag. There are many types of stall, which depend on the state of the lifting surface and it's shape. If there is no variation in angle-of-attack, then it is assumed that the conditions are static. In static conditions, stall properties depend mainly on the shape of the lifting surface. However, if variations in angle-of-attack are present, additional dynamics come into play. In this section, more details on said conditions will be provided.

2.1.1. Stall Types

There are three different types of static stall, which are differentiated by how flow separates on a wing. These types are: trailing edge (TE) stall, leading edge (LE) stall and thin foil stall. These stall types are described in more detail in the list below [16, 17]. The stall model used in this research, which will be described later in Section 2.3, is mainly based on the trailing edge stall.

1. **Trailing edge stall:** The boundary layer starts separating at the trailing edge of the airfoil and creeps forward with increasing of angle-of-attack α. In Figure 2.1. This type of stall is specific to airfoils with a large leading edge radius, which are typical for transport aircraft.
2. **Leading edge stall:** This type of stall usually causes a flow separation over the entire airfoil section, with its origin at the leading edge of the airfoil. In Figure 2.2, it can be seen that the suction peak at maximum lift coefficient is followed by a very steep adverse pressure gradient, compared to a more gradual decrease in lift coefficient of trailing edge stall, depicted in Figure 2.1.
3. **Thin airfoil stall:** This stall type is characteristic to very thin airfoils or thicker leading edge airfoils subjected to low Reynolds numbers. During this type of stall, a separation bubble forms at the LE, see Figure 2.3, which grows with increasing angle-of-attack. Eventually, after critical angle-of-attack, the flow separates and the airfoil stalls.

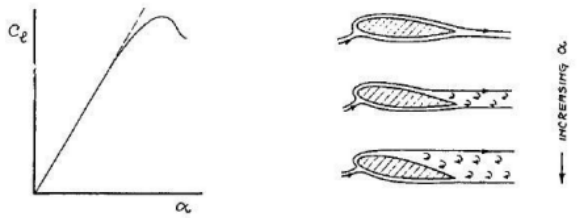

Figure 2.1: Trailing edge stall. Image acquired from [17].

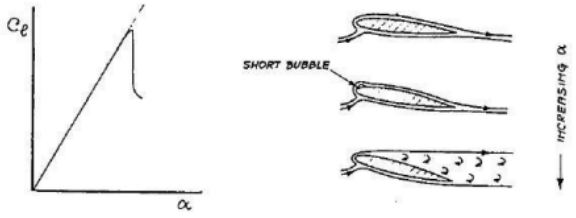

Figure 2.2: Leading edge stall. Image acquired from [17].

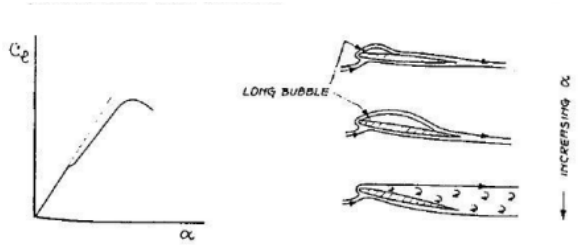

Figure 2.3: Thin foil stall. Image acquired from [17].

In addition to the static stall, a more complicated case is the dynamic stall. This type of stall occurs on an oscillating airfoil, of which the angle-of-attack increases very rapidly ($\dot{\alpha} > 0$). Therefore, the stall onset is pushed further back than in a static case, thus resulting in a higher maximum lift coefficient and critical angle-of-attack. On the other hand, once dynamic stall occurs, the effects of flow separation are more severe and prolonged [18]. Figure 2.4, provided by Choudhry et al. [19], compares static (steady) and dynamic (unsteady) lift coefficient curves. In addition to the already described effects, a sharp increase in the lift coefficient can be observed in step 4. For now, it is generally assumed that this is caused by the dynamic stall vortex (DSV) creating an additional suction at the leading edge of an airfoil, but the true reason is still being debated [19].

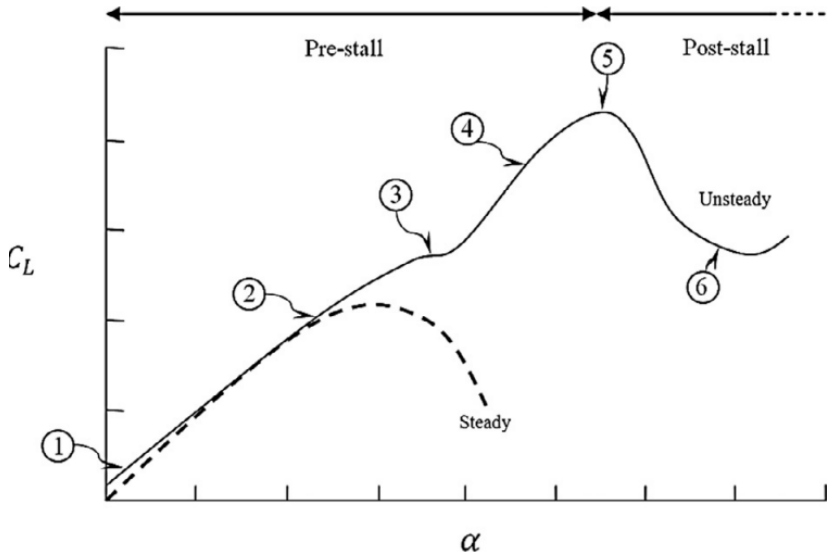

Figure 2.4: $C_L - \alpha$ plots of unsteady (dynamic) stall and steady (static) stall. Image acquired from [19].

2.1.2. Stall Buffet

When the aircraft approaches stall, a buffeting phenomenon can be observed. Ed Obert defines buffet as *"a form of airframe vibration caused by pressure fluctuations in separated flow"* [17]. Buffeting can be triggered by multiple reasons, such as strong shockwave formation fluctuations at high speeds, flow separation at low speeds or deliberate geometrical properties of the aircraft. In addition, vibrations caused by buffeting can be severe and thus regulators use buffet onset as a limiting factor of the aircraft operational envelope [17].

In this research, only the low-speed buffeting will be considered. It is one of the main cues of stall onset when approaching the critical angle-of-attack [13]. In addition, the threshold at which human can detect buffeting vibrations is low [17], therefore it is an important element in modeling the stall.

2.2. Relevance of Accurate Stall Simulation

Loss of Control in Flight (LOC-I) is the leading cause of fatal accidents for over 50 years [2]. While definitions of LOC-I tend to vary [20], IATA defines it as an aircraft deviation from intended flightpath or an adverse flight condition placing an aircraft outside its normal flight envelope, with pilot unable to maintain control of the aircraft [3]. Despite being only the 6th most common accident cause, it is responsible for the highest portion of all fatalities in aviation accidents, meaning that nearly every LOC-I accident was fatal. Statistics provided by IATA show that between 2009 and 2018, there were 64 LOC-I accidents identified, of which 94% involved human fatalities.

While there are many different categories of LOC-I causes, stall is identified as the most common one [3, 21]. As described previously, an aircraft enters stall when angle-of-attack reaches or exceeds a point of maximum lift coefficient, after which the flow on a wing separates [16], thus leading to loss of lift and control. If a stall is identified and acted upon correctly, an entry to a severe upset can be prevented. Therefore, aircraft manufacturers and regulators have implemented measures to ensure prevention and recovery from the stall. This has been done in two ways: first, by implementing stall warning (SWS) and protection (SPS) systems on board the aircraft; second, by providing Upset Prevention and Recovery Training (UPRT) to pilots.

With the introduction of aircraft stall warning and protection systems, the trend of LOC-I accidents has been decreasing [4], but the importance of UPRT still remains. Nowadays, many aircraft are equipped with SWS and SPS, such as a stick shaker and stick pusher. Additionally, the introduction of a fly-by-wire control system has allowed for more advanced stall prevention functions, such as ”flight envelope protection” or ”alpha protection” [22]. These systems assist in keeping the aircraft within a safe envelope of operations. However, there is always a risk of them becoming ineffective, due to their reliance on accurate signals and measurements from aircraft sensors, which can fail [22]. An example of such a case is Air France Flight 447 in 2009, where a potential ice buildup on the sensors lead to inconsistent airspeed indications, eventually resulting in the disengagement of the stall protection system [23]. As a consequence, inadequate actions and communication of the crew and a failure to identify cues leading to a stall resulted in a catastrophic crash. This highlights the importance of UPRT training, which enables pilots to accurately recognize and respond to natural stall cues, regardless of the presence of envelope protection systems [22].

To use flight simulation training devices (FSTD) for UPRT training, additional modifications are required. Most FSTDs used for pilot training (Type D and Level 7) are not designed to perform a full stall recovery and can only demonstrate stall to a very limited extent [6]. According to Advani et al. [7], only 56% of the UPRT objectives can be covered without modifying Level D or Type 7 simulators. Therefore, to use these simulators in UPRT, some upgrades are required, one of which is to improve the aircraft model. It is advised that the model includes accurate buffet onset, reduced control effectiveness and damping, Mach effects, stall protection system activation and more [7]. In addition, it is important that the implementation of new changes does not contribute to ”negative training”. Incorrect reaction and handling caused by negative training can lead to potentially fatal situations during LOC-I [6, 7]. Therefore, to benefit from FSTDs in UPRT training, special attention must be given when expanding the existing envelope, by ensuring that the accuracy of stall simulation is maintained at the highest level.

2.3. Modeling of Stall

One of the main aspects that needs to be improved to perform UPRT in FSTD is the aerodynamic post-stall model [7]. Therefore, a task force team has been created at TU Delft to perform research on this topic [24]. The research consist of creating and upgrading the aerodynamic stall model using flight test data [10, 12, 11, 25, 14, 26, 27] and performing tests [13, 28, 29] on the said model in a research simulator. To gather data, a research aircraft is used, which will be briefly described in Section 2.3.1. Then, Section 2.3.2 will explain the model philosophy and Section 2.3.3, Section 2.3.4 and Section 2.3.5 will describe the current state of the model developed at TU Delft.

2.3.1. Flight Test Vehicle

The flight tests for TU Delft aerodynamic stall model identification are performed using a modified Cessna Citation II jet, registered as PH-LAB, see Figure 2.5. PH-LAB is a research aircraft, owned by the Delft University of Technology together with the Netherlands Aerospace Center (NLR). The twin-jet aircraft features unswept tapered wings and a cruciform tail. To perform research flight tests, the aircraft is equipped

with an advanced flight test instrumentation system (FTIS), which is used to gather data while the aircraft is being operated, and an in-house-developed fly-by-wire control system. Lastly, the Cessna Citation II can be equipped with an air-data boom, which provides accurate measurements for angle-of-attack and sideslip [24].

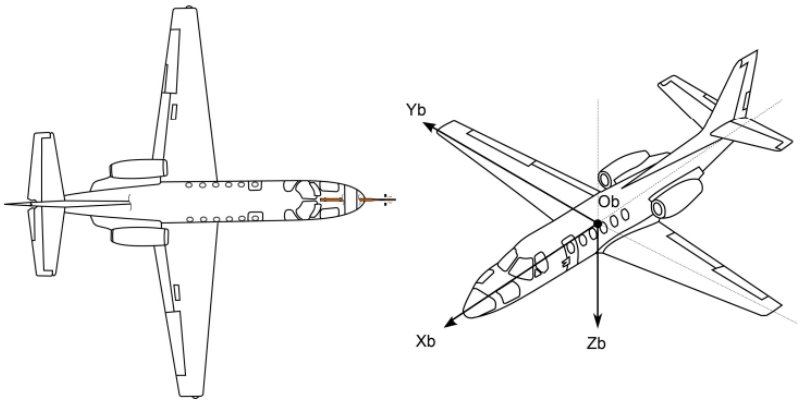

Figure 2.5: Schematic drawings of the Cessna Citation II, taken from [10]

2.3.2. Kirchhoff Stall Model

The aerodynamic stall models created at TU Delft are mainly based on Kirchhoff's theory of flow separation. Application of this theory for stall modeling was first introduced by Fischenberg in 1995 [30], which was further applied and built upon in research at TU Delft [10, 28, 29, 25, 11, 14, 12]. According to research by Fischenberg [30], one of the main variables describing the aerodynamic stall is X: a non-dimensional state, which shows the location of flow separation on the airfoil chord. This variable takes values in the range of $0 \leq X \leq 1$, where $X = 1$ means fully attached flow and $X = 0$ is fully separated flow. Using an approximation of Kirchhoff's theory of flow separation, wing lift can be modeled as a dependency on the flow separation point, shown in Eq.(2.1). In this case, the lift coefficient becomes a function of angle-of-attack α and variable X.

$$C_L(\alpha, X) = C_{L_\alpha} \left(\frac{1 + \sqrt{X}}{2} \right)^2 \alpha \tag{2.1}$$

In a steady stall case, where $\dot{\alpha} = 0$, the flow separation point depends only on the angle-of-attack and can be denoted as X_0. When using flight test data to identify steady flow separation X_0, Fischenberg proposed using an approximated function, see Eq.(2.2). According to Fischenberg, this function contains only two unknown parameters (a_1 and α^*) and the hyperbolic tangent tanh provides continuity across the entire range, which is essential for convergence of parameter estimation [30].

$$X_0(\alpha) = \frac{1}{2} \{1 - \tanh(a_1(\alpha - \alpha^*))\} \tag{2.2}$$

However, for unsteady (dynamic) flight conditions, where $\dot{\alpha} \neq 0$, $X_0(\alpha)$ cannot be used to model flow separation at high angles of attack. In this case, it is necessary to add additional parameters, which portray the effects of delayed stall onset. To model these conditions, two unsteady effects need to be taken into account:

1. Hysteresis effects, which delay the stall to a higher angle-of-attack. Hysteresis is proportional to $\dot{\alpha}$ and is caused by boundary layer effects and dynamic stall vortex. These effects are incorporated in X as shown in Eq.(2.3).
$$X(\alpha, \dot{\alpha}) = X_0(\alpha - \tau_2 \dot{\alpha}) \tag{2.3}$$
2. Unsteady aerodynamics, which describe response of forces to a change in a flow condition. This effect is time dependent and can be described in a form of ordinary differential equation (ODE). For

this, Fischenberg used an approximated Wagner or Theodorsen function [30], shown in Eq.(2.4), making X time dependent.

$$\tau_1 \frac{dX}{dt} + X = X_0 \left(\alpha - \tau_2 \dot{\alpha}\right) \tag{2.4}$$

Combining the steady flow separation approximation in Eq.(2.2) and unsteady effects described by Eq.(2.3) and Eq.(2.4), the final flow separation point function can be written as Eq.(2.5):

$$\tau_1 \frac{dX}{dt} + X = \frac{1}{2}\left\{1 - \tanh(a_1(\alpha - \tau_2 \dot{\alpha} - \alpha^*))\right\} \tag{2.5}$$

Parameters a_1, α^*, τ_1 and τ_2 in Eq.(2.5) are nonlinear stall parameters. Additionally, all of these parameters can be identified from flight test data. These are the parameters, that have been varied during Just noticeable Difference research [28, 13, 29] (more in Section 2.4.5), therefore understanding the role of each parameter is important when designing and analyzing the experiments. The list below describes each parameter in more detail:

1. a_1 **- Stall abruptness parameter:** the higher the value, the more abrupt the stall is. As can be seen in Figure 2.6, the stall abruptness appears as a more sudden drop in lift coefficient, which is caused by a more rapid flow separation near stall angle-of-attack. On the other hand, the angle-of-attack range, at which flow remains fully attached is bigger at high a_1 values.
2. α^* **- Stall angle-of-attack:** angle-of-attack value at which the flow separation point is halfway on the chord, i.e. $X = 0.5$. In Figure 2.7, it can be observed that the higher the value of α^*, the more flow separation is delayed, thus higher maximum lift coefficient at the stall angle-of-attack.
3. τ_1 **- Time lag:** a delay of flow separation point X dynamics, which can be interpreted as a delay of airflow reaction to sudden change in α. This effect can be seen in Figure 2.8.
4. τ_2 **- Hysteresis parameter:** describes hysteresis effects caused by circulation and boundary layer effects, proportional $\dot{\alpha}$. In Figure 2.9 it can be seen that the larger τ_2, the longer the flow stays attached. The value of this parameter depends on an airfoil shape [30].

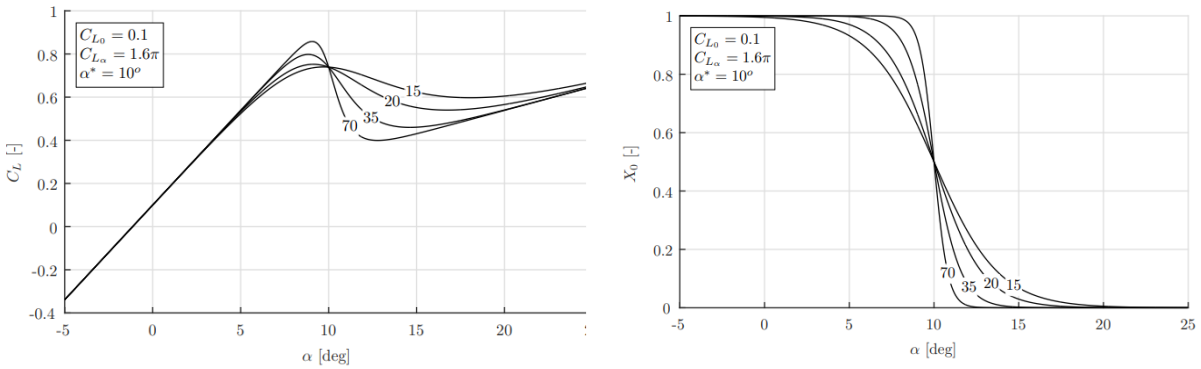

(a) Effects of a_1 value on lift curve. Image acquired from [25].

(b) Effects of a_1 value on flow separation point location. Image acquired from [25].

Figure 2.6: Effects of a_1 on flow separation.

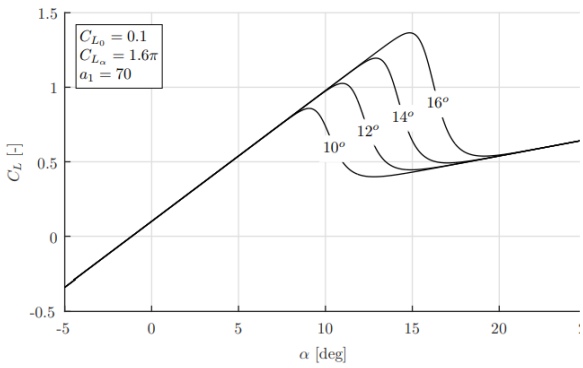

(a) Effects of α^* on lift slope. Image acquired from [25].

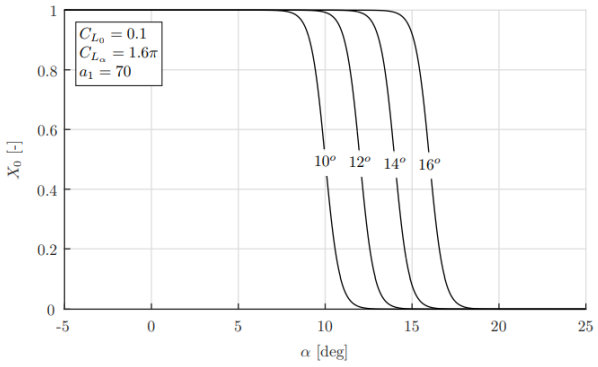

(b) Effects of α^* on flow separation point location. Image acquired from [25].

Figure 2.7: Effects of α^* on flow separation.

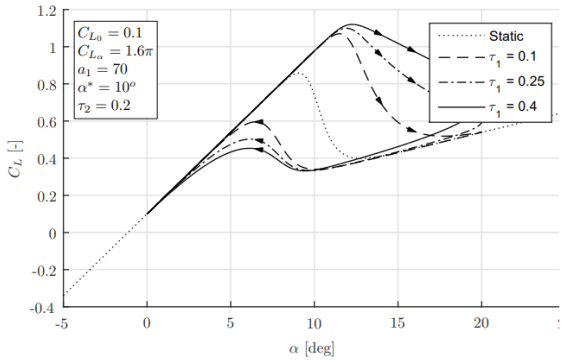

(a) Effects of τ_1 on lift slope. Image acquired from [25].

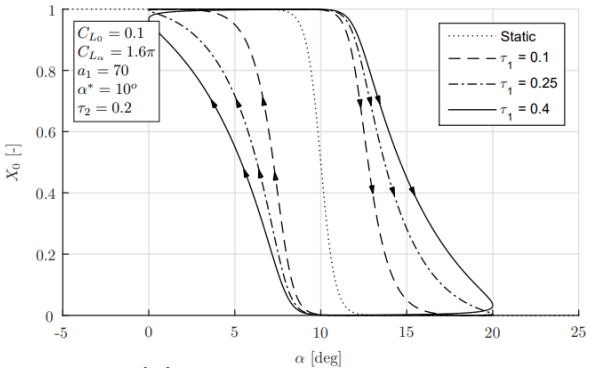

(b) Effects of τ_1 on flow separation point location. Image acquired from [25].

Figure 2.8: Effects of τ_1 on flow separation.

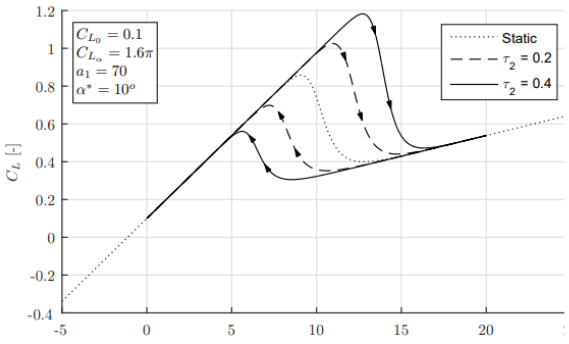

(a) Effects of τ_2 on lift slope. Image acquired from [25].

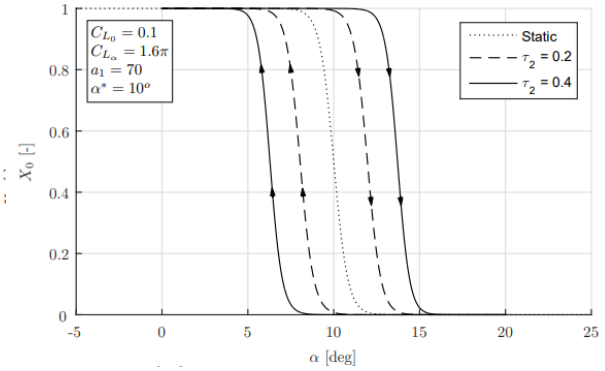

(b) Effects of τ_2 on flow separation point location. Image acquired from [25].

Figure 2.9: Effects of τ_2 on flow separation.

The parameters a_1 and α^* affect the steady part of a stall model, hence Figure 2.6 and Figure 2.7 depicts only a static stall, where $\dot{\alpha} = \frac{dX}{dt} = 0$. On the other hand, parameters τ_1 and τ_2 depict variations in

unsteady stall, therefore, a static case and dynamic cases are compared in Figure 2.8 and Figure 2.9 to show their effect.

2.3.3. TU Delft Stall Model

By using orthogonal model structure selection method and Kirchhoff's theory, Van Ingen et al. [10] developed the following longitudinal and lateral model structure:

$$\begin{aligned}
C_L &= C_{L_0} + C_{L_\alpha}\left(\frac{1+\sqrt{X}}{2}\right)^2 \alpha + C_{L_{\alpha^2}}(\alpha - 6^\circ)_+^2 \\
C_D &= C_{D_0} + C_{D_\alpha}\alpha + C_{D_{\delta e}}\delta_e + C_{D_X}(1-X) + C_{D_{C_T}}C_T \\
C_Y &= C_{Y_0} + C_{Y_\beta}\beta + C_{Y_p}\frac{pb}{2V} + C_{Y_r}\frac{rb}{2V} + C_{Y_{\delta_a}}\delta_a \\
C_l &= C_{l_0} + C_{l_\beta}\beta + C_{l_p}\frac{pb}{2V} + C_{l_r}\frac{rb}{2V} + C_{l_{\delta_a}}\delta_a \\
C_m &= C_{m_0} + C_{m_\alpha}\alpha + C_{m_{X\delta_e}}\mathsf{max}(0.5, X) + C_{m_{C_T}}C_T \\
C_n &= C_{n_0} + C_{n_\beta}\beta + C_{n_r}\frac{rb}{2V} + C_{r_{\delta_r}}\delta_r
\end{aligned} \tag{2.6}$$

Where $(\alpha - 6^\circ)_+^2$ is a spline term that is activated when the angle-of-attack is above 6°, otherwise it is equal to 0. A model selection algorithm used in the research by Van Ingen et al. [10] selected these parameters from a candidate pool based on the improvements in the model fit to the flight test data [10]. While the model displayed great performance, there were a lot of areas left for improvement.

One of the shortcomings of this model was that the pitching moment coefficient C_m did not contain a damping term C_{m_q}. In this case, the model structure selection algorithm did not include it, due to lower performance when fitting the flight test data. However, it was later discovered during experiments in a research simulator that the lack of pitch damping term indeed reduced the fidelity of the model [13]. Therefore, research by Van Wezel [12] tackled this issue and an alternative C_m model without a flow separation term was introduced, which showed a 55.9% improvement compared to the model by Van Ingen [10].

It can also be observed that in Van Ingen's model (see Eq.(2.6)) the asymmetric force and moment coefficients do not include the flow separation parameter X. Therefore, in asymmetric model research by de Fuijk [26], it was proposed to incorporate this parameter in rolling moment coefficient C_l by allowing wings to have separate flow separation points X (X_{left} and X_{right}) and local angles of attack. This way, the roll-off tendency, caused by one wing stalling before the other, was modeled [24].

2.3.4. TU Delft Buffet Model

In Section 2.1.2, the buffet was introduced as an important part of the stall. Therefore, in addition to a lateral and asymmetric stall, a buffet model was developed by Van Horssen [25]. This model contains accelerations both in vertical and lateral directions, albeit the latter one is less severe. The buffet model by van Horssen is assumed to be a white noise signal (intensity equal to 1), which was passed through a second-order shaping filter, with the filter being shown in Eq.(2.7). For the vertical case, one filter is used, while for the lateral case, two filters are added together to depict two dominant frequencies [25].

$$H(j\omega) = \frac{H_0\omega_0^2}{(j\omega)^2 + \frac{\omega_0}{Q_0}j\omega + \omega^2} \tag{2.7}$$

The model is made such that the buffet activation and intensity are linked to the flow separation value X. As the flow separates more, the buffet intensity increases. To model this, an additional scaling factor of $(1-X)$ was applied on the model, which can be seen on the left-hand side of a schematic in Figure 2.10 [24, 25]. Additionally, since the buffet starts at a certain point during stall onset, the buffet model has an activation threshold X_{thres} set by the flow separation point. This point is set to $X < 0.89$, meaning that once the separation point is a little more than 11% of the chord away from the trailing edge, the buffeting starts. These additions allow the buffet onset to be modeled more accurately.

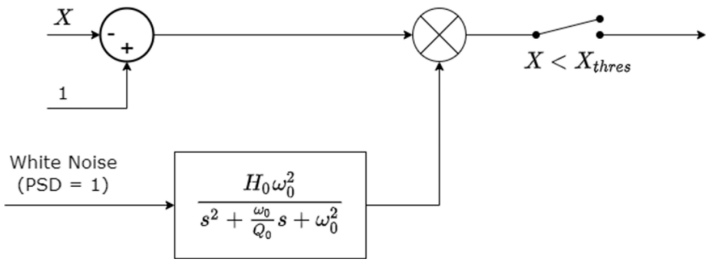

Figure 2.10: Schematic drawings of the buffet model, taken from [24, 25]

2.3.5. Modeling of a stall-strip and the Wing Separately

When the aircraft enters a stall, it is desired that the flow separation starts on the inboard part of the wing. At low speeds, the flow separation of a tapered and swept wing starts on the outboard section and travels inboard. This results in the ineffectiveness of control surfaces located on the outboard wing. Therefore, by stalling the inboard wing first, the flight controls remain effective and stall recovery is controllable. As a downside, the design maximum lift coefficient is reduced in exchange for control effectiveness during the stall [17].

To induce an inboard stall, the Cessna Citation II is equipped with stall-strips. Usually, when designing a wing for an inboard stall, the camber, twist and leading-edge radius are varied along the span. If this cannot be achieved, a small device called a stall-strip (also known as a breaker strip) can be installed at the leading edge of an inboard wing [17]. On the Cessna Citation II, the stall-strip is located on the de-ice boot. Schematics of the stall-strip and its location can be seen in Figure 2.11 and Figure 2.12.

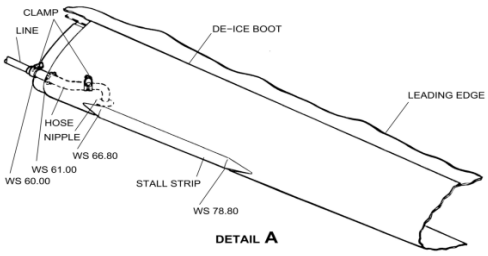

Figure 2.11: A close up schematic of the stall-strip from the aircraft manual. Image obtained from [14].

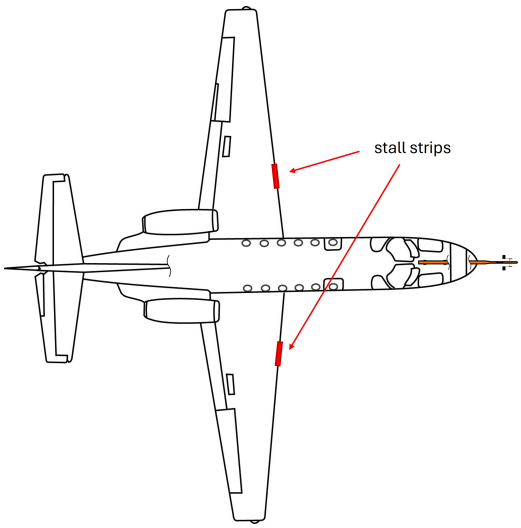

Figure 2.12: Top view of the Cessna Citation II with approximate stall-strip locations. Image obtained and edited from [10].

In the experiment data and research of Herbold [14], it was observed that the angle-of-attack at which the Cessna Citation II Stalls does not match with the simulation data of airfoils used in the aircraft. The Cessna Citation II model would stall at angle-of-attack around $\alpha^* \approx 12°$ [10], while the stall angle of NACA23012 airfoil found in wind tunnel tests lies in the range of $15°$ to $20°$ [31, 14]. This means the stall model, proposed by Van Ingen et al. [10], was simulating the stall-strip flow separation mechanics and not of the entirety of the wing. Therefore, in research by Herbold [14], a split was made in the flow separation of the stall-strip and the wing. As a result, the new longitudinal model by Herbold (see Equation 2.8) contains two flow separation states: X_{ss} (stall-strip) and X_w (wing).

$$
\begin{aligned}
C_L &= C_{L_0} + C_{L_{\alpha,ss}} \left(\frac{1+\sqrt{X_{ss}}}{2} \right)^2 + C_{L_{\alpha,w}} \left(\frac{1+\sqrt{X_w}}{2} \right)^2 \alpha + C_{L_q} \frac{q\bar{c}}{V} + C_{L_{\delta e}} \delta e \\
C_D &= C_{D_0} + C_{D_{C_T}} C_T + C_{D_{\delta e}} \delta_e + C_{D_{C_L^2}} C_L^2 + C_{D_{X_{ss}}} (1 - X_{ss}) + C_{D_{X_w}} (1 - X_w) \\
C_m &= C_{m_0} + C_{m_{C_T}} C_T + C_{m_q^*} \frac{q\bar{c}}{2} - l_{c.p.} C_L + C^*_{m_{X\delta_e}} \delta e
\end{aligned}
\tag{2.8}
$$

Where $l_{c.p.}$ is the position of the center of pressure and $C^*_{m_{\delta_e}}$ is the control effectiveness of the elevator, which depend on flow separation states. To support this new aerodynamic stall model, the Kirchhoff model described in Section 2.3.2 was modified to support two flow separation states:

$$
\begin{aligned}
\tau_{1,ss} \frac{dX_{ss}}{dt} + X_{ss} &= \frac{1}{2} \{1 - \tanh(a_{1,ss} \left[\alpha - \tau_{2,ss} \dot{\alpha} - \alpha^*_{ss} \right])\} \\
X_w &= \frac{1}{2} \{1 - \tanh(a_{1,w} \left[\alpha - \alpha^*_w \right])\}
\end{aligned}
\tag{2.9}
$$

As seen in Eq.(2.9), the flow separation point of the stall-strip X_{ss} is modeled by unsteady (dynamic) stall properties, while the wing flow separation point X_w is governed by steady stall.

With these changes, the longitudinal aerodynamic stall model by Herbold [14] shows significant improvements compared to the model by Van Ingen et al. [10]. The Mean Squared Error (MSE) was improved by 32%, 29% and 27% for lift, drag, and pitching moment coefficients respectively. In addition, the stall-strip and wing stall angles-of-attack were found to be $\alpha^*_{ss} = 11.2°$ and $\alpha^*_w = 18.7°$ respectively, which match the stall angles of the model and NACA23012 from the previous discussion. Lastly, the stall-strip abruptness parameter $a_{1,ss}$ was very high, thus matching the primary function of the stall-strip.

Lastly, when it comes to modeling the stall using two X states, a special attention needs to be given to the buffet model, provided in Section 2.3.4. As described before, the buffet model activation threshold and intensity depend on flow separation location X. However, with the introduction of *two* flow separation variables in Eq.(2.6), there is no clear indicator anymore to define a threshold and intensity of buffet onset. This was not addressed in the research by Herbold [14], so it is important to revisit the buffet model implementation before conducting experiments in a full-flight simulator.

2.4. Stall Model Simulator Experiments

As mentioned in Section 2.2, in order for FSTD simulators to be useful in UPRT training, a lot of improvements need to be implemented. One of the main addressed improvements was the implementation of the stall models to current FSTD simulators. There are a lot of already provided requirements by the regulation authorities on what the stall simulations should include [32], however, the requirements on the accuracy are still unclear. Therefore, this section will explore the research that has been performed to figure out the required model fidelity, in order for FSTDs to be beneficial in stall simulation and UPRT training. First, Section 2.4.1 will provide a list of known requirements on stall simulation in FSTDs by EASA. After that, Section 2.4.2 will explore external research done on simlating stall in FSTDs. The remaining subsections will explain the just-noticeable differences (JND) and related research performed by stall modeling task force at TU Delft.

2.4.1. Simulation Requirements for UPRT

In this section, a direct collection of important requirements from EASA flight simulator certification specification guide [32] will be provided. The following points were mainly taken from sections *"AMC9 FSTD(A).300"* and *"AMC10 FSTD(A).300"*.

The "Flight Simulation Training Device Standards" are defined as follows [32]:

- *"the unrealistic degradation of the FSTD functionality (such as degrading flight control effectiveness) to drive an aeroplane upset is not acceptable.."*
- *"the FSTD should be evaluated for specific upset recovery manoeuvres; a minimum set of manoeuvres: a) a nose-high wings level aeroplane upset; b) a nose-low aeroplane upset; and c) a high bank angle aeroplane upset;"*
  The aerodynamic stall modelling should include:

- *"degradation of the static/dynamic lateral directional stability;"*
- *"uncommanded roll response or roll-off requiring significant control deflection to counter;"*
- *"degradation in control response (pitch, roll, and yaw);"*
- *"apparent randomness or non-repeatability;"*
- *"changes in pitch stability;"*
- *"Mach effects; "*
- *"stall buffet;"*
- *"**as appropriate to the aeroplane type**, the model should be capable of capturing the variations seen in the stall characteristics of the aeroplane (e.g. the presence or absence of a pitch break, deterrent buffet, or other indications of a stall where present on the aeroplane);"*

Furthermore, the provided flight conditions for stall and approach-to-stall characteristic tests for FSTDs are [32]:

1. *"stall entry at wings level (1g);"*
2. *"stall entry in turning flight of at least 25° bank angle (accelerated stall);*

2.4.2. General Research on Simulating Stall

Before UPRT was introduced, there was already some research being performed on stall simulation in FSTDs. Already in 2012, research by Advani et al. [5, 33] explored what exact modifications were required to make FSTDs useful for future UPRT programs. Besides instruction and motion cueing, it was agreed that the mathematical model fidelity and realism of upset onsets is crucial.

The first experiment exploring pilot reaction to different aircraft stall models was performed by Schroeder et al. [8]. In this research, three different Boeing 737 aerodynamic stall models were compared in a full-flight simulator. The first two models contained stall models identified from either flight or wind tunnel data, while a third one was just an FSTD model with roll asymmetry added. While most attention was paid on how the pilots perform the recovery procedure, there were indications of participants pointing out differences and preferences between the models.

A few years later an investigation by Grant et al. [9] was made to assess how model fidelity difference can affect the full aerodynamic stall recovery training. This time, the aircraft models contained a nominal case and two varied parameter cases: mild and severe. This variation was designed to be within the uncertainty that is usually observed in the real development of aircraft models. Additionally, in this experiment pilots were actively flying the model. The results concluded that pilots would not observe any significant differences in fidelity between the models, however, some aspects were noticeable, such as roll-off effect. It is speculated whether the differences were large enough [34].

This research primarily concentrated on the fidelity of stall models and human perception within FSTDs. However, there remains a gap in understanding the precise point at which pilots can detect changes in the simulated stall fidelity. To address this, a few studies were dedicated at TU Delft. To find the margin, the methods of finding the Just-Noticeable Difference (JND) were used. Next sections will explain the JND and introduce the research done at TU Delft.

2.4.3. Just-Noticeable Differences (JND)

Humans are not machines and do not have perfect sensors. When a person is introduced to two very similar stimuli, it is very likely they are not going to notice a difference. A very commonly used illustration of this phenomena is by looking at how people react to weight. Imagine a person is holding a bag in each hand with an equal amount of glass marbles. If you add a marble to one bag while they are looking away, it is very likely, it will go unnoticed. However, if you keep slowly adding marbles to the same bag, at a certain amount of marbles, the person will notice the difference in the weight of the bags. This additional amount of marbles illustrates the concept of just-noticeable difference (JND) margin. A just-noticeable difference is defined as the minimum amount of change in stimuli between two signals in order to detect a difference.

However, if the initial bag of marbles was five times bigger, the amount of additional marbles from last time will not be enough for a difference to be detected. This means that if the intensity of the original

stimulus is larger, the difference needed to notice a change also tends to increase. This phenomenon is described by Weber's law, which can be written as Eq.(2.10):

$$\frac{\Delta I}{I} = Const. \tag{2.10}$$

According to Weber's law, the new amount of additional marbles would need to be at least five times larger, for a difference to be detected again. While the example here is very simple, JND margins can also be useful in detecting a minimum amount of change allowed in stall model parameters, before human can detect it. Knowing this margin can help to determine whether model fidelity is still suitable for UPRT training.

There are multiple ways to detect these JND margins. Two main methods used in previous research are the staircase (adaptive) and the method of constant stimuli (non-adaptive) [28, 29, 13]. In the staircase procedure, such as Up/Down, the next trial is determined by the the answer from the previous. When difference is detected, the next step size is decreased until the difference is undetectable [29, 28, 13, 35, 36]. To improve the level of correctness in the resulting value, modifications to staircase procedure can be applied [37]. In addition, a lot of attention needs to be put in formulating the question given after each comparison, such that the results to not get affected by bias influenced on a participant. The one Up/Down staircase method and more advanced variations were used in passive stall model parameter JND research [29, 28, 13].

The second option, the method of constant stimuli, is a bit more primitive. Instead of constantly adapting the next stimuli depending on the previous answer, this method uses already pre-determined pool of stimuli [38]. The range at which these stimuli lie is between almost always detectable and almost never detectable values. The results only contain a frequency on how often a stimulus was detected and the margin value is obtained by analyzing a psychometric function. This method was used in the active stall parameter JND experiment by Bootsma et al. [13].

2.4.4. Aparatus - SIMONA Research Simulator (SRS)

The SIMONA Research Simulator (SRS) is used to perform various human-in-the loop research at TU Delft. SIMONA is a 6-degree-of-freedom simulator, featuring a hydraulic hexapod motion base [39]. The SRS is equipped with classical washout filters [40], providing realistic motion cues. In addition, the visual ques are projected to a field of view of 180x40°, which is seen through a collimated mirror, with a visual update rate of 60Hz [41]. The SRS can simulate many different vehicles, such as cars [42], helicopters and, most importantly, aircraft. In addition, the software architecture used by SRS is DUECA (Delft University Environment for Communication and Activation), which reduces operational complexities and thus is accessible to researchers and students [41].

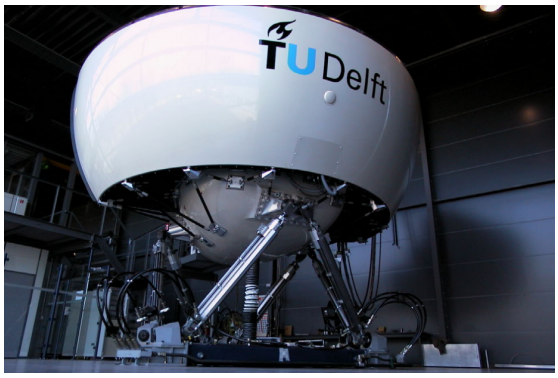

Figure 2.13: Exterior of SIMONA. Adapted from [41].

Figure 2.14: Flight deck inside SIMONA. Note yoke on the left and side-stick on the right. Adapted from [41].

During the experiment simulation, the flight deck can be configured to match the Cessna Citation II cockpit as closely as possible. Since it is a research simulator, both hardware and software can be

customized. This means that LCD cockpit screens can be easily modified to fit the additional experiment needs, such as displaying messages or providing tracking unusual ques. For visual cues, Flight Gear would be used. In addition, the roll,yaw and sway can be disabled, meaning that only quasi-static stall ques (pitch, surge, heave) will remain [43]. Finally, the cockpit is equipped with both side-stick and yoke, meaning that all participants will have to sit on one side only.

2.4.5. JND Research at TU Delft

The research performed in SIMONA by the TU Delft stall task force primarily focuses on detecting the JND margins of stall model parameters. While regulatory authorities provide certain requirements (see Section 2.4.1) for FSTDS in UPRT simulator training, there is no clear quantitative guidance on the required accuracy of aerodynamic stall model itself. As a result, it remains uncertain to what extent manufacturers should prioritize and allocate resources towards model fidelity. Therefore, to address this gap, the TU Delft stall modeling task force performed human-in-the-loop experiments in the SRS, using in-house developed stall models.

The first research conducted by Smets et. al. [28] measured the JND margins of key Kirchhoff parameters of the longitudinal stall model. These parameters were stall abruptness a_1 and time lag τ_1, whereas τ_2 and α^* were kept constant (see Eq.(2.5)). The τ_2 time constant was excluded due to experiment not including deep stalls, while α^* is a fixed value for an aircraft. To avoid giving too many distractions during the experiment, the participants were given to passively observe two consecutive quasi-static stalls flown by an autopilot and tell whether they notice a difference. To converge to a JND margin value, a staircase procedure was used, where answers ”yes” or ”no” in certain order would affect the next comparison, as well as eventually decrease in step size of parameter change as the experiment went on. As a result, it was found that for both parameters, the lower and upper JND margins were equal, as well as that participants were more sensitive to changes of a stall abruptness parameter a_1 that to τ_1.

Similar research was also done by Imbrechts et al. [29], but this case for the Cessna Citation II buffet model, mentioned in Section 2.3.4. While the buffet is both for vertical and lateral directions, only vertical model was considered in the experiment. The chosen parameters for the experiment were buffet threshold defining flow separation point X_{thres} and buffet characteristic frequency parameter ω_0. The experimental methods applied to find the JND margins were identical to the ones used by Smets et al. [28]. The main conclusions were that participants were more sensitive to lower buffeting threshold X_{thres} than the allowed tolerances provided by the regulators.

Lastly, the research conducted by Bootsma et al. [13] was a follow-up to work by Smets et al. [28], where several improvements were added to experiment set up. First, a more detailed passive experiment was performed using values found by Smets et al. [28] as a starting point. In this experiment, a different staircase method option was used and participants were asked to indicate which stall was more abrupt. These improvements helped to remove biases in participant answers. Second, an active experiment was introduced, where a pilots flew and recovered from stall themselves. To detect the JND margins constant stimuli paradigm was used. As a result, the passive case showed even lower margins than what was discovered in the experiment by Smets et al. [28], while actively flown experiment JND margins were found to be around five times higher, meaning pilots were less sensitive to abruptness parameter changes while being in control of the aircraft.

2.4.6. Issues Identified with Stall Models in JND Research

While previous research provided valuable insights in JND margins, there were also issues identified with the stall model. To date, the JND research performed at TU Delft has used only one Cessna Citation II stall model, created by Van Ingen et al. [10]. Initially, this model was used as a base in passive longitudinal stall and buffeting JND research by Smets et al. [28] and Imbrechts et al. [29]. In this research, the experiments were conducted passively, which means that the simulated flight was performed using an autopilot, while the participant was an observer.

However, it was later discovered by Boostma et al. [13], that if the same stall model is flown actively, i.e. controlled by the participant, the simulated flight characteristics did not match with the real flying qualities of Cessna Citation II. It was discovered that the said model displayed inaccurate pitch rate characteristics when controlled actively, which were previously masked by an autopilot. This was caused by a lack of a C_{m_q} term in aerodynamic coefficient equation, due to the nature of the parameter selection algorithm used

by Van Ingen et al. [10].

Before proceeding with the active JND experiment, Van Ingen's model had to be modified and tested to include a pitch damping term [10, 13]. In addition, this later lead to complete remodeling of the pitching moment coefficient equation, which was done by Van Wezel et al. [12]. This discovery highlighted the importance of validating stall models not only in passive simulations, but also by performing actively controlled tests in a flight simulator. This will therefore ensure accurate model handling qualities before moving on with further research.

Furthermore, most modifications (see Section 2.3.3) applied to TU Delft stall model were not yet tested in a full-flight simulator. Therefore, with the introduction of a more accurate stall model by Herbold [14], described in Section 2.3.5, it was decided to validate it in the flight simulator as the first step. In this model, the stall-strip and wing are modeled separately, which introduced two distinct flow separation point states on the wing. Additionally, it is also not yet clear how these changes will affect the noticeably of Kirchhoff parameter variations. Therefore, this study will focus on evaluating the improved aerodynamic stall model developed by Herbold and measuring JND margins of the new model parameters both passively and actively. Next chapter will introduce a research objective and questions on this topic.

3

Research Questions

In this research, the JND margins will be measured on the stall model developed by Herbold [14]. In addition, it is desired to quantitatively compare the results with the research done previously [13, 10], which used a different stall model by Van Ingen et al. [10]. Therefore, the research objective is as follows:

Research Objective

How much does the magnitude of JND margins of Kirchhoff stall parameters change when the flow separation is modeled separately for a stall strip and a wing, compared to previous research.

While trying trying to achieve the objective, the following research questions will help to provide a more step by step approach. Before JND experiment can be started, the model has to be validated. Therefore RQ 1 needs to be answered first.

Research Question 1

Is the model with stall strips an accurate representation of Cessna Citation II dynamics when flown actively in a simulator?

Once it is ensured that there are no major issues with the new model, a first comparison between baseline models can be done. This will be used to answer RQ 2. By having an idea on how the change is perceived, further actions can be taken in the main experiment design.

Research Question 2

How is the difference between the base model with stall strips and base model used in Boostma's research noticeable when flying actively?

When designing the experiment, it is important that the sensitivity analysis performed on the new Kirchhoff parameters answers RQ 3 and RQ 4.

Research Question 3

What could be a suitable parameter range when selecting the staircase procedure in passive experiment?

Research Question 4

What could be a suitable parameter range when performing an active experiment?

During the experiment, the goal will be to get quantitative measures of JND margins, using RQ 5 and RQ 6, which later can be used to answer the research objective.

Research Question 5

What are the JND margins of stall-strip Kirchhoff parameters when flying passively?

Research Question 6

What are the JND margins of stall-strip Kirchhoff parameters and wing when flying actively?

Research Question 7

What is the significance of separating a stall strip in a flow separation model for full flight simulation?

Lastly, RQ 8 will include a little side-track during the start of the project to find the best way to incorporate the buffet model with the new stall model. The buffet model is important for the stall cueing during the experiment, therefore multiple implementation options will be explored.

Research Question 8

How can buffet model be accurately applied when two flow separation parameters are present?

4

Project Plan

In this chapter, the methodology and planning to achieve the research objective is given. At the moment, the thesis research is still at early stage and therefore a lot of details and decisions still need to be finalized. Since the thesis research is split into two parts (Phase 1 and Phase 2), the sections will also be divided to reflect the flow. Section 4.1 will describe the methodology and next steps, then Section 4.2 will introduce to expected outcome of the research and, finally, the Section 4.3 will include a Gantt chart with the planning of each task throughout the next phases of the research.

4.1. Methodology

4.1.1. Phase 1 : Preparations

Model implementation

First, the new model will be implemented in SIMULINK. This process consists of two parts:

1. **Stall model implementation.** The model by Herbold [14] will be implemented using SIMULINK in DASMAT and verified with available data. This might require two SIMULINK files, one used for generating code in DUECA using C++.
2. **Buffet model adjustment.** As mentioned previously in Section 2.3.5, the new model contains two flow separation states - stall strip and wing, whereas buffet model from Section 2.3.4 depends on only on one. Additionally, in research by Imbrechts et al. [29] it was discovered that pilots are very sensitive to the preciseness of the X_{thres}, at which buffeting is activated. Therefore, a good strategy must be made in combining two flow separation states into one. In the list below, few preliminary approaches are provided:
   (a) Running a second model in the background based on dynamics by Van Ingen et al. [10].
   (b) Letting X_{ss} to be the determining state used as X in the buffet model.
   (c) Weighted average between X_{ss} and X_w. A few weight factor combinations can be explored.

Each of these strategies will be implemented and tested with ”stall autopilot” input and compared to buffet onset and magnitude results from the previous research.

Piloted Model Validation Using SIMONA

To ensure that the new stall model of Cessna Citation II is accurate, a small experiment will be conducted in the SIMONA Research Simulator, where it will be flown by an experienced pilot. In this experiment, the pilot will compare the handling characteristics of the stall model with those of the real Cessna Citation II jet. If any inconsistencies are observed, the model will be modified using received feedback and tested again. In addition, this experiment will be conducted without an active motion base.

For this small experiment, it is crucial that the stall and buffet models mentioned previously are fully implemented, as well as SIMONA and pilot participation are arranged in advance. The SIMULINK model from the earlier implementation will be transferred to DUECA framework. From there, input and state output data will be collected.

Additionally, this experiment will be used to perform first comparison between two models: the baseline

model used in Bootsma's et al. experiment [13] and the new stall strip model. The results will later be used during a detailed experiment design.

Sensitivity analysis

Once validation of the stall model is complete, a sensitivity analysis will follow. This analysis will be used to select most relevant Kirchhoff parameters from Equation 2.5, which will be varied during the main experiment. Since the new model contains more parameters and two flow separation states, the variation these parameters may provide different outcomes, compared to sensitivity analysis performed by Smets and Bootsma et al. [28, 13]. As a result, the selection of the parameters could potentially be different.

In the sensitivity analysis, multiple automated simulations will be performed with an artificial pilot input, such as done in the experiment by Smets et al. [28]. During these simulations, one parameter will be varied, while others will be 'frozen'. Then, a comparison of deviation from the baseline case will be performed. Lastly, this analysis will provide a good insight on the parameter behavior, when designing the experiment for both passive and active control.

Experiment Design

Once key parameters from sensitivity analysis are selected, the experiment will be designed in more detail. During the experiment design, the following aspects will be determined during the design:

1. hypotheses
2. independent variables (IV)
3. control variables
4. simulation settings
5. JND measuring methods (passive and active case)

This design of the experiment will be complete before the start of Phase 2.

4.1.2. Phase 2 : Experiment

During the mid-term evaluation, the experiment design will be approved. Once the approval is received, the preparations and experiment set up at SIMONA will start. To prepare for the experiment, first the model will be implemented and additional code using DUECA will be written. This code will include the set up (for example, the staircase experiment algorithm), the display and other cabin features, data logging, model implementation and more. After completing this, the implemented code will have to be tested, before moving further to the main experiment.

4.2. Expected Results

While it is hard to predict the exact results at this stage, some speculations can be done. For **Phase 1** it can be expected that:

1. For the buffet model, the selected flow separation parameter can be either from a second model running in the background or X_{ss}. The first solution is very straightforward, though some mismatches from two models may occur. On the other hand, the X_{ss} state also seems to be a good candidate, since the separation of the flow behind the stall strip is usually related to queuing of the buffet onset. In addition, state X_{ss} is more abrupt than X_w.
2. The small simulation experiment is expected to yield positive results in model validation and upgrading. In addition, some feedback on the buffet model implementation might also be available.
3. For the second part of the small experiment, it is not expected that the pilot will notice a large difference when flying actively. While the improvements in new model [14] are large compared to the previous model [10], the overall difference may not be as visible when flown actively [13, 9]. However, if compared passively, there is a high chance that a difference will be noticed, as discovered in previous research [28, 13]. In addition, it is also expected that the relationship between parameters will be a little different for the new model.
4. Sensitivity analysis is expected to yield similar results to previous research [28, 13].

For the main experiment in **Phase 2**, while the selected parameters and experimental procedures are not yet known, it can be expected that

1. For variable parameter selection, the most likely scenario will contain $a_{1,ss}$, τ_2 and $a_{1,w}$, as seen in [28, 13]. According to Smets et al. [28], the parameters α^*_{ss}, $\tau_{2,ss}$ and α^*_w do not influence the experiment and should remain fixed.
2. There will be a difference in JND margins between active and passive case, consistent with those found in the results by Bootsma et al. [13]. How the other parameters will be used, it is still yet to be determined.
3. There will be a difference in JND margins between stall strip parameters and wing parameters. Since stall strip has more abrupt flow separation, the changes in it might be more easily noticeable to pilots. On the other hand, the opposite might be possible too. A sensitivity analysis during Phase 1 may give better insight in result prediction.

A better result prediction will be available after completing the sensitivity analysis in **Phase 1**.

4.3. Planning

In this section, the planning of the research will be presented in a form of a Gantt chart. In Figure 4.1, an overview of the thesis span is given, without many details on the tasks. Figure 4.2, Figure 4.3 and Figure 4.4 show a more detailed view of each research phase with tasks. The color coding is as follows: blue is dedicated time-frame for a task, pink is public holidays and vacations, dark red indicates an important deadline and orange shades are available buffer zones for the deadlines. A lighter color (light pink or orange) indicates that vacation time or a deadline can be shifted within it.

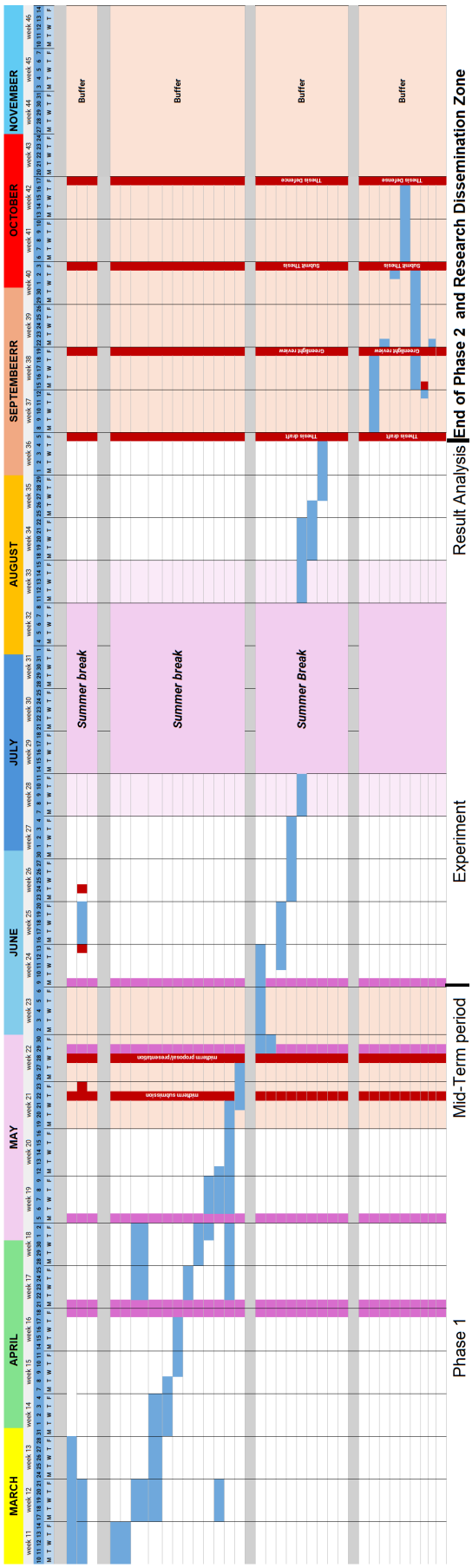

Figure 4.1: A 'bird's eye view' of the thesis research planning

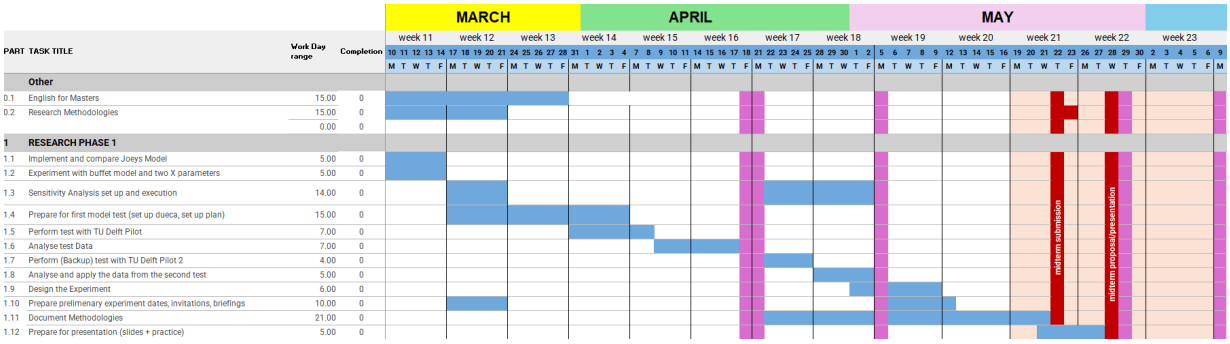

Figure 4.2: A close-up of Gantt chart for Phase 1 planning

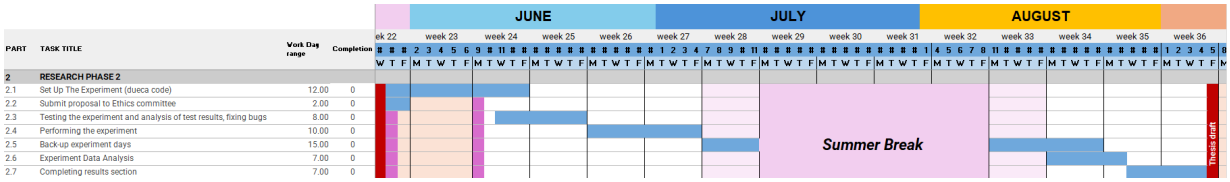

Figure 4.3: A close-up of Gantt chart for Phase 3 planning

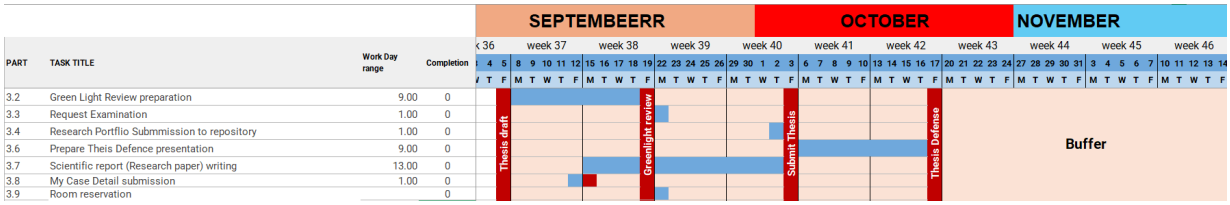

Figure 4.4: A close-up of Gantt chart for Phase 3 planning

Part II

Scientific Article

Evaluating Flow Separation Model Fidelity for Stall in Piloted Flight Simulation

Rasa Vaznelytė *
Delft University of Technology, Delft, Zuid-Holland, 2629HS, the Netherlands

Aerodynamic stall is a leading cause of fatal accidents in aviation. This has introduced regulatory changes to pilot training, where aerodynamic stall models are utilized in full flight simulators for mandatory stall recognition and recovery training. In this research, two longitudinal aerodynamic stall models of the Cessna Citation II were compared side by side to assess the fidelity of two different flow separation modeling options. The first model contains one flow separation state for the entire wing, while the second model models wing and stall-strip effects as two separate states. In previous research, the second model type showed approximately 30% improvement in matching flight test data. Pilot-in-the-loop tests were conducted in the SIMONA Research Simulator, where a Cessna Citation II test pilot actively flew quasi-steady stalls with both models. The tests revealed that the two-state flow separation model had better stall onset characteristics, but it lacked in recovery performance compared to the one-flow-separation model, often leading to higher oscillations. In addition, the tests showed that for an aircraft with reversible controls, an integrated control column with control loading and buffet feedback is required to further improve the model fidelity. The test data analysis revealed that elevator effectiveness variation, buffet cues, and the flow separation hysteresis time constant were the main contributors to oscillations in stall onset and recovery characteristic of the two-state flow separation model. However, the direct effects of having two flow separation states instead of one could not be fully isolated due to pitch model difference between the two stall models. The findings of this research provide guidance for future stall model development aimed at improving the fidelity and training effectiveness of full flight simulators.

Nomenclature

Abbreviations

AoA	=	Angle-of-attack
FSTD	=	Flight Simulation Training Device
FTIS	=	Flight Test Instrumentation System
IATA	=	International Air Transport Association
ICAO	=	International Civil Aviation Organization
JND	=	Just-Noticeable Difference
LOC-I	=	Loss of Control in Flight
MAC	=	Mean Aerodynamic Chord
PIO	=	Pilot Induced Oscillations
SIMONA	=	International Research Institute for Simulation, Motion and Navigation
SRS	=	SIMONA Research Simulator
UPRT	=	Upset Prevention and Recovery Training

Roman symbols

a_1	=	Flow separation abruptness parameter [-]
b	=	Wingspan [m]
$\bar{c}$	=	Mean aerodynamic chord (MAC) [m]
C_D	=	Aircraft drag coefficient [-]

*MSc. Student, Department of Control Simulation, Faculty of Aerospace Engineering

C_L	=	Aircraft lift coefficient [-]
C_{L_α}	=	Lift curve slope [-]
$C_{L_{\max}}$	=	Maximum aircraft lift coefficient [-]
C_m	=	Pitch moment [-]
C_{m_0}	=	Zero-lift moment coefficient [-]
C_{m_q}	=	Pitch damping coefficient [-]
C_T	=	Thrust coefficient [-]
$I_{(xx,yy,zz,xz)}$	=	Moments of inertia [kg·m^2]
$K_{\{q,x,z\}}$	=	Pitch, heave, and surge gain [-]
m	=	Empty mass [kg]
q	=	Pitch rate [rad/s]
S	=	Wing area [m^2]
V_∞	=	Free stream air velocity [m/s]
X	=	Non-dimensional flow separation point (used in model M1) [-]
X_{ss}	=	Non-dimensional flow separation point from the stall-strip (used in model M2) [-]
X_w	=	Non-dimensional flow separation point of the rest of the wing (used in model M2) [-]
$x_{c.g.}$	=	Aircraft center of gravity [m]

Greek symbols

α	=	Angle-of-attack [rad]
α^*	=	Stall angle of attack [rad]
$\dot{\alpha}$	=	Angle of attack rate [rad/s]
δ_e	=	Elevator deflection [rad]
τ_1	=	Flow separation delay time constant [s]
τ_2	=	Flow separation hysteresis time constant [s]
$\omega_{b\{q,x,z\}}$	=	Pitch, heave, and surge break frequency [rad/s]
$\omega_{n\{q,x,z\}}$	=	Pitch, heave, and surge natural frequency [rad/s]
$\zeta_{\{q,x,z\}}$	=	Pitch, heave, and surge damping coefficient [-]
θ	=	Pitch angle

I. Introduction

Loss of Control in Flight (LOC-I) has been the leading category of fatal accidents for over 50 years [1]. According to IATA, between 2009 and 2018, 94% of commercial aviation accidents in this category involved fatalities, making most of them catastrophic events [2]. One of the main reasons behind LOC-I accidents is the stall – a sudden loss of lift that leads to aircraft upset. In response to these statistics, mandatory Upset Prevention and Recovery Training (UPRT) was introduced in 2019 by ICAO [3]. To utilize current flight simulation training devices (FSTDs) for UPRT, many fidelity enhancements must be made to avoid negative training [4]. One of these is expansion of model fidelity into a post-stall region [5].

While the expansion of full flight simulator envelope fidelity is required for the training, there are no well-defined regulations on the accuracy of the stall simulation itself. Research has been done to explore this issue; Schroeder et al. [6] examined how pilots perceive stall models generated using different resources, while Grant et al. [7] explored whether changing fidelity parameters of an existing aircraft model was noticed by the pilots flying the simulation. In both experiments, it was observed that pilots were not as sensitive to these changes, but there was no clear conclusion on whether these changes can affect the quality of stall recovery training.

To contribute to this research, a group from Delft University of Technology has developed stall models incorporating Kirchhoff's flow separation theory, which were identified from flight test data of the Cessna Citation II. These models were then used in human-in-the-loop experiments using the SIMONA Research Simulator (SRS). The first stall model to be implemented in full flight simulation was by Van Ingen et al. [8–10]. This stall model contains a single flow separation state to describe the non-linear aerodynamics during stall and how it affects the aerodynamic forces and moments on the aircraft. However, since then, there have been new updates and improvements made to this stall model [10–13].

The most recent stall modeling addition by Herbold [13] in 2025 includes two flow separation states: the first one modeling separation effects behind a stall-strip on the inboard part of the wing, and the second one modeling effects for the remainder of the wing. This two-state flow separation model has showed a significant improvement in model fit to flight experiment data. In addition, recent tuft measurement flight tests by Deligios [14] have confirmed that flow separation on the stall-strip and on the wing occurs as two distinct separation regions. The resulting improvement in model fidelity has drawn interest on how this new way of looking at the wing stall model would perform in a full flight simulation.

Therefore, the goal of this paper is to compare the two-state flow separation model introduced by Herbold [13] and the single-state flow separation model developed by Van Ingen et al. [8] by conducting pilot-in-the-loop tests in the SRS and performing a detailed analysis of simulated aerodynamic force and moment contributions. For this test, a Cessna Citation II test pilot performed Quasi-Steady stall maneuvers and provided feedback on the differences observed between the models. Prior to the pilot-in-the-loop test, a few modifications were made to Herbold's two-state flow separation model [13] to enhance its quality and adapt it for full flight simulation. The pitch moment model C_m was updated to improve the initial state for trimmed flight and reduce pitch oscillations. In addition, a few alternative mass model model options were explored to improve consistency of the simulation. This resulted in a number of model variations, from which the best performing model was selected experimentally. This final two-state model was then used in the main pilot-in-the-loop test to be compared to the single-state flow separation model by Van Ingen.

This paper is structured as follows: section I provides an overview on how the principle of flow separation is generally incorporated in an aircraft model, followed by the introduction of the two Cessna Citation II stall models and flight test data used in this research. Then, section IV describes the methods used to modify the models and how the pilot-in-the-loop test was conducted in full flight simulation, which are then followed by the results in section V. Lastly, these results are discussed in section VI and the conclusions are presented in section VII.

II. Experiment Aircraft

The stall models used in this research were identified for the Cessna Citation II research aircraft, registered as PH-LAB. The research aircraft is in a joint ownership between TU Delft and the Netherlands Aerospace Center (NLR). The aircraft is equipped with a custom Flight Test Instrumentation System (FTIS), which is used to collect in-flight data [13]. The aircraft is illustrated in Figure 1 and a summary of aircraft parameters can be seen in Figure 4.

Table 4 Geometric and inertial (at Basic Empty Weight) properties of PH-LAB [13].

Dimension		Value	Unit
Wingspan	b	15.75	m
MAC	$\bar{c}$	2.013	m
Wing Area	S	30.0	m^2
Empty Mass	m	4161.3	kg
	I_{xx}	12392	$kg{\cdot}m^2$
	I_{yy}	31501	$kg{\cdot}m^2$
	I_{zz}	41908	$kg{\cdot}m^2$
	I_{xz}	2252.2	$kg{\cdot}m^2$

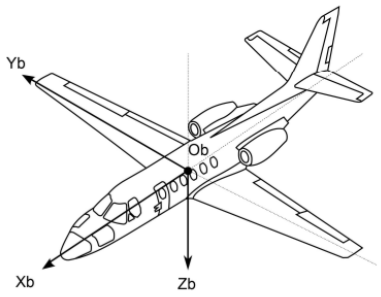

Fig. 1 Cessna Citation II PH-LAB, adapted from [15].

A. Cessna Citation II Flight Test Data

The stall models used in this research were previously identified in the work by Van Ingen et al. [8] and Herbold [13] using experimental datasets from 2016 and 2024 flight tests, see Table 5. The dataset contained a total of 46 stalls, consisting of three maneuver types: quasi-steady stalls, dynamic stalls and deep dynamic stalls.

Table 5 Summary of the flight test datasets.

Dataset	Maneuver Type	Description	No. of Sets	Flight Level	Used in
2016	Quasi Steady Wings Level (1g)	From trimmed flight, the airspeed is reduced at 1 kts/s until stall occurs. The stall is held for a few moments.	16	80–100, 110–150, 150–200	**M1, M2**
	Quasi Steady Accelerated (1.1g–1.4g)	From trimmed flight, the aircraft is banked between 30–45° and pitched up to maintain altitude. Airspeed is reduced at 1 kts/s until stall.	18	80–100, 110–150, 150–200	**M1, M2**
2024	Dynamic Stall	Starts with a positive angle-of-attack rate and sequential step inputs. Once stabilised and close to stall, oscillating elevator inputs are used to enter and exit the stall.	5	150–200	**M2**
	Deep Dynamic Stall	Starts with a positive angle-of-attack rate and sequential step inputs. Once stabilised, a constant elevator deflection is applied to keep the aircraft stalled. At 18–20° AoA, small elevator oscillations are applied within the stall.	7	150–200	**M2**

The 2016 dataset, containing two types of quasi-steady stalls, was used in the model by Van Ingen et al. [8], which is introduced later in Section III.B.1. For model by Herbold [13], discussed in Section III.B.2, all datasets were used, including dynamic stalls that contain $\dot{\alpha}$ excitation. In this research, a selection of quasi-steady wing-level stalls was used to evaluated the piloted simulation data in subsection V.D.

B. Cessna Citation II Stall Properties

The stall of a tapered wing, such as the one of the Cessna Citation II, initiates at the outer section of the wing and expands towards the root as the angle-of-attack increases. This is called a tip-stall. This type of stall is highly unstable, since separated flow at the wingtip reduces the aileron effectiveness, resulting in undesired roll moments and reduced lateral control of the aircraft [16]. One of the ways to improve stall characteristics of a tapered wing is by artificially inducing root-stall before the tip-stall critical angle-of-attack is reached [17, 18]. For the Cessna Citation II aircraft, this is done by placing a stall-strip at the leading edge of the inner wing, see Figure 3 and Figure 2. This device creates a flow separation at the inner section the wing, which expands with increasing angle-of-attack. This forces the aircraft to pitch down towards a recovery, while retaining the lateral control capabilities.

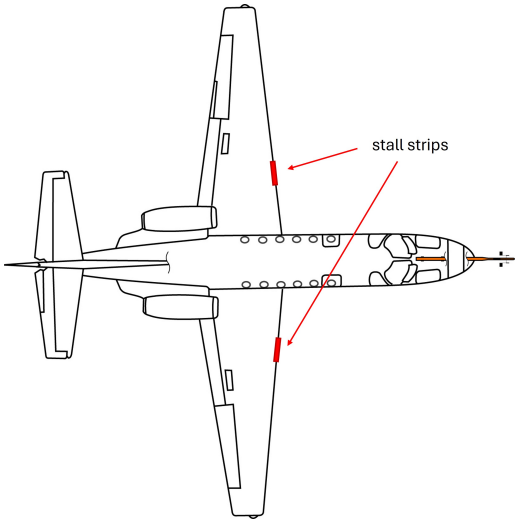

Fig. 2 Top view of the Cessna Citation II with approximate stall-strip locations. Image obtained and edited from [8].

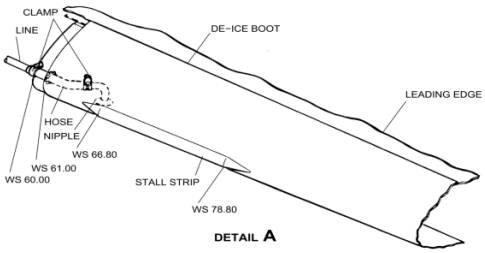

Fig. 3 A close-up of the stall-strip schematic from the aircraft manual. Image obtained from [13].

Next to improving the stall characteristics of the tapered wing, the stall-strip has additional effects on the aircraft. The most noticeable effect is an induced low-speed buffeting. This is caused by the engine nacelles and horizontal tail surface being engulfed in the separated flow from the stall-strip, causing vibrations in the cabin and the control column – a useful stall onset cue for the pilots [17]. The implementation of a stall-strip also comes at a cost: it reduces the maximum lift coefficient $C_{L_{\max}}$ of the aircraft [18]. This negative aspect of a stall-strip is usually accepted for the ensured controllable and stable recovery.

III. Kirchhoff Flow Separation Models

A. Kirchhoff Flow Separation Theory

Both the one-state and two-state aerodynamic stall models developed at TU Delft are based on Kirchhoff's theory of flow separation. This method is used to relate the lift and moment equations to the trailing edge flow separation acting on a wing during a stalled flight [19]. The flow separation point is defined as a non-dimensional state X, which is a normalized chord-wise distance. Therefore, the state X takes values in the range of $0 \leq X \leq 1$, where $X = 1$ means fully attached flow and $X = 0$ is fully separated flow. For example, according to Goman and Khrabrov [19], the lift

coefficient C_L can then be related to state X using Eq. (1):

$$C_L(\alpha, X) = C_{L_\alpha}\left(\frac{1+\sqrt{X}}{2}\right)^2 \alpha \tag{1}$$

Where α is an angle-of-attack (AoA) and C_{L_α} is a lift curve slope. Based on this theory, Eq.(2) was introduced by Fischenberg [20], for modeling the flow separation state as a function of time and incorporating hysteresis and unsteady aerodynamics effects:

$$\tau_1 \frac{dX}{dt} + X = \frac{1}{2}\{1 - \tanh(a_1(\alpha - \tau_2\dot{\alpha} - \alpha^*))\} \tag{2}$$

Here a_1 is a flow separation abruptness parameter, α^* is a stall angle of attack, $\dot{\alpha}$ is angle of attack rate, and time constants τ_1 and τ_2 represent the flow separation reactiveness to change and the hysteresis effect, respectively. All of these nonlinear stall model parameters and can be identified experimentally [20].

By manipulating previously described parameters, three cases of a flow separation model can be identified: **unsteady**, **quasi-steady** and **steady**. Since the model in Eq. (2) contains time constants τ_1 and τ_2, which are responsible for unsteady effects, and $\dot{\alpha} \neq 0$, it will be referred to as the **unsteady** case. In the **quasi-steady** case, the time constant τ_1 is equal to zero and therefore Eq. (2) simplifies to Eq. (3) :

$$X = \frac{1}{2}\{1 - \tanh(a_1(\alpha - \tau_2\dot{\alpha} - \alpha^*))\} \tag{3}$$

Lastly, the **steady** case refers to the condition where the flow separation state is only a function of the angle-of-attack and does not contain any unsteady effects. This means that $\dot{\alpha}$, τ_1, and τ_2 are equal to zero. The steady case is usually denoted as X_0, as shown in Eq. (4):

$$X_0 = \frac{1}{2}\{1 - \tanh(a_1(\alpha - \alpha^*))\} \tag{4}$$

B. Stall Models

In this section, two main structures of longitudinal models are introduced: **M1** and **M2**. These structures will serve as baseline models, which were obtained in previous research [8, 10, 13]. The key difference between these structures is the number of flow separation states, therefore it is represented with a number in the name. In this case, the notations can be interpreted as *"**M**odel, **1**-flow-separation-state"* and *"**M**odel, **2**-flow-separation-states"*. Any change applied and tested in the pilot-in-the-loop tests will be an expansion or modification of these two models, for which additional identifiers will be appended to **M1** and **M2**.

1. M1 model

The first longitudinal stall model identified by Van Ingen et al. [8] and modified by Bootsma et al. [10] is described in Equation 5 and will be referred as **M1**. This model contains only a single flow separation state X for the entire wing, which is modeled using the unsteady flow separation in Eq. (2). The modification introduced by Bootsma on the initial model by Van Ingen is adding a pitch damping coefficient C_{m_q}, which was used to reduce pitch oscillations during actively controlled flight in a full flight simulator [10]. This modification is already taken into account in Eq. (5).

$$\begin{aligned}
C_L &= C_{L_0} + C_{L_\alpha}\left(\frac{1+\sqrt{X}}{2}\right)^2 \alpha + C_{L_{\alpha^2}}(\alpha - 6^\circ)_+^2 \\
C_D &= C_{D_0} + C_{D_\alpha}\alpha + C_{D_{\delta e}}\delta_e + C_{D_X}(1-X) + C_{D_{C_T}}C_T \\
C_m &= C_{m_0} + C_{m_\alpha}\alpha + C_{m_{\delta_e X}}\max(0.5, X)\delta_e + C_{m_q}\frac{qc}{V_\infty} + C_{m_{C_T}}C_T
\end{aligned} \tag{5}$$

Where the term $(\alpha - 6^\circ)_+^2$ is zero for $\alpha \leq 6^\circ$, and for $\alpha > 6^\circ$ it is equal to $(\alpha - 6^\circ)^2$.

2. M2 model

The second longitudinal stall model **M2** introduced by Herbold [13] contains two flow separation states: X_{ss} and X_w, see Eq. (6). The state X_{ss} is computed using the unsteady flow separation model from Eq. (2) and models the effects of the flow separation caused by a stall-strip, while the state X_w is obtained using a steady flow separation model as defined in Eq. (4) and models the flow separation of the rest of the wing. Compared to the **M1** model, this model has shown a reduction in mean square error (MSE) of C_L, C_D and C_m with respect to flight test data by 32% , 29% and 27%, respectively [13].

$$
\begin{aligned}
\tau_{1,ss}\frac{dX_{ss}}{dt} + X_{ss} &= \frac{1}{2}\{1 - \tanh(a_{1,ss}\left[\alpha - \tau_{2,ss}\dot{\alpha} - \alpha^*_{ss}\right])\} \\
X_w &= \frac{1}{2}\{1 - \tanh(a_{1,w}\left[\alpha - \alpha^*_{w}\right])\} \\
C_L &= C_{L_0} + C_{L_{\alpha,ss}}\left(\frac{1+\sqrt{X_{ss}}}{2}\right)^2\alpha + C_{L_{\alpha,w}}\left(\frac{1+\sqrt{X_w}}{2}\right)^2\alpha + C_{L_q}\frac{q\bar{c}}{V_\infty} + C_{L_{\delta e}}\delta e \\
C_D &= C_{D_0} + C_{D_{C_T}}C_T + C_{D_{\delta e}}\delta_e + C_{D_{C_L^2}}C_L^2 + C_{D_{X_{ss}}}(1 - X_{ss}) + C_{D_{X_w}}(1 - X_w) \\
C_m &= C_{m_0} + C_{m_{C_T}}C_T + C_{m_{q^*}}\frac{q\bar{c}}{V_\infty} - l_{c.p.}C_L + C^*_{m_{X\delta_e}}\delta_e \\
\text{where: } l_{c.p.} &= -C_{m_{K_0}} - C_{m_{c.g}}\frac{x_{c.g.}}{\bar{c}} - C_{m_{K_{1,ss}}}(1 - X_{ss}) - C_{m_{K_{1,w}}}(1 - X_w) \\
C^*_{m_{X\delta_e}} &= C_{m_{\delta_e}} + C_{m_{X_{ss}\delta_e}}X_{ss}
\end{aligned}
\tag{6}
$$

The coefficient values of the **M1** and **M2** models are listed in Table 6. A schematic representation between flow separation states predicted by **M1** and **M2** can be seen Figure 4.

Table 6 A list of M1 and M2 flow separation and aerodynamic coefficient parameter values.

	M1			M2		
	Name	**Unit**	**Value**	**Name**	**Unit**	**Value**
Flow Separation Parameters	τ_1	[s]	0.2547	$\tau_{1,ss}$	[s]	0.4191
	τ_2	[s]	0.0176	$\tau_{2,ss}$	[s]	0.3391
	a_1	[-]	27.6711	$a_{1,ss}$	[-]	70.2846
	α^*	[rad]	0.2084	α^*_{ss}	[rad]	0.1956
				$a_{1,w}$	[-]	13.9276
				α^*_w	[rad]	0.3267
C_L Parameters	C_{L_0}	[-]	0.1758	C_{L_0}	[-]	0.2318
	C_{L_α}	[-]	4.6605	$C_{L_{\alpha,ss}}$	[-]	1.3851
	$C_{L_{\alpha^2}}$	[-]	10.7753	$C_{L_{\alpha,w}}$	[-]	2.5961
				C_{L_q}	[-]	8.0747
				$C_{L_{\delta e}}$	[-]	-0.3403
C_D Parameters	C_{D_0}	[-]	0.0046	C_{D_0}	[-]	0.0165
	C_{D_α}	[-]	0.2372	$C_{D_{C_T}}$	[-]	0.3917
	$C_{D_{\delta e}}$	[-]	-0.1857	$C_{D_{\delta e}}$	[-]	-0.1894
	C_{D_X}	[-]	0.0732	$C_{D_{C_L^2}}$	[-]	0.0258
	$C_{D_{C_T}}$	[-]	0.3788	$C_{D_{X_{ss}}}$	[-]	0.0555
				$C_{D_{X_w}}$	[-]	0.2062
C_m Parameters	C_{m_0}	[-]	0.0183	C_{m_0}	[-]	0.0659
	C_{m_α}	[-]	-0.5683	$C_{m_{C_T}}$	[-]	0.0794
	$C_{m_{\delta e X}}$	[-]	-1.023	$C_{m_{q^*}}$	[-]	-1.7502
	C_{m_q}	[-]	-22	$C_{m_{\delta e}}$	[-]	-0.7431
	$C_{m_{C_T}}$	[-]	0.1443	$C_{m_{c.g}}$	[-]	-0.9616
				$C_{m_{K_0}}$	[-]	3.2316
				$C_{m_{K_{1,ss}}}$	[-]	-0.0517
				$C_{m_{K_{1,w}}}$	[-]	-0.0681
				$C_{m_{X_{ss}\delta_e}}$	[-]	-0.2576

Figure 4(a) shows flow separation point values as a function of an angle-of-attack for **M1** model at the top panel and **M2** model at the bottom panel. Here, time-dependent parameters were excluded and therefore the flow separation equations were reduced to a static form of Eq. (4). In Figure 4(b), an impression of flow separation points on a wing is shown for three selected angles of attack. At low angles-of-attack, such as $\alpha = 5^\circ$ in the top right panel, both models predict a fully attached flow. In middle right panel where $\alpha = 13^\circ$, the stall-strip X_{ss} fully separates and wing separation X_w is starting to develop, while for the **M1** model, state X shows a separation across entire wing, with its value around 20% of the chord. Finally, at the highest AoA at 22° shown in the bottom right panel, the X state for the **M1** model is fully separated, while separation of the X_w is not fully complete for the **M2** model.

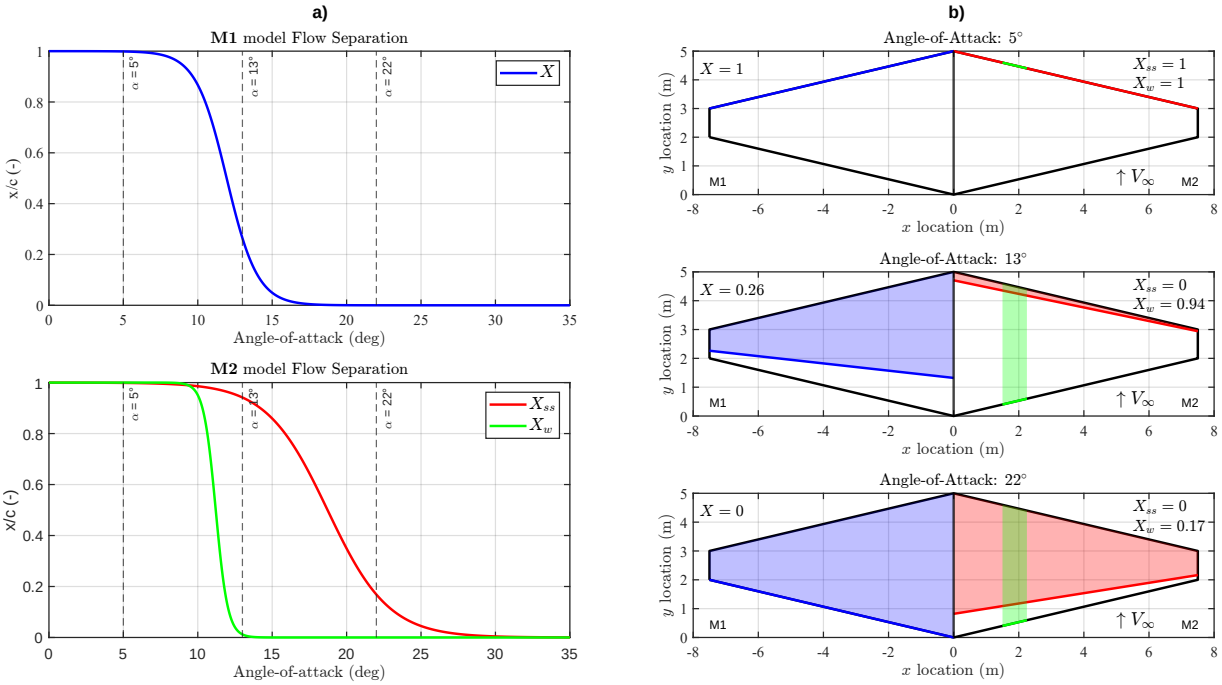

Fig. 4 Left side : flow separation parameter values with angle of attack; Right side: schematic representation of the flow separation parameter meaning.

Besides the flow separation, another notable difference between the **M1** and **M2** model equations (Eq. (5) and Eq. (6)) is the term used for a stabilizing pitch-down moment. The **M1** model contains the $C_{m_\alpha}\alpha$ term, which increases linearly with angle-of-attack, while the **M2** model's stabilizing pitch-down moment depends on a C_L regressor, multiplied by the function describing center-of-pressure location $l_{c.p.}$. This means that with increasing angle-of-attack, unlike $C_{m_\alpha}\alpha$, the negative moment contribution of $l_{c.p.}C_L$ can reduce after achieving $C_{L_{max}}$. In addition, both $l_{c.p.}$ and C_L are functions of flow separation parameters, which could result in strong coupling effects and moment fluctuations in stall. The effects of this difference are discussed more in detail in Section V.B.1.

C. M2 Modifications

In its published form [13], the longitudinal M2 model was not ready for pilot-in-the-loop testing. When implemented in the equations of motion, the **M2** model had a high control sensitivity and uncontrollable oscillations related to the pitch model. Several issues with the pitch moment model were identified. Firstly, the pitch damping of **M2** was not as suitable compared to the reference model **M1**, for which the value of C_{m_q} was manually tuned using the SIMONA Research Simulator [10]. Secondly, the C_{m_0} value was high compared to **M1**, which causes the trim algorithm to be unstable. It was therefore decided to implement some modifications on model **M2** and refine it before applying it in the full flight simulation.

1. Pitch Damping Correction

The C_{m_q} of **M2** was set from -1.75 to -22 to reduce pitch oscillations. When the original **M2** model was simulated using equations of motion, it was observed to have high oscillations when given active control inputs. This was caused by the low magnitude of the pitch damping coefficient. For the reference model **M1**, the pitch damping value was experimentally found to be -22 [10], while the C_{m_q} of **M2** was only -1.75. When testing with active controls, it was observed that the C_{m_q} value of -22 was also suitable for the **M2** model.

2. Zero-lift Moment Correction

The C_{m_0} of **M2** was changed from 0.0659 to 0.02 in order to match the trim state of the aircraft. The C_{m_0} of **M2** is 0.0659, which around three times higher than previous models by Van Ingen et al. [8] and Van Horssen et al.

[21], 0.0183 and 0.021, respectively. As a result, the trim function could not find an equilibrium point or provided a mismatched trim elevator setting compared to the measured flight data. For example, at the trim point of $\alpha = 8°$, the resulting elevator deflection of model **M2** was around zero degrees, while the deflection value in the flight experiment data was around $-4°$. Therefore, it was decided to reduce the value of C_{m_0} to around -0.02 to better match the flight data and provide a more fair comparison in the pilot-in-the-loop test against model **M1**.

3. Elevator Effectiveness

During initial active control testing of both models (after modifications in Section III.C.1 and Section III.C.2 were applied), it was observed that even at high AoA stall conditions ($\alpha \geq 20°$), the **M2** model still had potential to pitch up to extremely high pitch angles. If recovery was not initiated at a specified maximum angle, any additional elevator deflection would enable the **M2** model to reach pitch angles of 40° and above. This pitch range during the stall is unrealistic and the elevator control effectiveness was reduced from 80% at full flow separation to around 50%, which is similar to **M1**, see Figure 5. This means that the $C_{m_{\delta_e}}$ was modified from -0.794 to -0.5 and $C_{mX_{ss}\delta_e}$ went from -0.2576 to -0.5007. These changes in elevator effectiveness are shown in Figure 5, plotted for an analytical cosine variation in AoA.

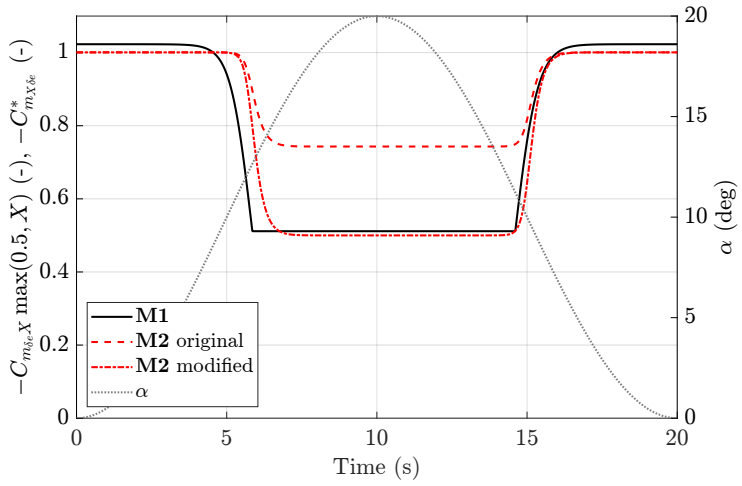

Fig. 5 Elevator Effectiveness change with angle-of-attack.

4. Buffet Implementation of Model M2

The buffet of the **M1** model, developed by Van Horssen et al. [21], contains vertical accelerations that are activated at flow separation values $X < 0.89$. In addition, the intensity of these buffet accelerations is regulated by a scaling factor $(1 - X)$. Since re-identifying the buffet model for the X_{ss} state of the **M2** model is outside the scope of this research, a separate state X matching the **M1** model was added to the **M2** model to ensure a matching buffet response. This state contains exactly the same flow separation coefficients and buffet threshold as in **M1** to suit the previous buffet model. This makes the full flight simulation model **M2** have three flow separation states: X_{ss}, X_w and X. However, X is only used for the buffet and does not play any role in aerodynamic force equations.

5. Mass Model Options

While implementing the **M2** model into the equations of motion, it was found that the mass model used for **M1** had a much lower total weight compared to the total weight of the aircraft during flight tests. While the mass model of **M1** had a total weight of 4970 kg, the flight tests and identification were performed with a total weight of 6082 kg. In addition, the center of gravity $x_{c.g.}$ of the two mass models differed, therefore the effect of shifting the center of gravity was also explored. Table 7 contains a summary of selected mass models that were explored in initial testing of the **M2** model, as described in subsection IV.C. In Figure 22, the mentioned mass model options are mapped to the center-of-gravity and moment envelope of the Cessna Citation II, from the aircraft's documentation [13].

Table 7 Mass Model options explored in this research.

Mass Model Option	Total mass, (kg)	$x_{c.g.}$ location, (m)	Origin
1	4970	7.096	M1 simulation [9, 10]
2	6082	7.135	Flight experiments [13]
3	4970	7.135	Combined

IV. Methodology

Two separate pilot-in-the-loop tests were performed in the SIMONA Research Simulator (SRS) to assess the subjective differences between the stall characteristics of the **M1** and **M2** models. The SRS specifications are described in more detail in subsection IV.A. The first initial test was used to assess the **M2** model stall characteristics and the effects of proposed modification. The goal of this test was to select the best performing **M2** model version to be compared to **M1**. The details about this first test are given in subsection IV.C. The pilot-in-the-loop test consisted of a direct comparison between the **M1** and **M2** models to evaluate the potential fidelity benefits of two flow separation parameters and determine which model represents the Cessna Citation II stall characteristics best. The details of the main test can be found in subsection IV.D. In both piloted tests, a Cessna Citation II test pilot performed a symmetrical quasi-steady stall maneuver, which is described in subsection IV.B.

Two types of data were collected in these tests: subjective pilot feedback, and maneuver log data which involves aircraft model states, parameters, etc. The pilot feedback was used to evaluate the model fidelity with respect to the real aircraft stall characteristics, while the log data was used to evaluate which parameters are responsible for various aspects of the **M1** and **M2** model dynamics.

A. SIMONA Research Simulator

Both pilot-in-the-loop tests were performed in the SRS (shown in Figure 6 and Figure 7) located at the Delft University of Technology. The SRS is a six degree-of-freedom motion simulator, powered by a hydraulic hexapod motion platform. The motion cues are provided using a classical washout filter [22]. The washout filter settings used during this research are listed in Table 8. These settings are almost the same as those used in the in the experiment performed by Bootsma et al. [10], except that the pitch high-pass filter gain K_q was corrected to 0.5 instead of 0.7. Since only the longitudinal motion was used, the roll, sway, and yaw washout filter settings were set to zero and are not shown in the table.

Fig. 6 The SIMONA Research Simulator. Adapted from [23].

Fig. 7 The cockpit inside the SIMONA Research Simulator. Adapted from [10].

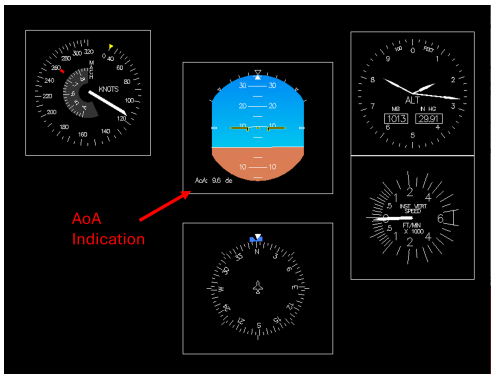

Fig. 8 The primary flight display used in the pilot-in-the-loop tests.

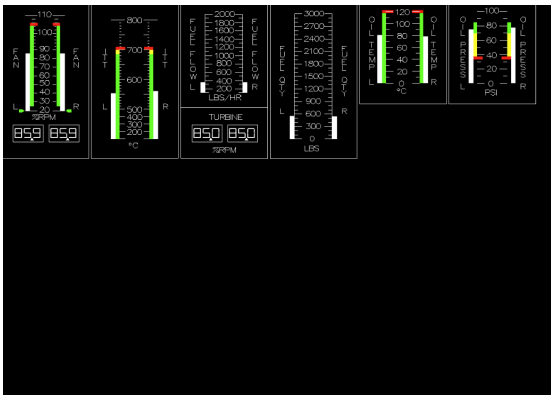

Fig. 9 The engine display used in the pilot-in-the-loop tests. Adapted from [10] and [23].

Aside from the motion cueing, the visual cues were provided using cockpit display screens and outside visuals. The primary flight display in front of the pilot was used to present aircraft attitude, airspeed, climb rate, altitude, and angle-of-attack indications. This layout can be seen in Figure 8. Next to the primary display, a second display, shown in Figure 9, provided the pilot with engine parameters. In addition to the cockpit displays, external visual cues were generated using the FlightGear visual database, which were displayed on a collimated mirror by three LCD projectors with a resolution of 1280×1024 each. The field of view of the collimated mirror is 180°×40° [22].

Table 8 Washout filter settings for pitch, heave and surge.

High-pass filter						Low-pass filter	
ω_{n_q}	1.0 rad/s	ω_{n_z}	2.0 rad/s	ω_{n_x}	1.2 rad/s	ω_{n_x}	2.4 rad/s
ζ_q	0.7	ζ_z	0.7	ζ_x	0.7	ζ_x	0.7
ω_{b_q}	0 rad/s	ω_{b_z}	0.3 rad/s	ω_{b_x}	0 rad/s		
K_q	0.5	K_z	0.5	K_x	0.5		

B. Maneuver

For the modification test and comparison test, the same setup was used. The pilot was seated on the left hand side of the cockpit (i.e., captain's seat) with a yoke control column configuration. The yoke was used to provide elevator inputs to the model, while the autopilot disengage button was used to start or to re-start the run. The simulation and model settings were controlled from the SRS operator room.

The maneuver performed during the simulation was a symmetric quasi-steady stall, with recovery initiation at 16°. In this maneuver, the aircraft was first decelerated at approximately 1 kt/s^2 by setting the throttles back and reducing thrust. At the same time, the pilot provided a negative elevator deflection to keep the aircraft attitude constant and thus increasing the angle-of-attack. When the angle-of-attack of 16° was achieved, a recovery message was displayed and the pilot pitched the aircraft down to around 0° to -3° of pitch angle. Once the airspeed increased, the pilot leveled out the aircraft by adjusting pitch up and increasing thrust. The recovery angle-of-attack was chosen to match the previous experiments by Bootsma et al. and Smets et al. [9, 10] and to assess how well the **M2** model would perform. For **M2**, this angle-of-attack contains both full stall-strip flow separation and slight wing trailing edge separation.

In this research, the flight director guidance, used in active Just-Noticeable Difference (JND) experiments by Bootsma et al. [10] was not incorporated. However, an explicit angle-of-attack indicator was added to help the test pilot provide more consistent data, see Figure 8. In previous research [9, 10], the maneuver was started roughly at angles-of-attack of 10° to keep the duration of the stall short. For this research, it was chosen to start the stall maneuver at 8.4° of AoA, just before flow starts to separate and the buffet begins. This way the entry to stall is smoother. Since the pilot-in-the-loop test runs started at lower angles-of-attack than in previous research [9, 10], the flight director guidance led to more pitch overshoot corrections, which were distracting from the stall itself.

On the other hand, the pilots did not see angle-of-attack indications during test flights, therefore this new addition

negatively affected the realism of a stall. Since these tests were not intended to obtain quantitative measures, such as parameter JND thresholds, the implementation of AoA indication was considered acceptable.

C. M2 Model Modification Test

Before the comparison of the **M1** and **M2** models, preliminary evaluations of several **M2** model modifications were performed in the SRS. These tests were performed by a single Cessna Citation II test pilot. The goal of this test was to assess the fidelity of the **M2** model and select the most realistic modification. The most realistic modification selected based on test pilot feedback was subsequently applied in the comparison against model **M1** in the second pilot-in-the-loop test.

In this first test, for each modified **M2** model version, two quasi-steady stall maneuvers described in subsection IV.B were performed. In addition to the previously described 16° AoA recovery, a second deeper stall with a 20° AoA recovery was performed to push the model performance to its limits. In total, 5 **M2** modifications were compared, which are summarized in Table 9.

Table 9 M2 model options explored during the first test.

ID	Pitch Moment Modifications	Mass Model	Elevator Effectiveness
M2.a	✓	1	*original*
M2.b	✓	3	*original*
M2.c	✓	2	*original*
M2.d	✓	2	*reduced*
M2.e	✓	3	*reduced*

D. M1 and M2 Model Comparison Test

After the first test described in subsection IV.C, the selected **M2** model was compared side-by-side with the **M1** model. The aim of this test was to evaluate subjective differences in stall characteristics between these two models. This pilot-in-the-loop test was performed by the same test pilot, who performed the first **M2** model modification test.

In this test, four combinations of stall comparisons were made: **A**, **B**, **C** and **D**, see Table 10. The **A** and **B** combinations compared two identical models, while **C** and **D** compared two different models. To randomize the sequence of these comparison combinations, a Latin square design was used. The columns of the Latin square were then shuffled and each row resulted in a set of 4 comparisons. These sets were executed sequentially from set 1 to set 4, see Table 10. This resulted in 32 stalls in total, 16 stalls for each model.

Before the start of the comparison test, a short training session was conducted, during which a type **C** comparison between **M1** and **M2** models was performed to familiarize the pilot with the test procedure.

Each comparison consisted of two consecutive quasi-steady stalls with a 16° AoA recovery, as described in subsection IV.B. Both models were initialized at an angle-of-attack of 8.4°, for which the elevator trim condition and airspeed were nearly identical. At this angle-of-attack, the simulation started just before the buffet threshold and each stall lasted 50 seconds. This enabled a smooth entry into the stall and gave the pilot enough time to perform a full recovery.

After completing two consecutive stalls, the pilot was asked the first question: *"Did you notice a difference in stall models?"*. If the response was ***YES***, two follow-up open-ended questions were asked: *"What was different?"* and *"Which model resembles Cessna Citation II stall better?"*. If the answer to the first question was ***NO***, no follow-up questions were asked and the test proceeded to the next comparison. The comparison test was completed once all 16 comparisons from 4 sets were performed.

Table 10 Comparison test sequence order of the randomized Latin Square.

Comparison type			Column 1	Column 4	Column 2	Column 3
A	M1-M1	Set 1	**A**	**B**	**D**	**C**
B	M2-M2	Set 2	**B**	**C**	**A**	**D**
C	M1-M2	Set 3	**C**	**D**	**B**	**A**
D	M2-M1	Set 4	**D**	**A**	**C**	**B**

V. Results

In this chapter, the data collected during the pilot-in-the-loop tests, described in section IV, is analyzed. First, the pilot feedback of both pilot-in-the-loop tests is summarized in subsection V.A and Section V.B.1. The subsequent sections analyze the logged aircraft model data. In Section V.B.2, the **M1** and **M2** models are compared side by side, while in subsection V.D they are both verified against flight test data. Additionally, based on pilot-in-the-loop test data, a modification was applied to the stall autopilot from previous research [9, 10] and is discussed in subsection V.C.

A. M2 Model Modification Test

The best performing **M2** model was **M2.e**, which contains the mass model number **3**, pitch moment modifications and reduction in elevator effectiveness. From now on, this model will be regarded as the **M2** model. The pilot chose it for more realistic forces on the stick and performance of the model. On the other hand, it was observed to have more oscillations during recovery compared to the **M2.b** model, which can be seen in Figure 10a and Figure 10b.

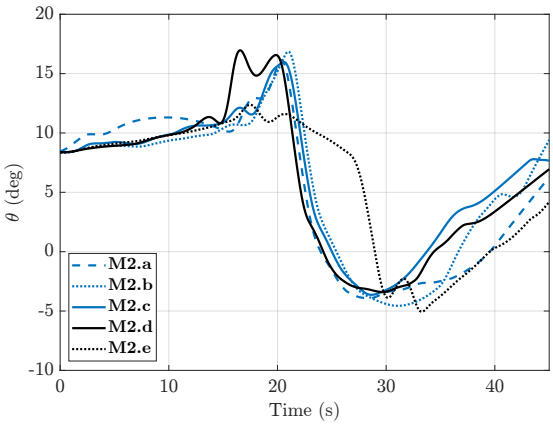

(a) Pitch angle value of each model from Table 9 during a 16° AoA stall maneuver.

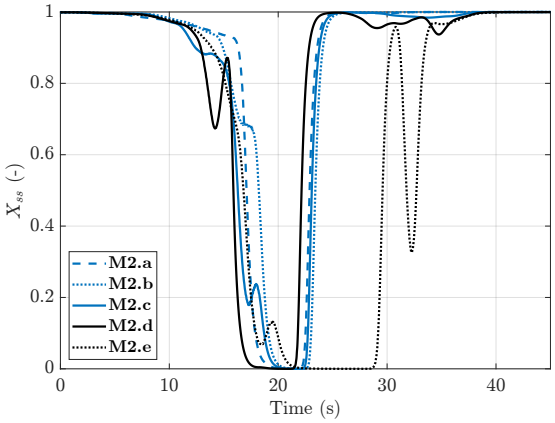

(b) The stall strip flow separation parameter value X_{ss} of each model from Table 9 during a 16° AoA stall maneuver.

In addition to the selected model, a few observations were made. First observation was that the pilot indicated to partially rely on buffet cues when entering and exiting stall. In the recovery phase, the pilot described "shedding off the buffet" as a cue that lift on the wing has been restored. The pilot also noted the lack of buffet feedback on the control column. It was described that when approaching stall, slight elevator deflections are experienced due to flow separation affecting the horizontal stabilizer. In the aircraft, these slight variations are felt through the control column, since the aircraft controls are reversible. However, the control column used in the test setup did not contain any force feedback – only an increasing force with deflection.

The second observation was that one of the main deciding factors for the pilot was the deflection force on the control column. This means that the pilot's preference included models with reduced elevator effectiveness. While this emulates the control column force and aircraft's tendency to force itself into recovery, the elevator deflections required to reach 16° AoA become significantly larger than in the flight test data, sometimes even approaching the maximum elevator limits, see Figure 11a. Moreover, the additional reduction of elevator effectiveness also slightly intensified oscillation in stall onset and recovery, which can also be seen in Figure 10a and Figure 10b. This means that for a more realistic stall simulation, a control column that simulates the reversible control system with force feedback is crucial.

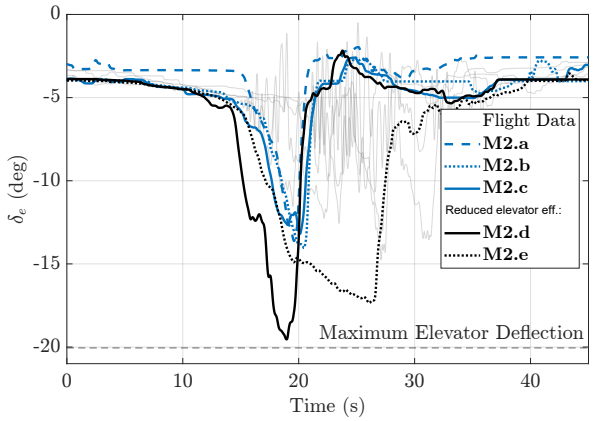

(a) Elevator deflection required to perform a 16° quasi-steady stall for all models from Table 9. The black lines contain models with reduced elevator effectiveness, while matching line-style represents the same mass model.

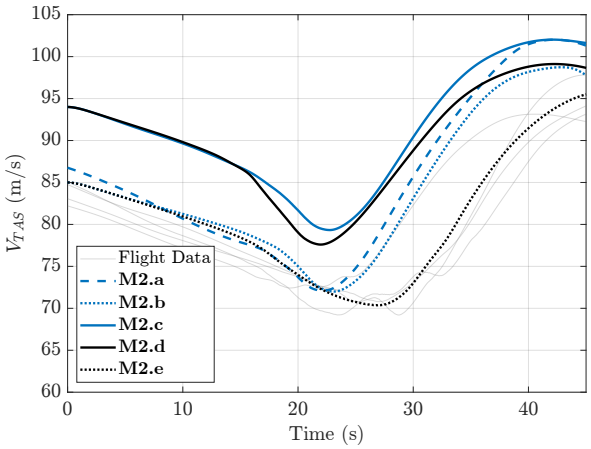

(b) Airspeed corresponding to the 16° AoA quasi-steady stall for all models from Table 9. The M2.c and M2.d contain the mass model number 2 from the flight test.

Finally, no significant differences were observed when shifting the center-of-gravity of the mass model. However, shifting $x_{c.g.}$ aft improved stability of the trim function. Additionally, it was expected that increasing aircraft mass would result in a sluggish model dynamics, instead, it resulted in more reactiveness, especially during oscillations. In addition, the higher aircraft weight from the flight test mass model number 2 resulted in increased overall airspeed, see Figure 11b, which did not match the flight test data compared to mass model 1 or 3.

B. M1 and M2 model Comparison Test

1. Subjective Assessment

When the **M1** and **M2** models were compared directly side by side, the pilot's subjective assessment showed that **M2** had a more realistic stall onset, while **M1** performed better in the recovery phase of the stall. Starting with the approach to the target stall angle, the tendency of **M2** to resist stall was more pronounced and it had more pitch oscillations compared to **M1**, see Figure 12. In contrast, during the recovery phase, **M2** model would often lead to Pilot Induced Oscillations (PIO) when trying to keep the aircraft at a target pitch angle, whereas **M1** was more stable and controllable. Since the Cessna Citation II aircraft has both resistance to stall and no PIO during recovery, the pilot's choice for the optimal realism was a mix of both models. In addition, for both **M1** and **M2**, when comparing the model against itself, the deciding factors for model preference were control column forces, length of the stall onset and recovery. In the end, the pilot concluded that both models felt comparable to the real aircraft.

2. Model Responses

In addition to the subjective pilot feedback, further analysis was done on the collected data. An immediate observation is that the **M1** model is more consistent than **M2** in stall onset. In Figure 12 it can be seen that the recovery initiation at 16° AoA varies more with time for **M2** than for **M1**. This is possibly due to the sensitivity of the **M2** model to pilot input, causing irregular oscillations of the X_{ss} state and therefore pitching moment, which are explored more in detail in Section V.B.5. These oscillations delay the time at which the recovery AoA is reached and the number of oscillations corresponds to the length of the delay. Figure 13 shows how the stall delay of **M2** increases with a lower gradient of elevator deflection δ_e, causing more oscillations in X_{ss}. To see what causes the observed differences between the **M1** and **M2** models, the aerodynamic coefficients and Kirchhoff parameters are examined.

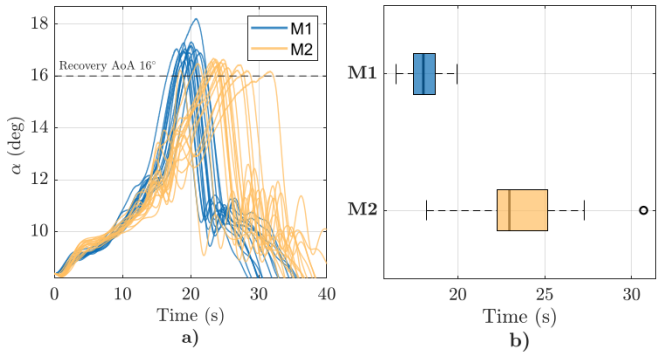

Fig. 12 a) AoA distribution of all 32 stalls. b) Box-Plot showing a time scatter of each model when recovery AoA was achieved.

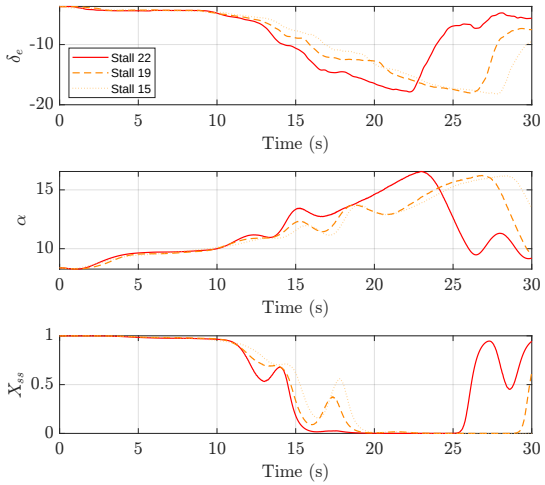

Fig. 13 Oscillation variation of M2 model outputs due to pilot input.

3. Lift Coefficient Modeling

The following analysis compares the longitudinal aerodynamic coefficients C_L, C_D and C_m for the **M1** and **M2** models using side-by-side figures that show both the total coefficient and its component contributions over the maneuver. Since the **M1** model was more consistent, only one performed run will be presented - *stall 20*. In contrast, the **M2** model responses vary more than **M1**, therefore two versions will be shown to give a more complete picture: a more stable *Stall 12* with minimal initial X_{ss} oscillation, and a more 'average' *Stall 30* containing a few stall onset and recovery oscillations. All other stalls are listed in Appendix C. This results in Figure 14 for C_L, Figure 16 for C_D and Figure 17 for C_m. To keep the legend of these figures short, each contribution to the total value is named after the coefficient related to it, but shows the product of the coefficient and its regressor. For instance, in Figure 16 of **M1**, the $C_{m_{\delta_e X}}$ plot contains entirety of '$C_{m_{\delta_e X}} \max(0.5, X)\delta_e$' from Eq.(5).

Starting with Figure 14, the C_L coefficient of the **M1** and **M2** models differs mainly by reaching $C_{L_{max}}$ at different phases of the maneuver. The $C_{L_{max}}$ of for **M1** is achieved during stall onset until flow separation AoA is reached, after which it starts to reduce. Just before reaching the recovery angle of attack, the C_L value slightly increases again due to the $C_{L_{\alpha^2}}$ contribution, the wing lift component. On the other hand, the **M2** model reaches its maximum C_L value right before the recovery. This is due to the wing lift component $C_{L_{X_w}}$ positively contributing after the $C_{L_{X_{ss}}}$ has reduced from separated flow. While X_w is already slowly separating as well, the angle of attack increase outweighs the effects of the decrease in the $C_{L_{X_w}}$ component due to X_w. In addition, the elevator deflection also contributes a non-negligible amount of lift right before the recovery, making C_L even higher in this region. These differences make the flow separation moment induce an oscillation in the C_L value in **M2** (see *stall 30* in Figure 14), as opposed to a rapid decrease seen in **M1**. This is also visible in Figure 15a. Lastly, the C_L magnitude for **M1** during leveling-out in recovery is significantly higher than for **M2**.

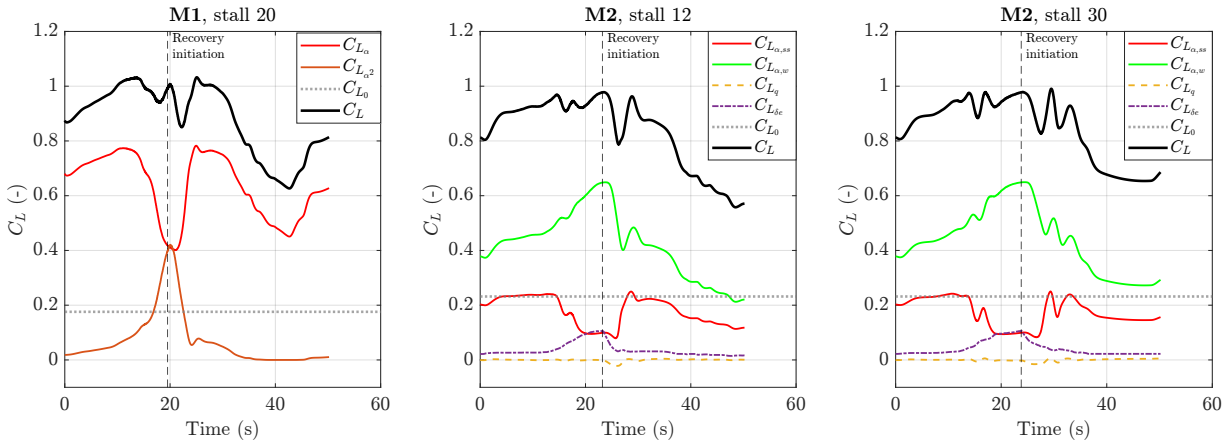

Fig. 14 C_L decomposition of M1 and M2 models.

A small detail can be observed for the $C_{L_{\alpha,ss}}$ component of the **M2** model: when the aircraft starts to recover, it unexpectedly decreases at first. This is caused by a lag in the hysteresis loop of the flow separation state X_{ss}, which is caused by a large τ_2 value, see Table 6. Looking at Figure 15b, the **M2** flow around the stall strips X_{ss} remains fully separated for angles-of-attack between 12°-14° in the recovery loop, while in the **M1** model, X has already started recovering. Combining this with Eq. (6), it can be seen that while the X_{ss} is constant, the drop in α reduces the magnitude of the $C_{L_{\alpha,ss}}$ component. Once X_{ss} starts increasing again, the total value of $C_{L_{\alpha,ss}}$ picks back up.

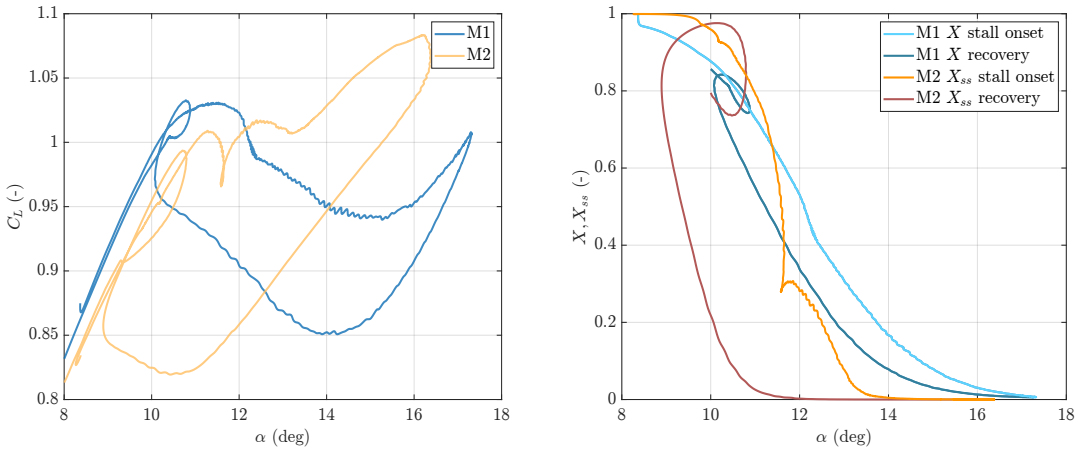

(a) Lift curve hysteresis loop. **(b) Flow separation point hysteresis loop.**

Fig. 15 Hysteresis loop comparison of M1 stall 20 and M2 stall 12.

4. Drag Coefficient Modeling

The simulated drag coefficient C_D curve is very similar between the **M1** and **M2** models throughout the entirety of the maneuver, as can be seen in Figure 16. The only noticeable differences are the individual contributions of the lift components (α or C_L) and C_{D_0}. For **M2**, the α lift contribution is replaced by a C_L regressor, and its magnitude is lower than the C_{D_α} value of **M1**. On the other hand, the C_{D_0} of **M2** has increased in value to compensate it. The C_L regressor also lacks the peak of the continuously increasing α regressor of **M1**, but this is compensated by a wing flow separation contribution $C_{D_{X_w}}$. As a result, the overall pattern of the drag coefficient is the same, and did not make a noticeable difference in full flight simulation. On the other hand, the **M2** model provides a better C_D model decomposition by separating the drag caused by flow separation around the stall strip and on the remainder of the wing.

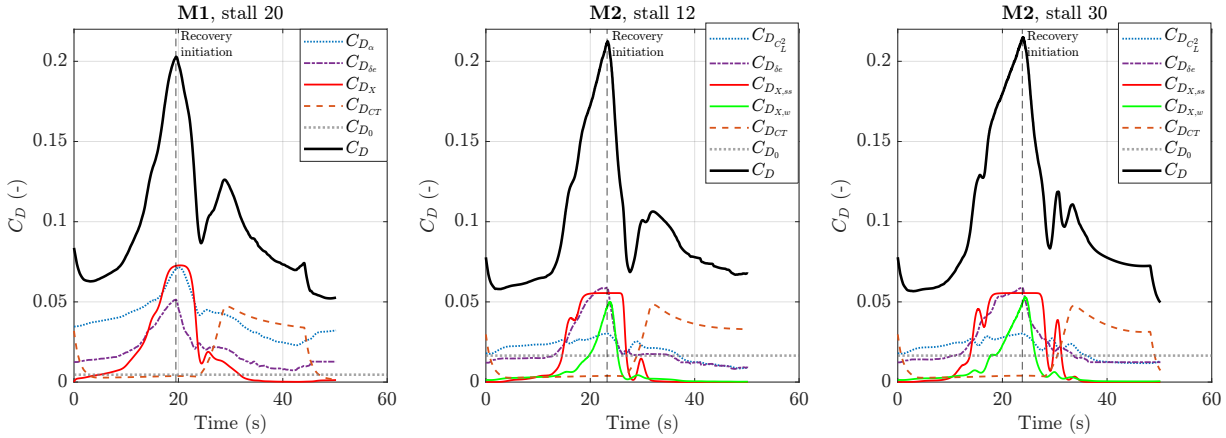

Fig. 16 C_D decomposition of M1 and M2 models .

5. Pitch Coefficient Modeling

Next, the pitch coefficient C_m is compared in Figure 17. When comparing the total C_m value, the overall curve is similar between the **M1** and **M2** models, but the oscillation peaks and their origins make a substantial difference in a piloted simulation. In stall onset, the oscillations, caused by flow separation, were often onserved between 10th second and recovery initiation mark, see Figure 17. For **M1**, the most common case was a single oscillation, whereas the **M2** model was prone to at least two oscillations. In addition, the **M2** model oscillations often have a higher magnitude, like the one depicted in *stall 30* of Figure 17. When looking at the individual terms, a general trend can be seen for both models in Figure 17 that the elevator component is creating a positive moment to increase the pitch angle, while at the same time the lift related component compensates this with a negative moment. For **M1** this lift component is governed by the angle-of-attack α, while for **M2** it is driven by C_L multiplied with the $-l_{c.p.}$ function, as defined in Eq. (6).

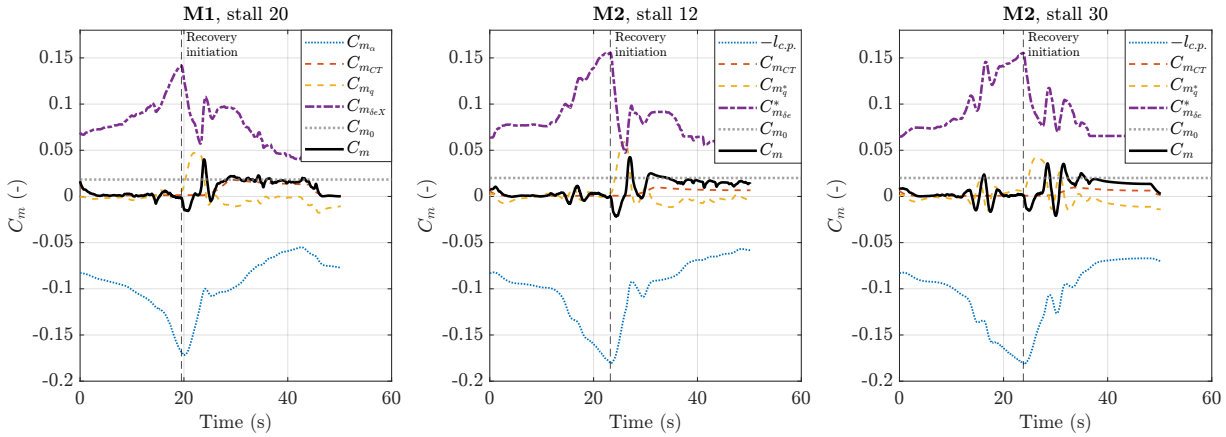

Fig. 17 C_m decomposition of M1 and M2 models .

When analyzing the oscillations, an unexpected outcome was observed in the **M1** model, where the pitch-down motion of the aircraft resisting the stall was created by the elevator component only. A more detailed visualization of this phenomena can be seen in Figure 18, where the total C_m shown in the top graph is shown aligned with its main contributions: the lift-related moment $C_{m_\alpha}\alpha$ in the second graph, the total elevator-related moment $C_{m_{\delta_e X}} \max(0.5, X)\delta_e$ (shortened to $C_{m_{\delta_e X}}\delta_e$ for simplicity) and δ_e in the third graph, and the elevator effectiveness term $C_{m_{\delta_e X}}$, flow separation X and angle of attack α plotted together in the bottom graph.

At the 'min $C_{m_{\delta_e X}}$' mark, indicated with a vertical dashed line, it can be seen that the pitch-down moment in total C_m matches exactly the moment when the elevator contribution $C_{m_{\delta_e X}}\delta_e$ experiences a dip. This dip in $C_{m_{\delta_e X}}\delta_e$ is

caused by two factors: sudden $C_{m_{\delta_e X}}$ decrease due to flow separation, and a reduced elevator deflection (δ_e) rate. Once the δ_e stagnates, the decreasing $C_{m_{\delta_e X}}$ creates a dip in the $C_{m_{\delta_e X}}\delta_e$ moment contribution. Since the $C_{m_\alpha}\alpha$ continues to decrease at a similar or lower rate, the outcome is a total pitch-down moment, i.e., $C_m < 0$.

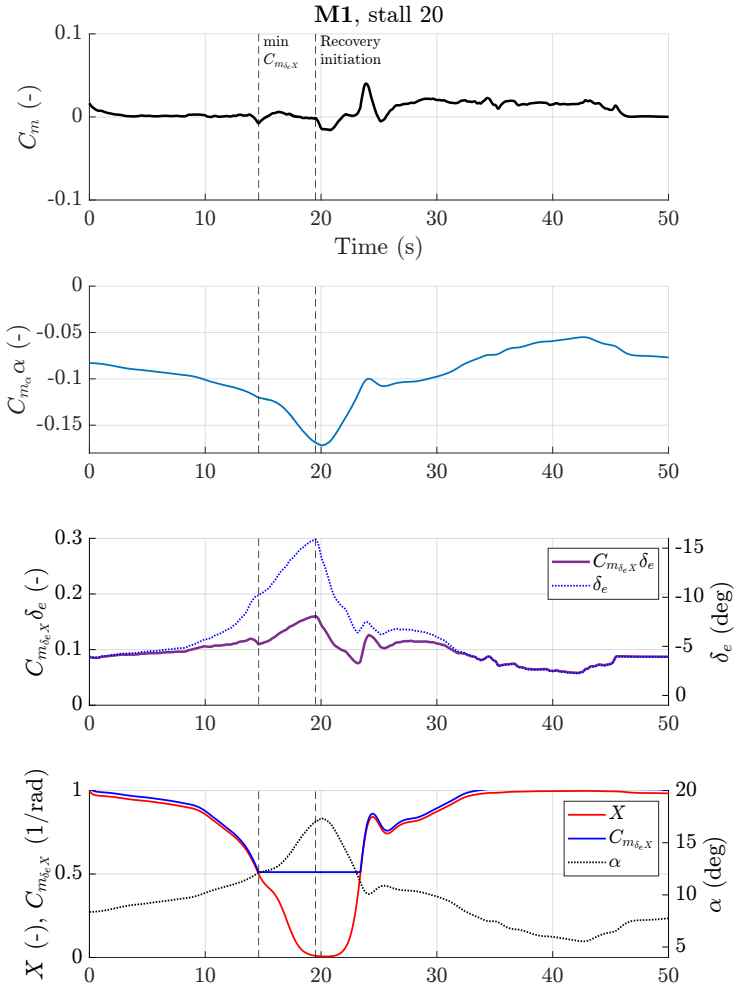

Fig. 18 A more detailed C_m component comparison of model M1.

In contrast to the previous model, the **M2** stall onset oscillations are more frequent and caused by a combination of the elevator contribution and the lift term. The details are shown in Figure 19, which has the same structure as Figure 18, but shows the **M2** model coefficients from Eq. (6). It is also important to highlight that $-l_{c.p}$ is not a coefficient, but a function of flow separation parameters, scaled by a function of C_L. Looking at the second row of Figure 19, it can be seen that starting from line 1, the negative $-l_{c.p}.C_L$ slope suddenly steepens more than for the **M1** model as the flow separates. At the same time, the elevator loses its effectiveness, creating a combined pitch-down moment at a higher magnitude than in the **M1** model.

When comparing the oscillations between stalls 12 and 30 in Figure 19, the slopes of $-l_{c.p}.C_L$ are very similar between line 1 and line 2, while the the magnitude of the elevator effectiveness differs more. There is a possibility that the more staggered elevator deflection of *stall 30* is the cause of these higher oscillation magnitudes. Once the elevator effectiveness is given a chance to reach a lower magnitude, the aircraft recovers more, making the flow separation parameter fluctuate. This fluctuation then leads to more oscillations.

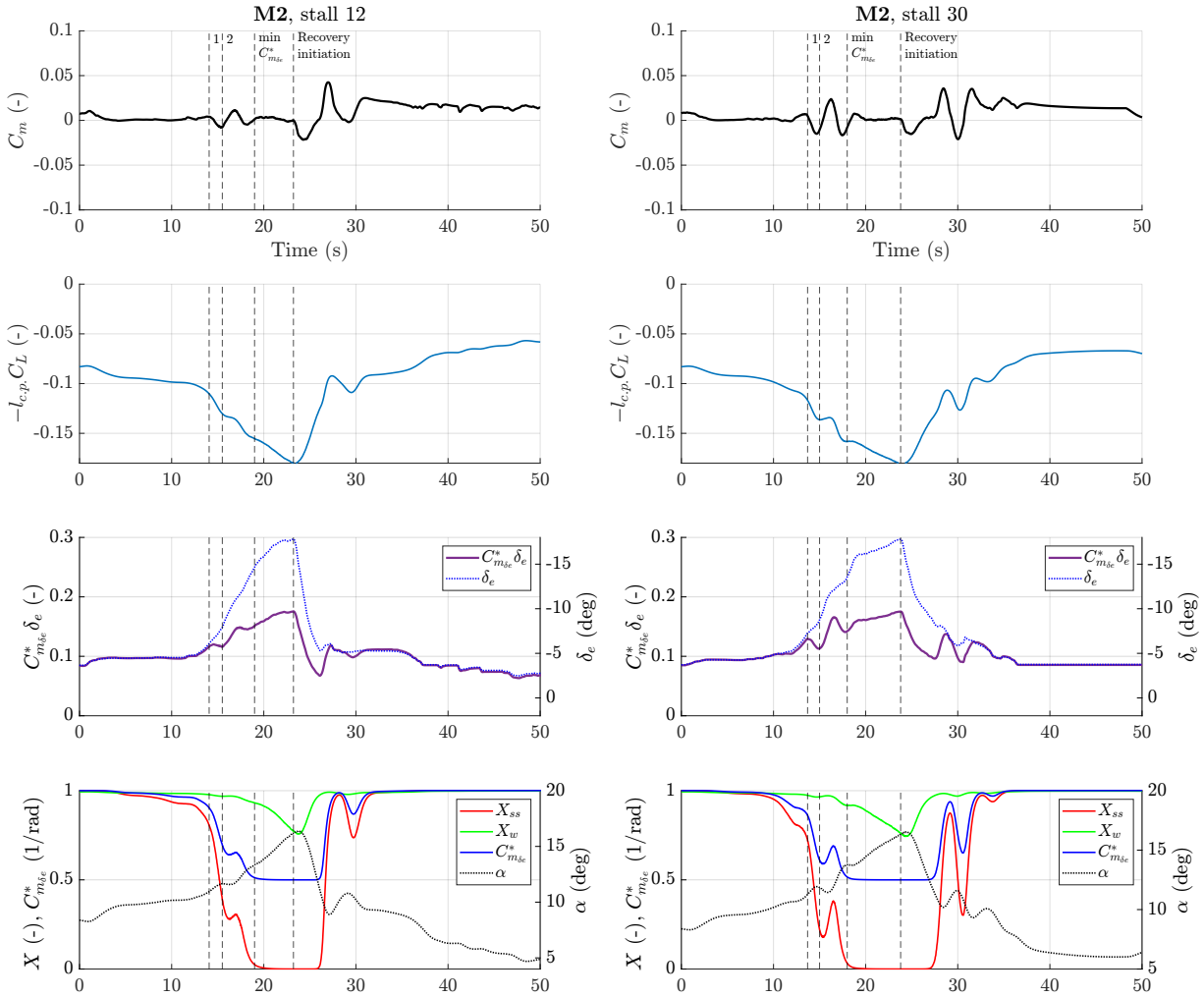

Fig. 19 A more detailed C_m component comparison of model M2.

Similarly, the pitch effects described for the stall onset contribute to oscillations observed for the **M2** model recovery. From recovery initiation onward, the pilot applies a more rapid elevator input and tries to pitch down to around -2°-0° degree pitch attitude. As the pilot tries to follow this target, more corrective deflections are applied than in the stall onset. At the same time, the elevator effectiveness changes rapidly, causing overshoots and over-corrections. Since the **M2** model state X_{ss} recovers later compared to the X state of the **M1** model, as discussed in Section V.B.3, the lag caused by $\tau_{1,ss}$ and $\tau_{2,ss}$ in recovery can also be a contributing to the delay in elevator effects, and therefore oscillations.

Lastly, Figure 18 and Figure 19 provide an explanation to the pitchover issues in **M2**, described in Section III.C.3. In both figures, the total pitch moment C_m is very close to zero between maximum flow separation and start of recovery. This is caused by the lift-related component of the moment canceling out the elevator moment. For the **M1** model, this negative lift-related moment depends on α, which, if forced, can continuously increase with more elevator deflection and therefore successfully cancel out the elevator moment. On the other hand, for model **M2** in Figure 19, the moment opposing the elevator depends on the C_L component, which, unlike α, reaches a local maximum point. Any additional elevator moment above this point will allow the aircraft to constantly pitch up. As a result, with the original **M2** elevator effectiveness, little effort was needed to overcome this opposing moment during the stall and continue pitching up.

C. Pilot-in-the-Loop Test Data and Offline Simulation Data Comparison

The **M2** data measured from the second pilot-in-the-loop test was compared to offline stall simulation data. The offline stall simulation data was generated by using a stall autopilot as created by Smets et al. [9]. In its published state,

the stall autopilot masked most of the oscillatory dynamics of the **M2** model. After gathering the piloted test data, new gains were tuned to match the autopilot behavior better with test pilot's and compare it again.

As shown in Figure 20, the first observed difference is that the angle-of-attack rate $\dot{\alpha}$ undergoes slightly larger variations during stall onset in the piloted test compared to the original stall autopilot. The original stall autopilot maintains the $\dot{\alpha}$ close to zero throughout the entire stall onset, preventing the τ_2 parameter to take an effect and therefore masking X_{ss} oscillations of the **M2** model. In the middle graph of Figure 20, it can be seen that the flow separation reproduced by the original stall autopilot does not show any oscillation in tall onset, compared to the pilot-in-the-loop test or updated autopilot output. By increasing the stall autopilot altitude reference tracking gain from 0.2 to 9, larger variations are introduced to $\dot{\alpha}$, exciting oscillations in the X_{ss} parameter as a result. In addition, the new autopilot gains improve the match of the pitch angle to the piloted test data, by removing an initial pitch decrease in stall onset of the original stall autopilot.

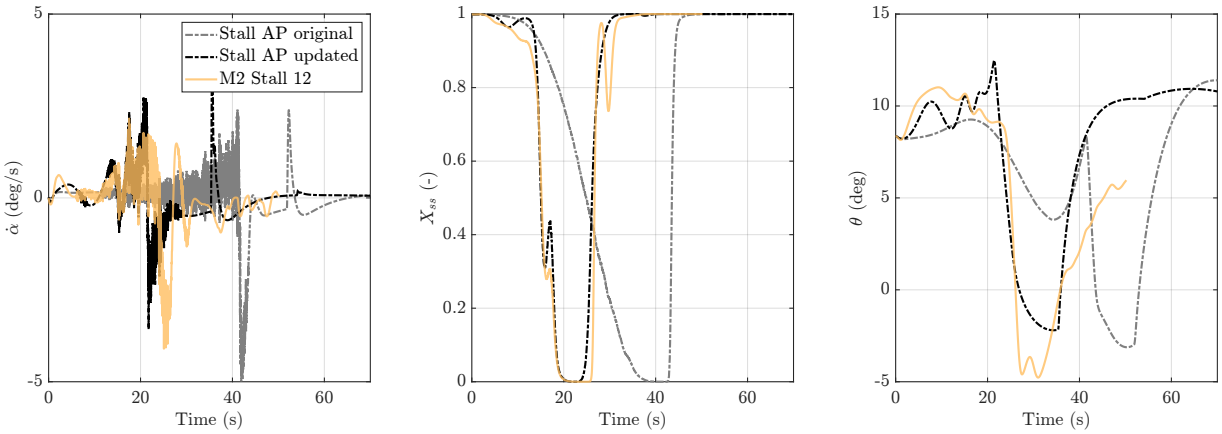

Fig. 20 Two stall autopilot versions compared to model M2 (stall 12).

D. Pilot-in-the-Loop Test Data and Flight Test Data comparison

The stall sets used in Figure 21 are taken from the 2016 flight test dataset collected by Van Ingen et al. [8] only. From the 2016 dataset, the five most consistent stalls were selected. Only one stall from "set 7" is a clean quasi-steady stall with no additional surface deflections used for model identification, such as doublets or quasi-random inputs, therefore it is used to directly compare $C_L - \alpha$ with the piloted simulation experiment data. In all sub-figures of Figure 21 this maneuver is highlighted in black, while other four sets are colored gray and are only present in aircraft state sub-figures. Note that the "set 7" maneuver reaches an AoA of only 13°, therefore it is not a good measure of the correctness of the piloted test data.

The $C_L - \alpha$ plot in the top left corner of Figure 21 shows the slope of the curve matching both **M1** and **M2**. At around 13° of AoA, the $C_{L_{\max}}$ of the flight test data is higher than any of any model, though the **M2** model comes close.

Unfortunately there is no flight test data for the maneuver hysteresis at higher angles-of-attack, and no further conclusion can be drawn. Looking at the aircraft state plots of Figure 21, both models, despite the limited availability of clean in-flight data, fall within the envelope of the flight-test measurements. Only the elevator deflection δ_e does not match: it is larger for the for the piloted simulation models due to high loss of elevator effectiveness during flow separation. This reaffirms that an alternative solution needs to be found for the control column accuracy.

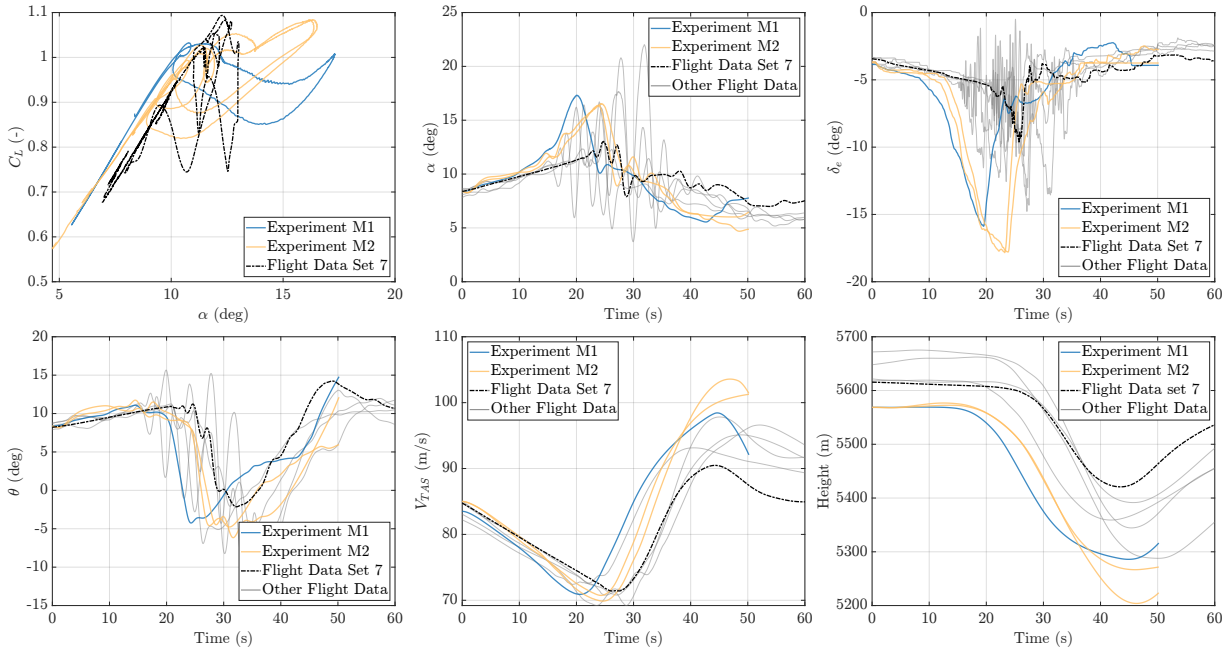

Fig. 21 Model M1 (stall 20) and M2 (stall 12 and 30) comparison against the flight test data.

VI. Discussion

Overall, from the test pilot feedback, both **M1** and **M2** simulated a symmetric quasi-steady stall in a satisfactory manner, however, both had their own drawbacks. The **M2** model in particular had a higher tendency to lead into oscillations, which were especially pronounced during the recovery. From the pilot-in-the-loop test log data analysis, several causes and recommendations were identified, which are discussed below.

A. Elevator Effectiveness and Control Forces

From the gathered pilot-in-the-loop test data and pilot feedback, the modification made to decrease the **M2** elevator effectiveness $C_{m_{\delta e}}$ was, in hindsight, a misleading choice. In Section III.C.3 it was explained that the goal of applying this change was to fix the pitching moment performance at high AoA and provide a more realistic control column force to the pilot. While initially this seemed to be the best choice when comparing the original and the modified elevator effectiveness, the downsides of this modification were revealed in later tests. Two main drawbacks were identified: increased oscillations during the recovery phase of a stall maneuver and unrealistic elevator deflections.

The most noticeable issue was severe oscillations during recovery phase, where the pilot pitches the nose down and follows an attitude target of $\theta \approx 0$. During this maneuver, X_{ss} transitions from full flow separation to full attachment and at the same time the elevator effectiveness goes from the lowest value to its maximum. As this happens, the initial pilot deflection suddenly causes the aircraft to overshoot the pitch target, requiring corrections that result in more overshoots. The reduction in elevator effectiveness increased the lowest-to-highest range, amplifying overshoots and aggravating the oscillations.

A second downside was an unrealistically high elevator deflection magnitude which was required to reach the 16° AoA recovery angle. While this provided a good control column force that matches what pilot experiences in real flight, the resulting elevator deflection value was close to the limits of the Cessna Citation II elevator range. Such high elevator deflection introduced offsets in C_L, C_D and C_m values which could significantly affect the stall model fidelity.

In addition to these drawbacks, the pilot-in-the-loop test data analysis showed that stall onset oscillations were caused by a combination of elevator effectiveness reduction and fluctuations in lift-induced moment coefficient. Due to this partial dependence on the elevator input provided by the pilot, the stall onset of the **M2** model varied on each run, sometimes leading to unwanted oscillations. In the correlation matrix from research by Herbold [13], the elevator effectiveness reduction parameter was found to have a high negative correlation to lift parameters responsible for nose-down moments. This means that eliminating the elevator effect tied to flow separation would reduce the oscillation

dependency on pilot input, while still maintaining the flow separation induced moments.

On the other hand, the **M1** model did not produce such oscillations, despite having similar reduction in elevator effectiveness as the modified version of **M2** model. Unlike the **M2** model modification, the 50% elevator effectiveness reduction during flow separation in the **M1** model was not arbitrary, but resulted from orthogonal model structure selection and identification by Van Ingen et al. [8]. Furthermore, during the 16° AoA stall maneuver, the flow separation parameter X of the **M1** model behaved similarly to X_{ss} of the **M2** model. Nevertheless, the **M1** model was more stable and did not contain as large oscillations as **M2**. Therefore, the elevator effectiveness modification for the **M2** model was not a cause, but only a contributing factor to the oscillations. The oscillatory behavior likely stems from the flow separation dynamics, such as flow separation delay $\tau_{1,ss}$ or hysteresis parameter $\tau_{2,ss}$.

B. Buffet Model Implementation

In addition to the elevator effectiveness, another factor contributing to the oscillations in the recovery of the **M2** model could have been the buffet model. Pilot feedback from the first test indicated that the disappearance of buffet was used as a reliable cue to determine when to level out the aircraft. As explained in Section III.C.4, the simulated buffet start and intensity were directly tied to the flow separation parameter X. For the **M2** model, this results in a potential mismatch, as the aerodynamics are related to X_{ss} and X_w. In Figure 15b it can be seen that the flow separation state X_{ss} recovers later than X due to time constant parameter τ_2 of the **M2** model being 19 times larger than for **M1**. Thus, the buffet ends before the X_{ss} state—and hence the elevator effectiveness—has a chance to fully recover. As a result, the pilot may initiate the recovery as the elevator effectiveness was changing, leading to overshoots and potential PIO. It is therefore advised to identify a new buffet threshold for the **M2** model that depends on the X_{ss} state for future experiments that involve an active recovery from a stall.

C. Control Column Fidelity

A possible solution to reduce these issues and improve model fidelity is by implementing realistic reversible controls through control loading on the column. In this research, a passive spring loaded control column was used in the test, which provides increasing resistance with displacement, but does not react to changes in aerodynamic forces, such as variation in dynamic pressure. In contrast, the Cessna Citation II aircraft has a reversible control system, meaning all forces acting on the elevator are directly felt by the pilots. Additionally, pilots report that the buffeting can also be felt in the control column. Previous research at DLR shows that, for aircraft with reversible control system, such as the Dornier Do328, an integration between control loading and aircraft aerodynamic model was required to reach level-D simulator fidelity, while it was not required for a C160 with hydraulic controls [24–26]. Implementing control loading on the column would therefore allow to achieve fidelity of high stick-forces at a smaller elevator deflection, eliminating the need to artificially reduce elevator effectiveness and result in more realistic pilot inputs to the model.

D. τ_2 effects

It is possible that the influence of the $\tau_{2,ss}$ parameter on the stall model dynamics was greater than anticipated. In research by Van Ingen et al. [8], a sensitivity analysis of the τ_2 parameter during model identification showed only minor changes in model fit, resulting in a wide range of τ_2 values with little effect on the overall fit quality for quasi-steady stalls. In addition, Smets et al. [9] reported that variations in the τ_2 parameter produced negligible differences in stalls executed using a stall autopilot. This could have happened for two reasons. Firstly, the τ_2 magnitude change between 0.006s to 0.029s was too small compared to the $\tau_{2,ss}$ value of 0.3391, which is more than 10 times higher than the highest value of the analysis. Secondly, from findings in subsection V.C it seems that the original stall autopilot simulation did not excite the $\dot{\alpha}$ value enough compared to pilot-controlled simulation, therefore masking the effects of the $\tau_{2,ss}$ parameter.

In the experiment, the large $\tau_{2,ss}$ value likely contributed to the **M2** model's tendency to oscillate, by creating a lag effect during flow re-attachment. This effect was amplified more after introducing a higher elevator effectiveness dependency on the **M2** model, which lead to higher oscillation magnitudes than in the baseline version of **M2**, as presented in subsection V.A.

This shows the effects of $\tau_{2,ss}$ variation can be better understood experimentally in active control scenarios and therefore further investigation is required.

E. Effect of Two Flow Separation States Compared to Single Flow Separation State

The objective of the pilot-in-the loop tests was to assess the differences between one flow separation state and two flow separation states in stall modeling, but in practice, it was not possible to completely isolate and observe this effect. Since the **M1** pitch model depends on angle-of-attack, it does not include pitch moment variations due to changes in $C_L(X_{ss}, X_w, \ldots)$ that are present in the **M2** model. In addition, other flow separation effects, such as elevator effectiveness, couple together with the mentioned aerodynamic moments, making it difficult isolate and observe the differences in piloted simulation. Therefore, to better assess the separation effects, the aerodynamic contribution to pitch needs to be re-identified to contain similar regressor terms.

Despite this limitation, retaining two flow separation states is considered necessary from a modeling perspective, as it provides a clear physical separation of aerodynamic effects that cannot be captured using a single flow separation state. As discussed in Section V.B.4, having two flow separation states provides a better drag model structure by separating the drag caused by wing flow separation from the lift effects (C_L or α). Furthermore, it has been verified by tufted flight tests that the Cessna Citation II stall strip causes a distinct local flow separation before the full wing stall [14].

Lastly, having split flow separations states for wing and stall-strip can assist in further six-degree-of-freedom stall model development. One of the functions of the stall-strip is to control the wing roll moment by creating symmetric flow separation on both wings [17]. As a result, the wing roll typically occurs deeper in the stall, when one wing loses more lift than the other one. In addition, these wing roll moments can also be caused by sideslip angle creating asymmetry in aircraft wing dihedral effect. By having a dedicated wing flow separation state, the roll and sideslip stall effects can be more easily modeled.

F. Future Steps and Experiments

A next step in improving the baseline **M2** model is the implementation of a reversible control model for force feedback on the control column. This would improve model fidelity both in terms of cockpit similarity and buffet cue perspective, while also providing more realistic pilot control inputs to the aerodynamic model. The reversible control effect on the model should be evaluated in full flight simulation using a baseline **M2** model, with pitch damping modifications if required.

In addition, the aerodynamic model requires re-identification to better match the expected values of pitch damping C_{m_q}, zero-lift pitching moment C_{m_0} and flow separation time constants $\tau_{1,ss}$ and $\tau_{2,ss}$. By incorporating the visual tuft data [14] for flow separation parameter and C_L model predictions, the time constant predictions can be improved. It is especially important, since parameters of C_D and C_m models are directly affected by flow separation and C_L prediction results. In addition, more dynamic stall data might also improve the quality of the model fit. Once the re-identified aerodynamic model is integrated with the control loading system, the stall model needs to be tested by multiple pilots to assess its fidelity.

Finally, for future JND experiments of the improved longitudinal **M2** model, the sensitivity of stall-strip separation parameter X_{ss} should be tested. In addition to previously assessed τ_1 and a_1 parameters, variations in τ_2 may also provide further insights if full recovery is performed during the experiment. On the other hand, the wing separation X_w parameters may not be as relevant for the JND experiments of the longitudinal **M2** model. Because the X_w is a more steady state compared to X_{ss}, its effects are unlikely to become apparent until very high angles-of-attack. At these angles, the aircraft is more prone to asymmetric wing roll-off moments and thus a strictly longitudinal model does not provide realism in this region. Therefore the JND assessment of X_w parameters may not be relevant for a longitudinal **M2** model.

VII. Conclusion

The main objective of this research was to implement the two-flow-separation-state model **M2** developed by Herbold et al. [13] in full flight simulation and compare it in terms of model fidelity to the already tested one-flow-separation-state **M1** model by Van Ingen et al. [8]. To evaluate this, two active pilot-in-the-loop tests were performed by a test pilot in the SIMONA Research Simulator: first a modification test to assess the readiness of the **M2** model, and then the main comparison test, comparing the **M2** model to **M1**. Before the main comparison test, the **M2** model was modified to improve pitch moment characteristics, namely damping, trim and control effectiveness. While both models demonstrated satisfactory performance, clear differences were observed. The **M2** model induced more pitch oscillations than **M1** both in stall onset and recovery. While this improved the stall onset fidelity, the recovery often lead to severe oscillations resembling PIO that are not characteristic to the Cessna Citation II. Subjectively, the test pilot preference was for the **M2** model for the stall onset and the **M1** model for recovery performance. Furthermore,

the tests revealed that the importance of force feedback on the control column for stall simulation was higher than initially anticipated and strongly affects simulator assessments of model fidelity. This was further confirmed in the pilot-in-the-loop test data analysis, which showed that recreating more realistic stick forces by artificially reducing elevator effectiveness in stall may have contributed to the **M2** oscillations. Furthermore, the $\tau_{2,ss}$ parameter, C_L and buffet model were identified as important contributors to pitch oscillations and their interactions need to be further investigated to further improve the stall model fidelity. In the end, it was not possible to fully isolate the differences of one flow separation state against two, due to pitch model differences between **M1** and **M2**. However, the benefits of two-state flow separation was observed in C_D model structure as well as in further expansion to asymmetric stall modeling.

Acknowledgments

The author would like to express her gratitude to the test pilot who volunteered to participate in the experiment at the SIMONA Research Simulator, as well as to the academic staff, daily supervisors, aircraft technicians and members of the stall task force for their guidance, insights, and support throughout the academic project.

References

[1] Boeing Commercial Airplanes, "Statistical Summary of Commercial Jet Airplane Accidents Worldwide Operations 1959–2023," Tech. rep., Boeing, 8 2024. URL `https://www.boeing.com/content/dam/boeing/boeingdotcom/company/about_bca/pdf/statsum.pdf`.

[2] International Air Transport Association, "Loss of Control In-Flight Accident Analysis Report, 2019 edition," Guidance material and best practices, Montreal–Geneva, 2019. URL `https://www.iata.org/contentassets/b6eb2adc248c484192101edd1ed36015/loc-i_2019.pdf`.

[3] Advani, S. K., Schroeder, J. A., and Burks, B., "What Really Can Be Done in Simulation to Improve Upset Training?" *AIAA Modeling and Simulation Technologies Conference*, American Institute of Aeronautics and Astronautics Inc. (AIAA), 2012. https://doi.org/10.2514/6.2010-7791.

[4] Jacobson, S., "Aircraft Loss of Control Causal Factors and Mitigation Challenges," *AIAA Guidance, Navigation, and Control Conference*, 2010. https://doi.org/10.2514/6.2010-8007.

[5] Advani, S. K., and Schroeder, J. A., "Global Implementation of Upset Prevention & Recovery Training," *AIAA Modeling and Simulation Technologies Conference*, American Institute of Aeronautics and Astronautics Inc. (AIAA), 2016. https://doi.org/10.2514/6.2016-1430.

[6] Schroeder, A. J., Burki-Cohen, J. S., Shikany, D., Gingras, D. R., and Desrochers, P. P., "An Evaluation of Several Stall Models for Commercial Transport Training," *AIAA Modeling and Simulation Technologies Conference*, American Institute of Aeronautics and Astronautics Inc. (AIAA), 2014. https://doi.org/10.2514/6.2014-1002.

[7] Grant, P. R., Moszczynski, G. J., and Schroeder, J. A., "Post-stall Flight Model Fidelity Effects on Full Stall Recovery Training," *AIAA Modeling and Simulation Technologies Conference*, American Institute of Aeronautics and Astronautics Inc. (AIAA), 2018. https://doi.org/10.2514/6.2018-2937.

[8] Van Ingen, J. B., de Visser, C. C., and Pool, D. M., "Stall Model Identification of a Cessna Citation II from Flight Test Data Using Orthogonal Model Structure Selection," *AIAA SCITECH 2021 Forum*, American Institute of Aeronautics and Astronautics Inc. (AIAA), 2021, pp. 11–15 & 19–21. https://doi.org/10.2514/6.2021-1725.

[9] Smets, S., de Visser, C., and Pool, D., "Subjective Noticeability of Variations in Quasi-Steady Aerodynamic Stall Dynamics," *AIAA SCITECH 2019 Forum*, American Institute of Aeronautics and Astronautics Inc. (AIAA), 2019. https://doi.org/10.2514/6.2019-1485.

[10] Bootsma, S., de Visser, C. C., and Pool, D., "Comparing Active and Passive Just Noticeable Difference Thresholds for Stall Abruptness in Symmetric Stall," *AIAA SCITECH 2025 Forum*, American Institute of Aeronautics and Astronautics Inc. (AIAA), 2025. https://doi.org/10.2514/6.2025-0975.

[11] Brill, P. A. R., de Visser, C. C., and Pool, D. M., "Improved Kirchhoff Stall Model Parameter Estimation Accuracy Through Optimal Data Slicing," *AIAA SCITECH 2025 Forum*, American Institute of Aeronautics and Astronautics Inc. (AIAA), 2025. https://doi.org/10.2514/6.2025-1248.

[12] Van Wezel, C., de Visser, C. C., and Pool, D. M., "Identifying Dynamic Stall Effects on the Pitching Moment From Cessna Citation II Flight Test Data," *AIAA SCITECH 2025 Forum*, American Institute of Aeronautics and Astronautics Inc. (AIAA), 2025. https://doi.org/10.2514/6.2025-1252.

[13] Herbold, J. A., "Improved Longitudinal Stall Modeling with Separable Nonlinear Least Squares and Dynamic Stall Maneuvers," Master's thesis, Delft, Zuid-Holland, 2629HS, the Netherlands, January 2025.

[14] Deligios, P., "Modeling Flow Separation from Quantified Tuft Motions," Master's thesis, Delft, Zuid-Holland, 2629HS, the Netherlands, November 2025.

[15] TU Delft, "Laboratory Aircraft," https://www.tudelft.nl/lr/organisatie/afdelingen/control-and-operations/facilities/laboratory-aircraft, 2025. Accessed: 2025-07-13.

[16] Lachmann, G. V., "Aerodynamic and Structural Features of Tapered Wings," *The Journal of the Royal Aeronautical Society*, Vol. 41, No. 315, 1937, p. 161–237. https://doi.org/10.1017/S0368393100104420.

[17] Hinson, M., "Devices for Improvement of Controllability at Stall," SAE Technical Paper 830723, 1983. https://doi.org/10.4271/830723.

[18] Obert, E., *Aerodynamic Design of Transport Aircraft*, IOS Press, Amsterdam, The Netherlands, 2009. URL http://ebookcentral.proquest.com/lib/delft/detail.action?docID=448784.

[19] Goman, N., and Khrabrov, A., "State-Space Representation of Aerodynamic Characteristics of an Aircraft at High Angles of Attack," *Astrodynamics Conference*, AIAA, 1992. https://doi.org/10.2514/6.1992-4651.

[20] Fischenberg, D., "Identification of an unsteady aerodynamic stall model from flight test data," *20th Atmospheric Flight Mechanics Conference*, American Institute of Aeronautics and Astronautics Inc. (AIAA), 1995. https://doi.org/10.2514/6.1995-3438.

[21] Van Horssen, L., de Visser, C. C., and Pool, D. M., "Aerodynamic Stall and Buffet Modeling for the Cessna Citation II Based on Flight Test Data," *2018 AIAA Modeling and Simulation Technologies Conference*, American Institute of Aeronautics and Astronautics, 2018. https://doi.org/10.2514/6.2018-1167.

[22] Stroosma, O., van Paassen, M. M., and Mulder, M., "Using the SIMONA Research Simulator for Human-Machine Interaction Research," *AIAA Modeling and Simulation Technologies Conference and Exhibit*, Austin, Texas, 2003. https://doi.org/10.2514/6.2003-5525.

[23] Imbrechts, A., de Visser, C. C., and Pool, D., "Just Noticeable Differences for Variations in Quasi-Steady Stall Buffet Model Parameters," *AIAA SCITECH 2022 Forum*, American Institute of Aeronautics and Astronautics Inc. (AIAA), 2022. https://doi.org/10.2514/6.2022-0510.

[24] Weiss, S., Gockel, W., Moennich, W., and Rohlf, D., "Identification of Dornier-328 reversible flight control systems," *AIAA Modeling and Simulation Technologies Conference and Exhibit*, AIAA, Boston, United States, 1998. https://doi.org/10.2514/6.1998-4163.

[25] Mönnich, W., and Jategaonkar, R. V., "Data Base Development for Level D Simulators - Lessons Learned," *System Identification for Integrated Aircraft Development and Flight Testing*, RTO Systems Concepts and Integration Panel (SCI) Symposium, Madrid, Spain, 1999, pp. 14–1–14–8.

[26] Jategaonkar, R. V., and Möennich, W., "Identification of DO-328 aerodynamic database for a Level D flight simulator," *AIAA Modeling and Simulation Technologies Conference and Exhibit*, AIAA, New Orleans, LA , United States, 1997. https://doi.org/10.2514/6.1997-3729.

A. Mass and Balance Chart of Cessna Citation II

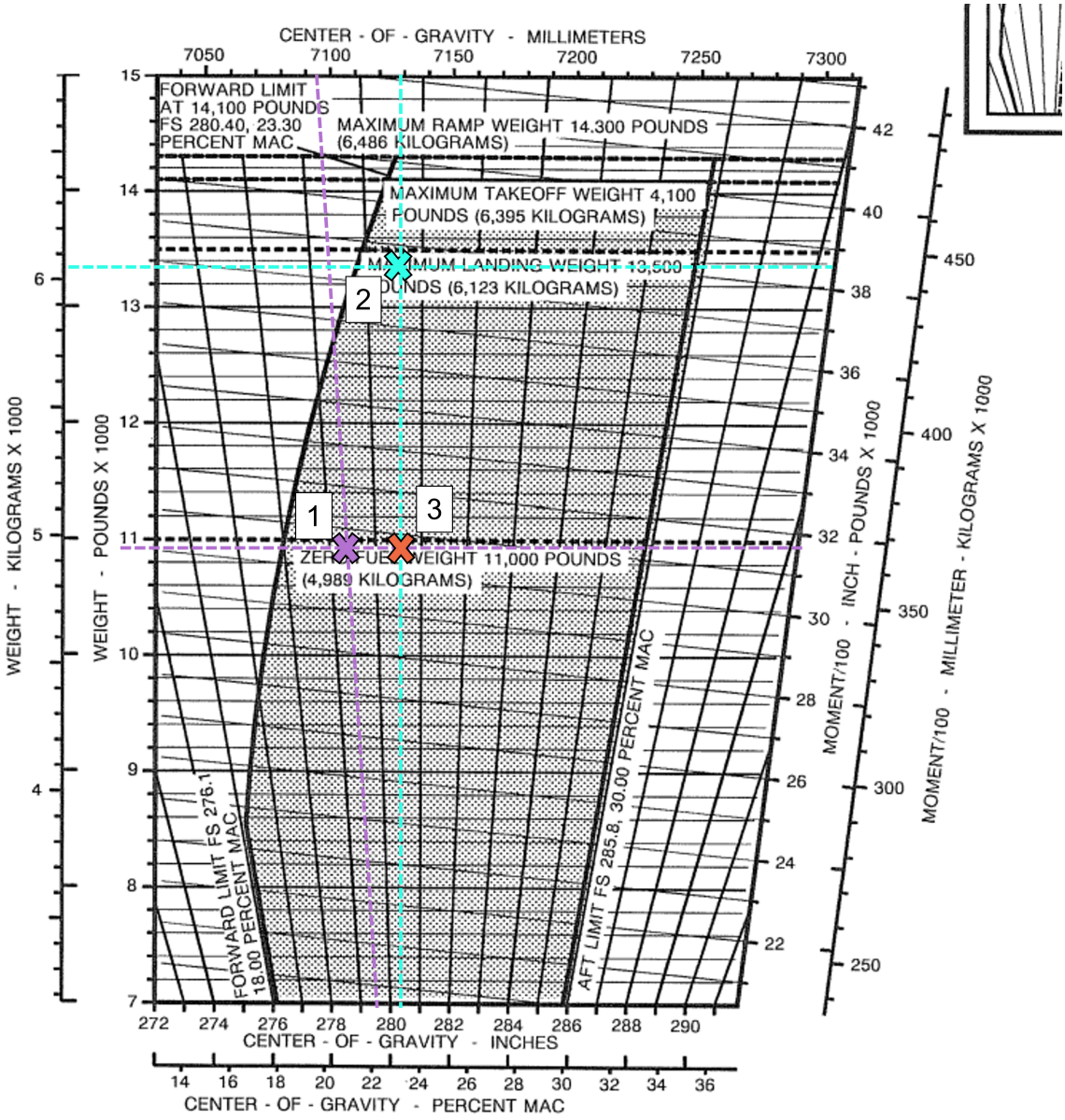

Fig. 22 The mass and balance chart of Cessna Citation II with highlighted model options from Table 7. The chart is obtained from [13].

B. Modification Pilot-in-the-Loop test results

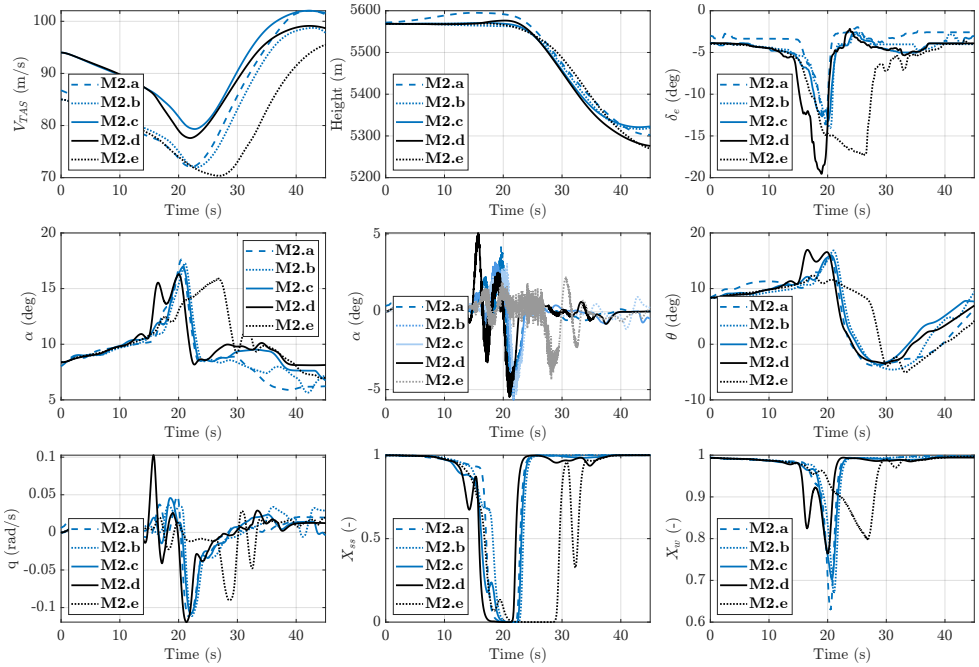

Fig. 23 Modification test state outputs for 16° AoA quasi-steady stalls.

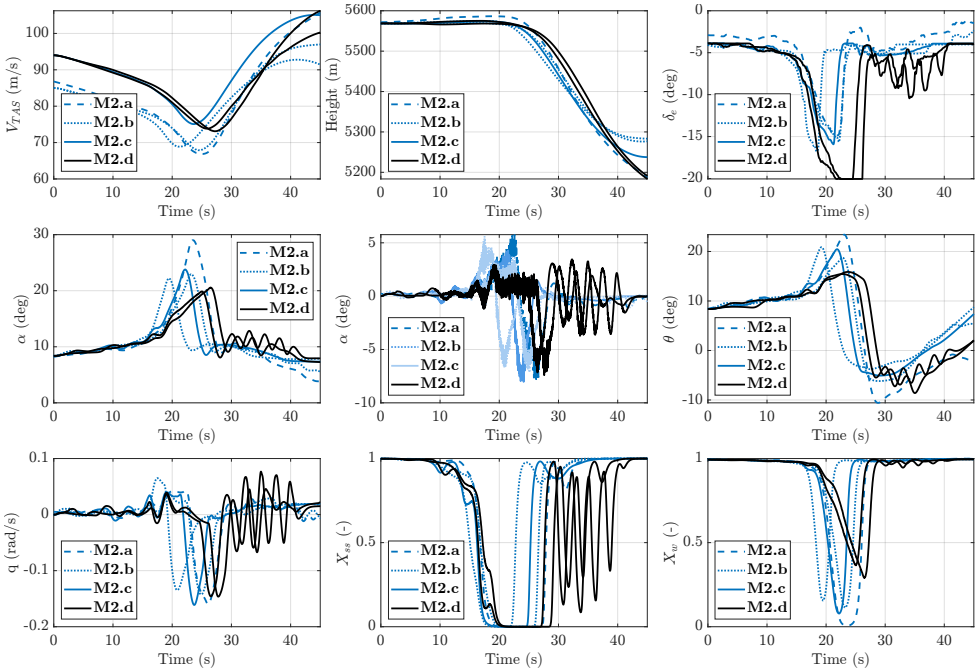

Fig. 24 Modification test state outputs for 20° AoA quasi-steady stalls.

C. Comparison Pilot-in-the-Loop test results

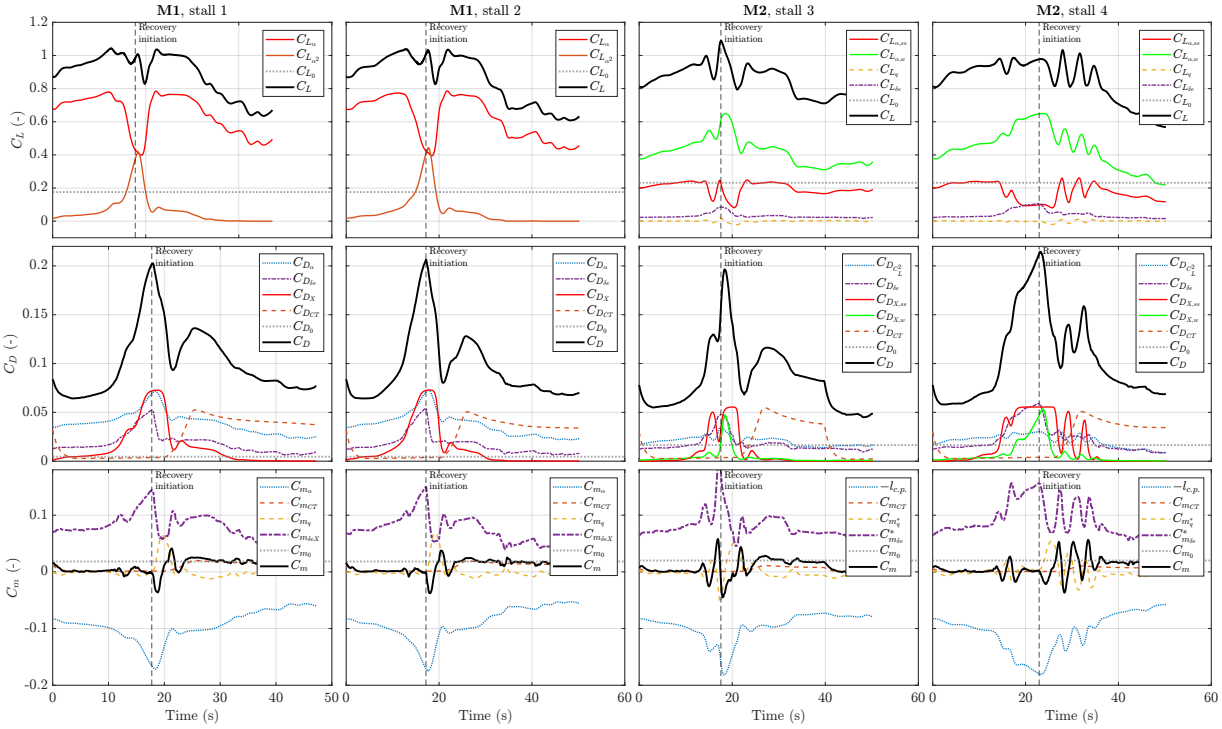

Fig. 25 Aerodynamic Coefficients and their components of stall 1, stall 2, stall 3, and stall 4.

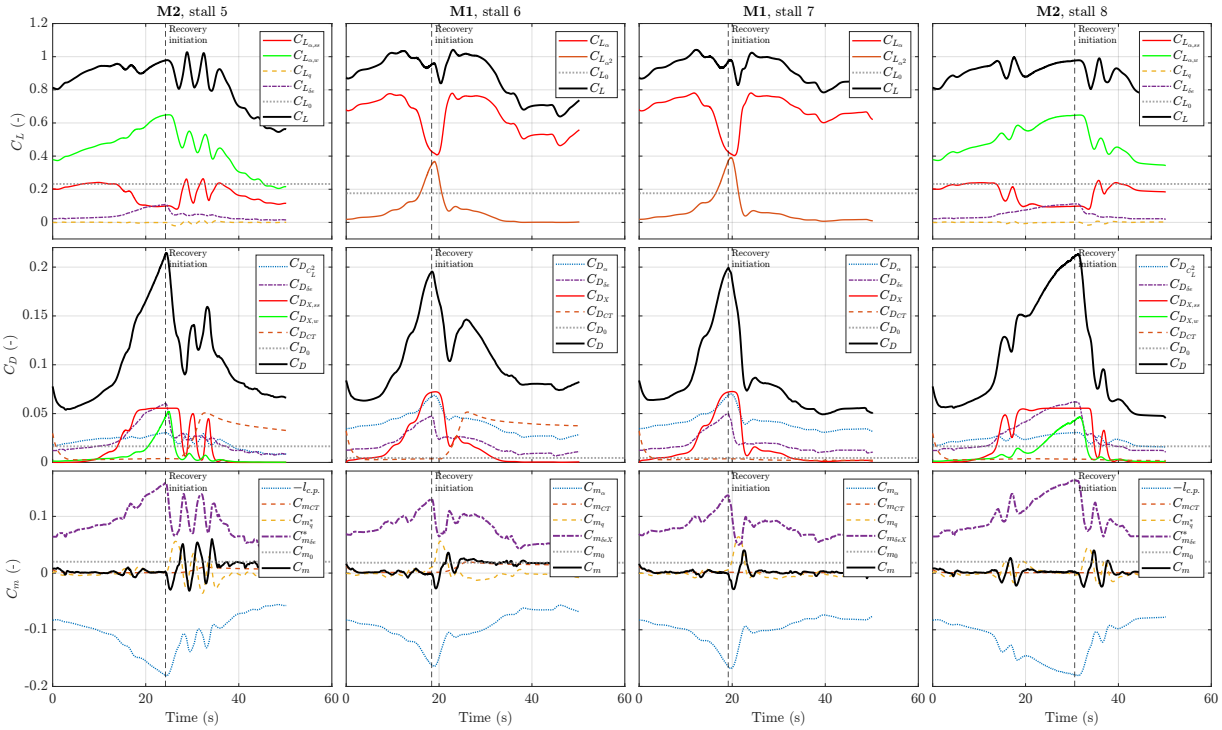

Fig. 26 Aerodynamic Coefficients and their components of stall 5, stall 6, stall 7, and stall 8.

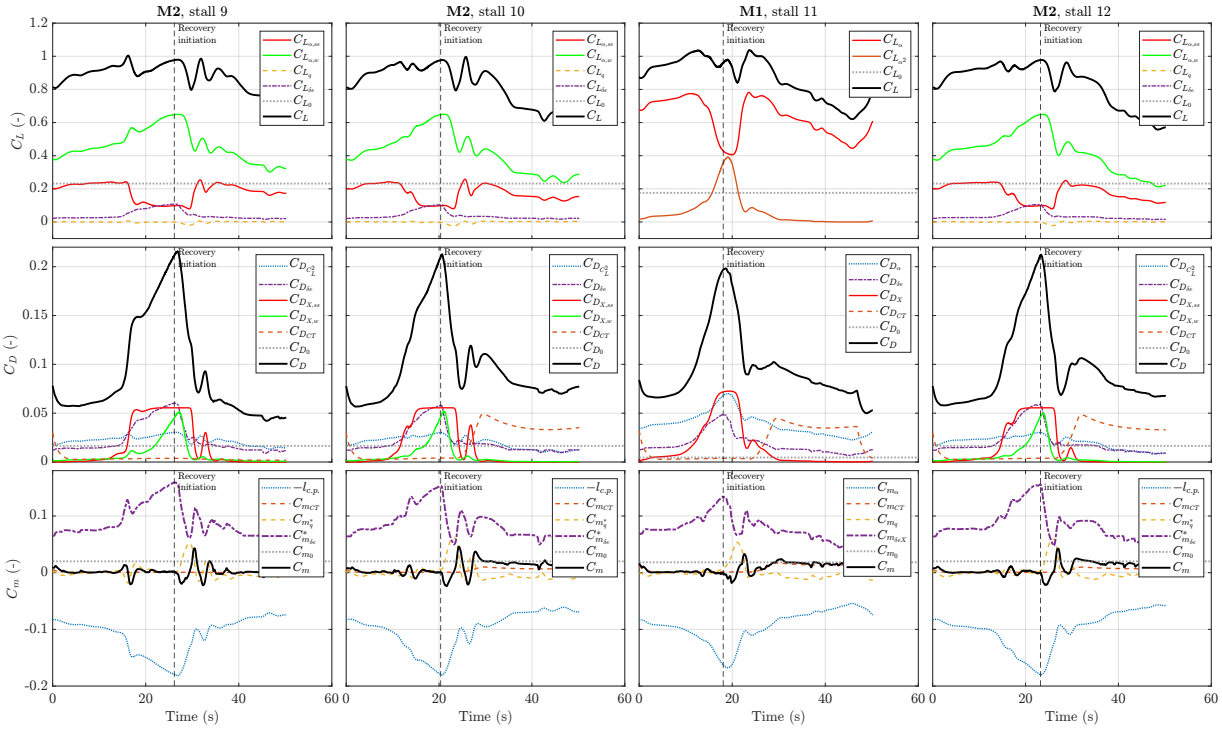

Fig. 27 Aerodynamic Coefficients and their components of stall 9, stall 10, stall 11, and stall 12.

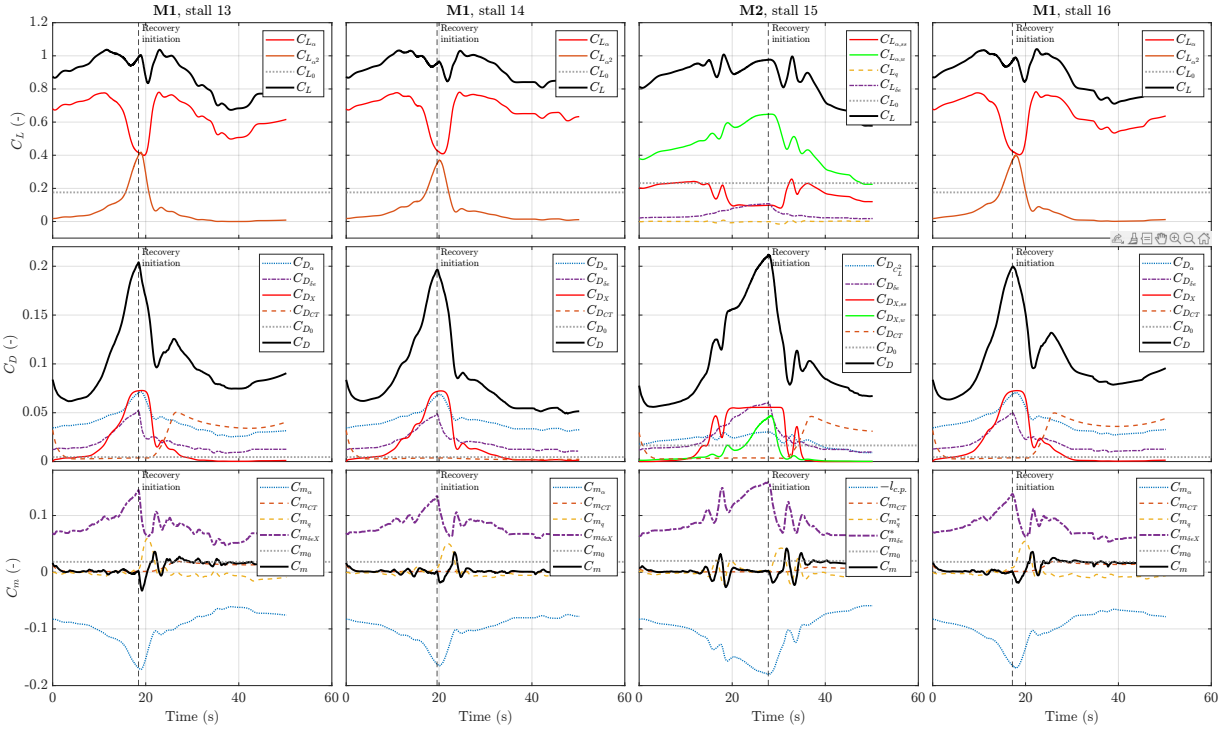

Fig. 28 Aerodynamic Coefficients and their components of stall 13, stall 14, stall 15, and stall 16.

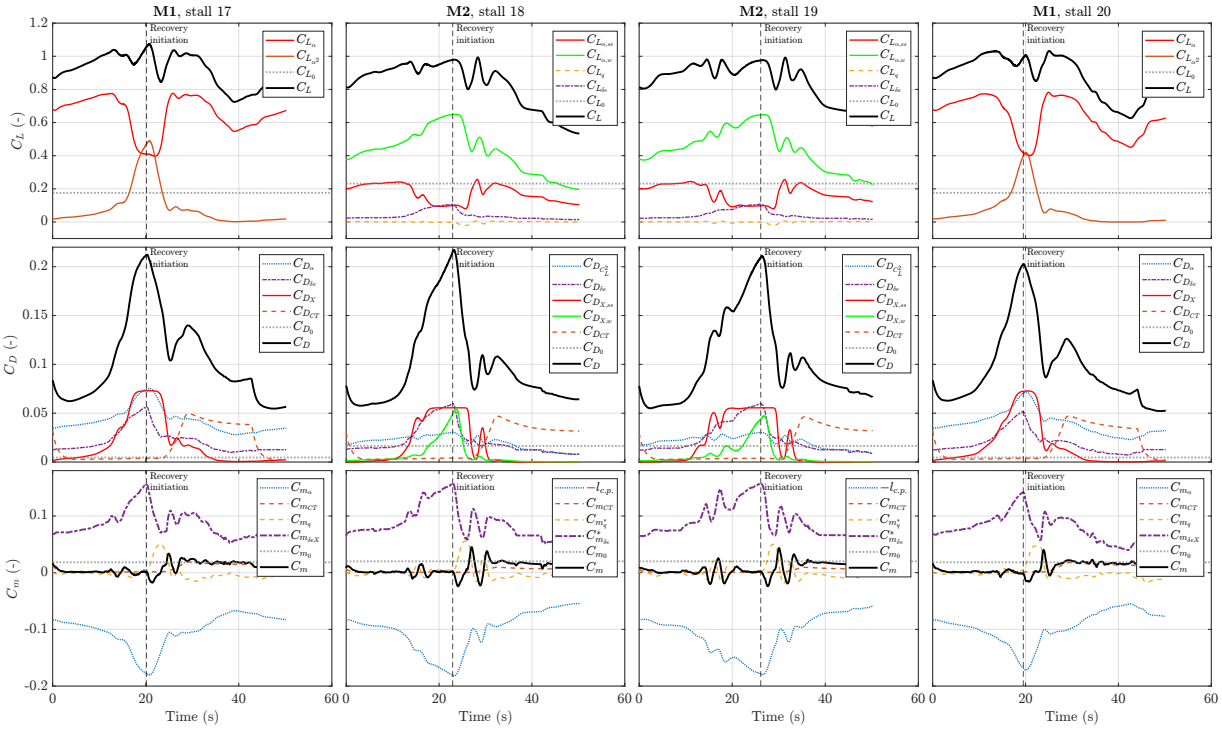

Fig. 29 Aerodynamic Coefficients and their components of stall 17, stall 18, stall 19, and stall 20.

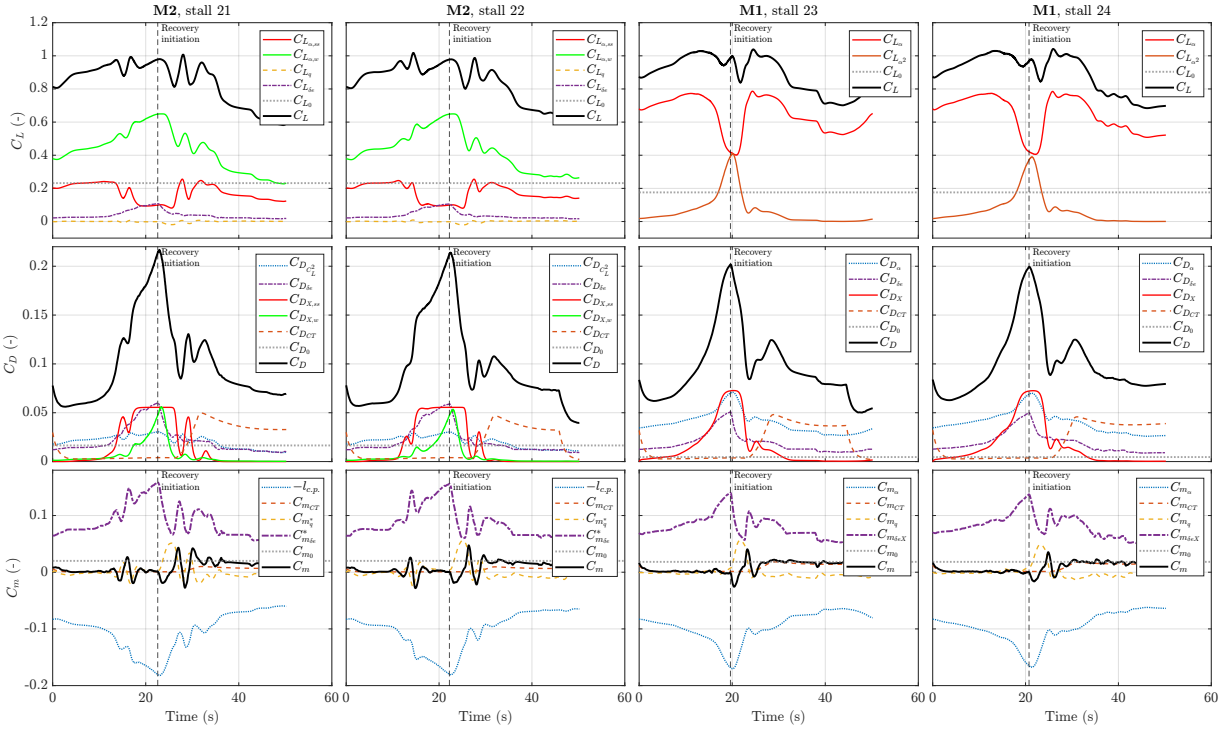

Fig. 30 Aerodynamic Coefficients and their components of stall 21, stall 22, stall 23, and stall 24.

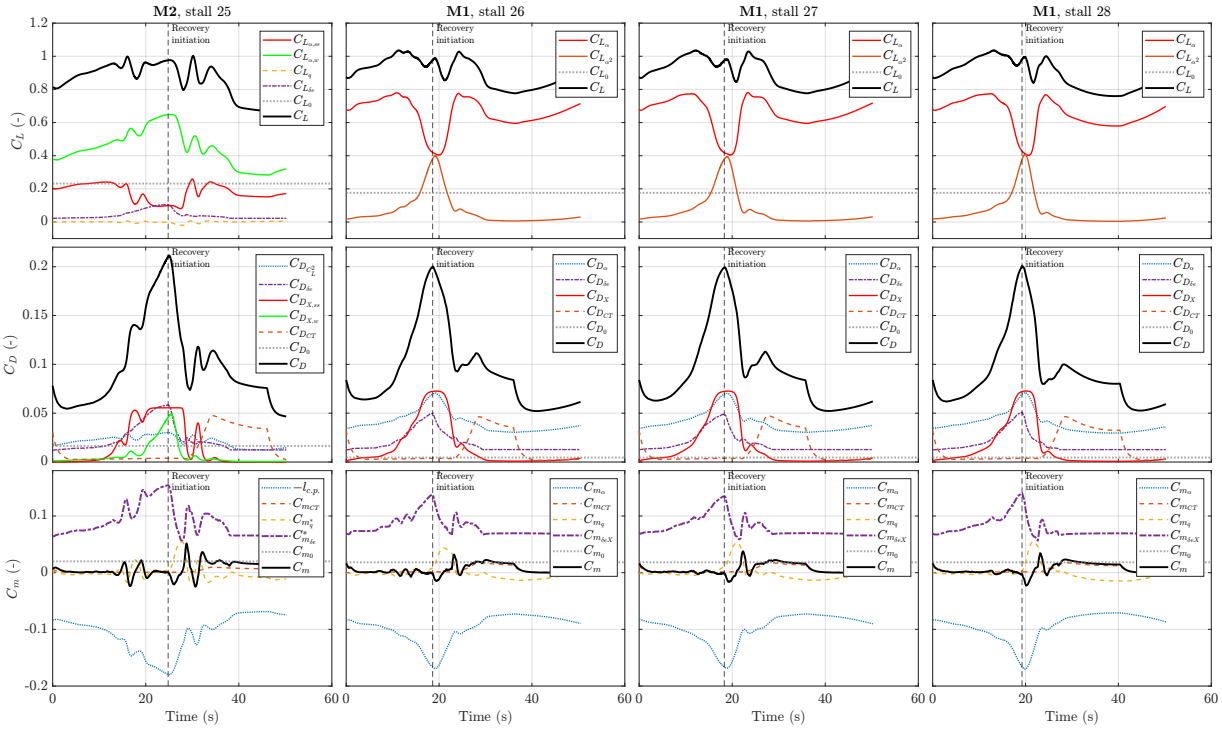

Fig. 31 Aerodynamic Coefficients and their components of stall 25, stall 26, stall 27, and stall 28.

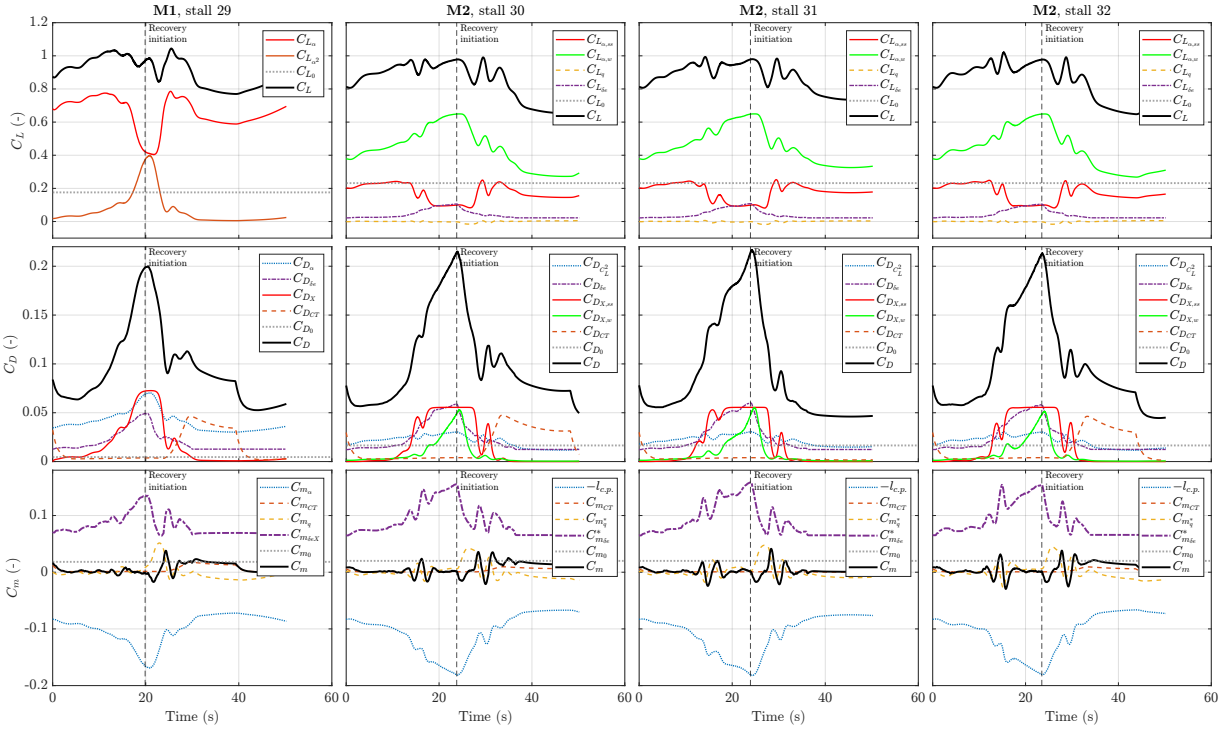

Fig. 32 Aerodynamic Coefficients and their components of stall 29, stall 30, stall 31, and stall 32.

Part III

Additional Results

6

Updated Research Questions

While implementing the **M2** model after the project proposal phase, it was revealed that the model was not suitable yet for the JND experiments. The model had issues with large oscillations in active control and difficulties in trim. In addition, some discrepancies between the identification and model simulation settings were detected, requiring a more in depth analysis of their effects. Taking into account the thesis duration, it was therefore decided to narrow down the scope of the project. This resulted to the following research objective and questions:

Research Objective

The research objective is to compare the two-state flow separation stall model **M2** [14] of the Cessna Citation II with the single-state flow separation stall model **M1** [10] by performing actively controlled quasi-steady stalls in SIMONA research simulator.

While trying trying to achieve the research objective, the following research questions will help to provide a more systematic approach. First, the measured data needs to be checked for inaccuracies. Since the model is chosen based on how well it fits the measured flight data, namely the aerodynamic coefficients, it is important that data it self is an accurate representation of the aircraft's flight. Therefore, the RQ1 is as follows:

Research Question 1

To what extent is the measured data processing done in the stall model identification is performed robustly?

Secondly, the **M2** model with its original coefficients may not be controllable when implemented into the full flight simulation for the first time. If that happens, some changes may need to be applied, therefore the RQ2 is:

Research Question 2

What changes need to be applied to the original **M2** model to implement it in full flight simulation?

One of the main known limitations in determining the pitch and drag models of the Cessna Citation II stall model lies in the correction for the thrust effects in the pitching moment data. During the flight, the entire pitching moment of the aircraft is recorded, meaning that it contains both moments caused by aerodynamics acting on an airframe and the moment caused by the engine thrust. Therefore, the moment caused by engine thrust needs to be removed from the data before identifying the aerodynamic pitching moment. Currently, the engine thrust is obtained from JT15D-1 model, however, the engine used by Cessna Citaion II is a more powerful JT15D-4, meaning that the current correction is not truly accurate. Therefore, the research question RQ3 is as follows:

Research Question 3

How large are the differences between JT15D-1 and JT15D-4 engine models and how do they affect the flight path reconstruction and model identification?

Once the engine model and the measured data is updated, a few modifications will be applied to the **M2** model. When the initial version of the **M2** model by Hebold [14] was implemented into equations of motion, it was observed the C_m had low pitch damping characteristics and produced inaccurate trim states. Therefore, it was decided to explore a few different C_m model versions with new regressors for the **M2** model. Therefore the RQ4 is as follows:

Research Question 4

What are the candidates for the **M2** stall model that have accurate pitch damping and trim characteristics?

Once the models are defined, they should be validated by running the experiment in the SIMONA Research Simulator. The goal will be to compare the performance of a few chosen **M2** models and their modifications. Then one model with the best resemblance of the Cessna citation II stall will be chosen. The chosen model will be used to answer the research question 5 and 6:

Research Question 5

How accurately can the modified and re-identified aerodynamic models of **M2** capture the stall of the Cessna Citation II compared to measured data and offline simulation? To what extent does the **M2** model need to be modified to be applicable in piloted simulation?

Research Question 6

What is the difference in the quasi-steady stall between **M1** and **M2** models in full flight simulation?

The remaining research question is additional aspect to keep in mind during research, but not to be analyzed extensively:

Research Question 7

How can the buffet model be accurately applied when two flow separation parameters are present?

7

Engine Model Evaluation in Stall Model Identification

The longitudinal models **M1** and **M2**, defined in the scientific article from Part II, contain a thrust coefficient C_T regressor term in C_m and C_D coefficients. According to results obtained by Van Ingen et al. [10], adding this term has greatly improved the model fit and it is believed that it represents an error correction for a discrepancy between the true thrust and the modeled thrust. Given this interpretation of C_T as a thrust-model compensation term, the re-identification of the **M2** model trim parameter C_{m_0} prompted an investigation into whether the corresponding $C_{m_{CT}}$ value, and therefore C_{m_o}, could be reduced.

The current look up table used in model identification comes from Pratt & Whitney JT15D-1 engine, while the PH-LAB is equipped JT15D-4. The JT15D-4 engine is around 10% more powerful than the previous engine. However, it was later discovered that the look-up table used in stall model identification did not contain an altitude correction, while the engine model used for piloted simulation did. It was therefore decided to explore alternative ways to achieve the thrust and see the effect it has on the aerodynamic data reconstruction and the aerodynamic model.

7.1. Engine Thrust Models

Three options were explored: a simple altitude correction formula applied on JT15D-1 look up table, a 3D look-up table constructed from JT15D-4 values found in the engine manual [44], and an implementation of an existing engine model used as a course material (SVV-algorithm). These resulting options were then plotted against the original engine thrust data, which can be seen later in Figure 7.2.

The first option is the altitude correction applied to the JT15D-1 look up table. The original table takes $N1$ (engine fan speed) and Mach number as inputs, however, the output values are rated for sea level only. This means that the original look-up table overestimated the value of the of the engine thrust for a given input. A common way to obtain the engine thrust at an altitude is by applying a correction factor seen in Eq.(7.1). Here, P is static pressure at an altitude, P_0 is the sea level pressure (130325 atm) and T_{LT} is look-up table thrust at sea level. For the flight test envelope altitude of around FL150-FL200 (between 4.5-6km), this results in thrust reduction of around 45% in standard atmosphere conditions.

$$T = T_{LT}\frac{P}{P_0} \tag{7.1}$$

The second option is a reconstructed 3D look-up table based on interpolated table data from the JT15D manual from Pratt and Whitney [44], which can be seen in Appendix A. These tables contain the engine thrust output data for altitudes of 0 ft, 10.000 ft and 20.000ft for Mach numbers from 0.2 to 0.5. This nearly fits the envelope of all test-flight maneuvers, only the thrust values at just bellow Mach 0.2 were rounded up to the value at 0.2 Mach. This resulted in 3D look-up table shown in Figure 7.1, which takes Flight-Level, fuel-mass-flow and Mach number as inputs.

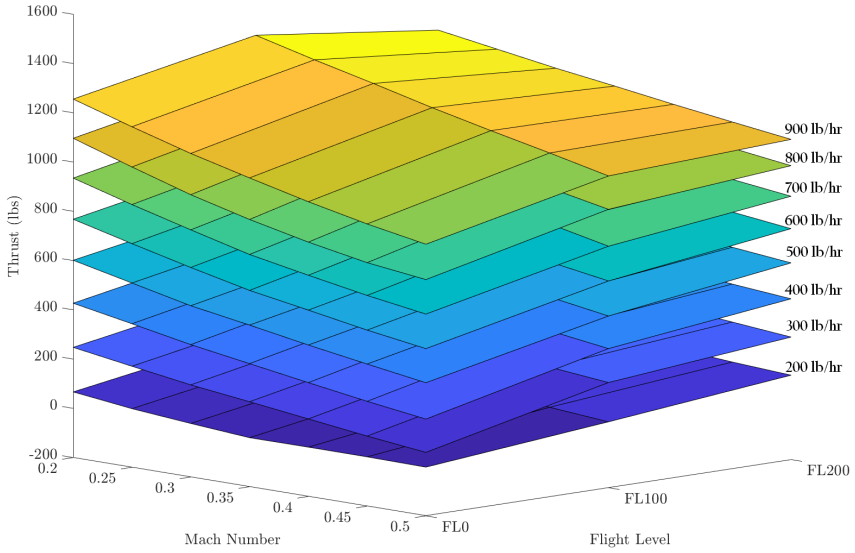

Figure 7.1: Interpolated JT15D-4 look-up table from data provided by the engine handbook [44].

The last model, SVV-algorithm, is a JT15D-4 model created at Delft University of Technology in early 1990s, based on turbomachinery equations. This function takes an altitude, fuel-mass-flow and a Mach number as inputs. One of the drawbacks of this function is that at low thrust values, the input bounds are often exceeded. As a result, missing data and glitches are present in the output. This affects the results, since the quasi-steady stall maneuver involves a very low throttle setting.

In Figure 7.2, the engine thrust output results are shown for three different maneuvers: dynamic stall, deep dynamic stall and a quasi-steady-stall. It can be seen that the SVV-algorithm and 3D look-up table outputs are in between the sea-level and corrected JT15D-1 thrust. This is expected, since JT15D-4 is more powerful than JT15D-1, but the output is already corrected for altitude effects. The overall shape, except for magnitude, is similar between all plots. Since the SVV-algorithm and the 3D look-up table depend on fuel-mass-flow input instead of $N1$, their outputs contain different thrust rates or peaks that are not present on JT15D-1 related plots. It can also be seen that the 3D look-up table output is generally higher than the SVV-algortithm, especially at a higher thrust output. Lastly, the SVV-algorithm exhibits glitches and missing data at low fuel-mass-flow settings during quasi-steady stalls due to engine inputs exceeding its envelope bounds.

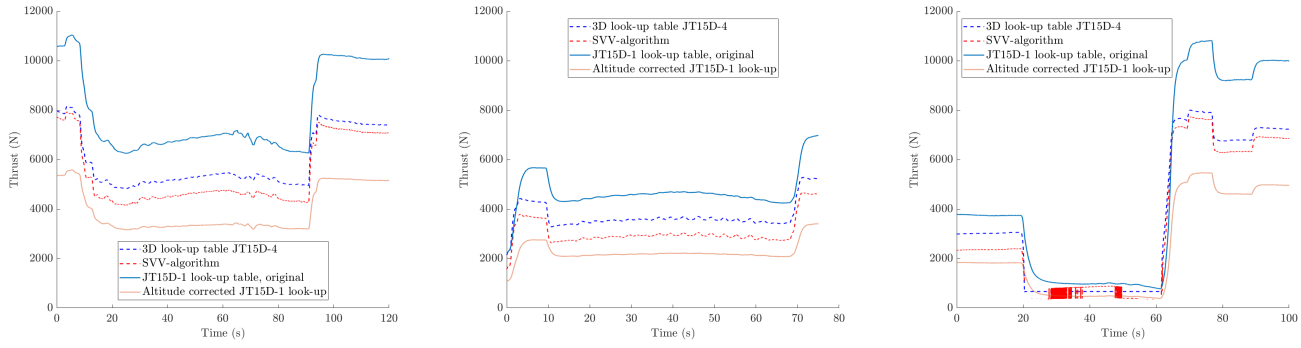

(a) Deep dynamic stall, set 002. **(b)** Dynamic stall, set 001. **(c)** Quasi-steady stall, set 012.

Figure 7.2: Engine thrust model outputs for deep dynamic, dynamic, and quasi-steady stalls.

The thrust output difference between 3D look-up table and SVV-algorithm can be displayed in the same manner as the thrust output tables from the JT15D handbook [44], shown in Appendix A. Figure 7.3,

Figure 7.4, and Figure 7.5 show that for each fuel-mass flow value, the 3D look-up table thrust is slightly higher than SVV-algorithm and the error is more prominent at lower fuel-mass-flow rates. However, the overall error decreases with increasing altitude. This means that the most consistent predictions of these methods are at high thrust values and high altitudes.

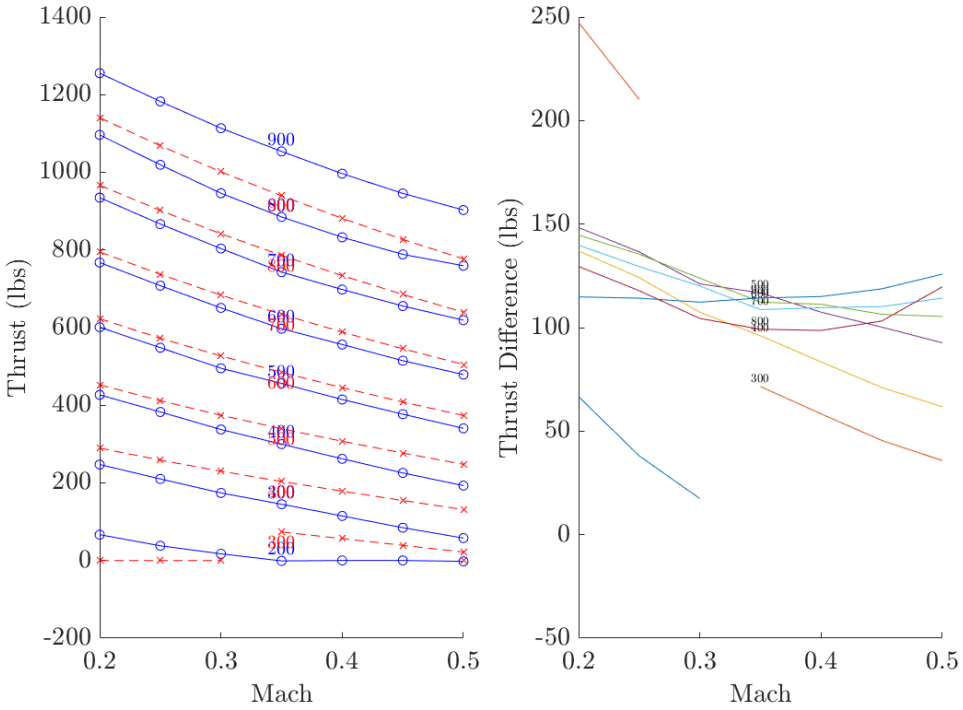

Figure 7.3: Thrust output of the 3D look-up table (blue circles) and the SVV-algorithm (red crosses) for sea level conditions and thrust error for each fuel mass flow input.

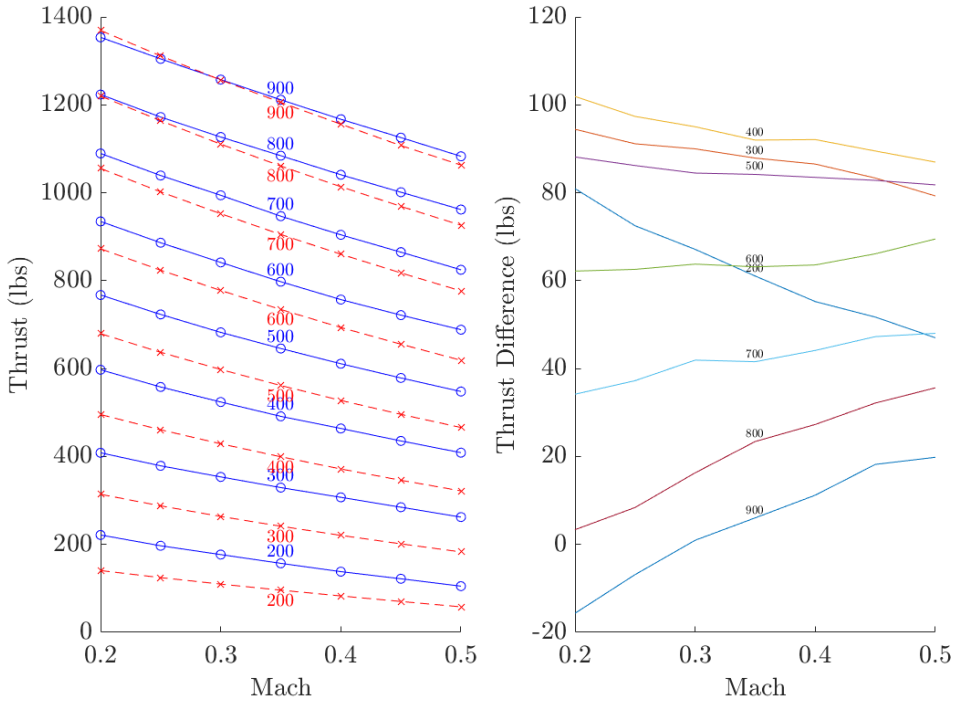

Figure 7.4: Thrust output of the 3D look-up table (blue circles) and the SVV-algorithm (red crosses) for FL150 conditions and thrust error for each fuel mass flow input.

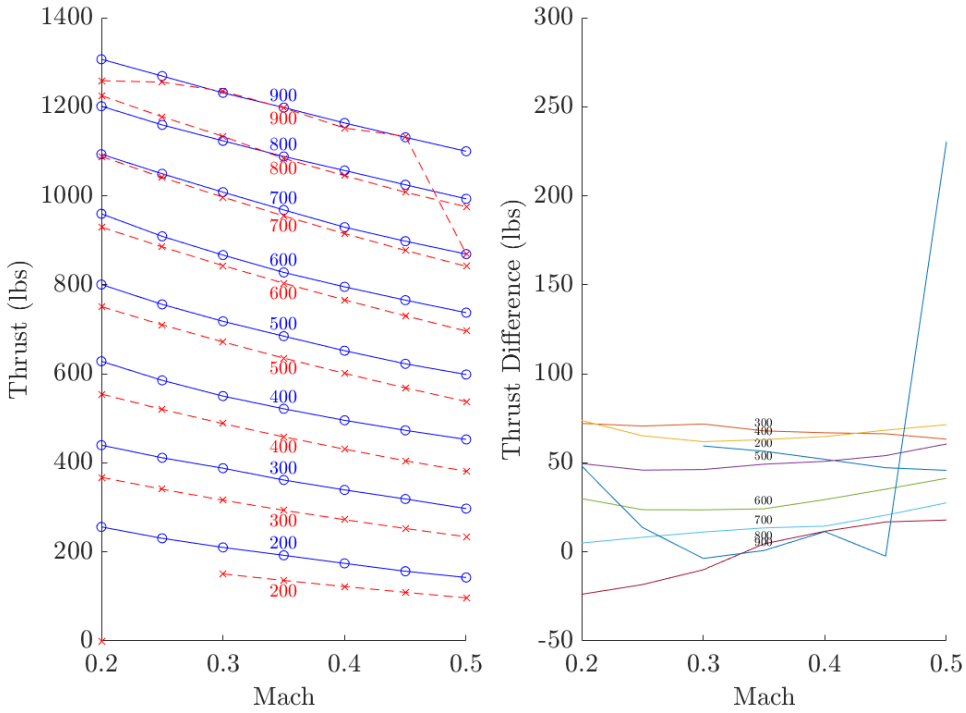

Figure 7.5: Thrust output of the 3D look-up table (blue circles) and the SVV-algorithm (red crosses) for FL200 conditions and thrust error for each fuel mass flow input.

7.2. N1 Fan Speed Noise Filtering

A median filter was applied on the measurements of the engine fan speed $N1$ to remove glitches. Most of these glitches took place in 2016 experiment dataset [10]. This meant that every spike in $N1$ would directly translate to a peak in the fitted pitch or drag data, since the thrust, which takes $N1$ as an input, is used to refine the pitch and drag measurements. These glitches were resolved by applying a 1D median filter (`medfilt1(data, 25, 'truncate')`) and then applying a 4th order low-pass filter.

7.3. Engine Thrust Effect in Flight Path Reconstruction

In this section, the effect of using JT15D-4 engine model against the original JT15D-1 look-up table, used in research by Van Ingen et al. [10] and Herbold [14], will be shown. Due to SVV-algorithm containing glitches, the 3D look-up table was chosen as the JT15D-4 engine model. Figure 7.6 shows that the main change is seen in the measured drag coefficient C_D at the initiation and recovery phase of the maneuver, where the engine thrust output is highest. A similar effect is also observed for the measured C_m output, but the magnitude of the difference is smaller. As a result of model re-identification using the Separable Nonlinear Least Squares (SNLS) introduced by Herbold [14], the JT15D-4 model has reduced the corrective $C_{D_{CT}}$ term by 61% for **M1** model and by 51% for **M2** model, see Table 7.1. A smaller change of 12% and 29% of $C_{m_{CT}}$ parameter can be seen for the **M1** and **M2** models respectively. On the other hand, the model fit statistics show a slightly worse fit to the new C_D and C_m values. Despite the good results in engine parameter data, the C_{m_0} has not changed significantly.

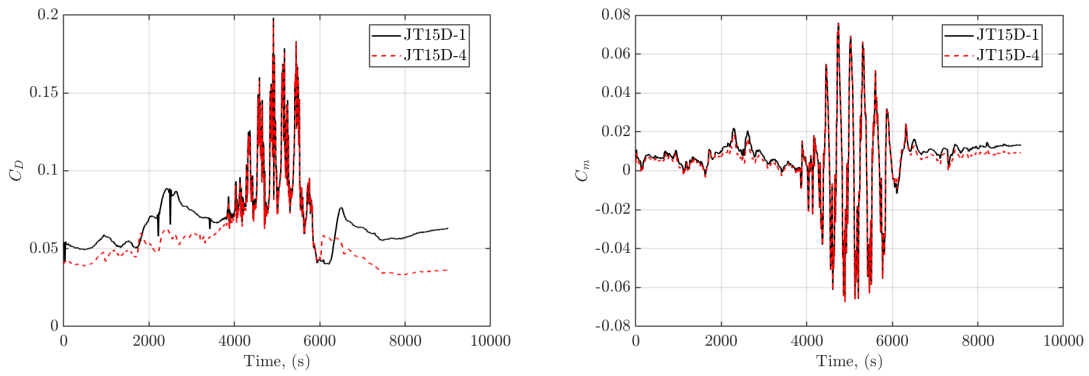

(a) C_D. **(b)** C_m.

Figure 7.6: Change in C_D and C_m measurements from different thrust models for a quasi-steady stall.

Table 7.1: The effects of engine thrust output on parameter values and model fit.

		M1			**M2**		
		JT15D-1	JT15D-4	*change %*	JT15D-1	JT15D-4	*change %*
C_D	$C_{D_{CT}}$	0.3454	0.1345	61.06	0.3945	0.1914	51.48
	MSE	0.000187	0.0001898	-1.50	0.000168	0.000167	0.77
	R^2	0.8988	0.8832	1.74	0.9091	0.8956	1.48
C_m	$C_{m_{CT}}$	0.09325	0.08158	12.51	0.07886	0.05632	28.58
	MSE	0.0001739	0.0001738	0.06	0.000144	0.0001426	0.70
	R^2	0.748	0.7406	0.99	0.7916	0.7872	0.56

8

Alternative Pitch Model Identification

The original **M2** model as introduced by Herbold [14] has some known drawbacks when it comes to implementation to real-time simulation. The first issue is high oscillations, which are likely linked to the small C_{m_q} value of -1.7502, whereas other known models have values as large as -22 [13]. In addition, the model trims at a lower elevator deflection compared to the **M1** model and flight test data. This is possibly caused by a C_{m_0} value of 0.0659 compared to the **M1** model value of 0.018, causing an elevator deflection offset at the same initial condition. Lastly, it was observed by Herbold that $C_{m_{K_0}}$ and $C_{m_{c.g.}}$ are highly correlated [14] and therefore may not be reliable at simulating the pitch model.

To resolve these issues, it was decided to modify the **M2** model during the identification process, before moving to full flight simulation and piloted experimentation. For this, two approaches were explored: modification of the identification maneuver database and modification of the **M2** model pitching moment.

8.1. M2 Model Identification Database Modifications

For modifying the identification database, three options were explored. The first version includes the baseline **M2** model identification dataset containing quasi-steady stalls collected in 2016 and dynamic stalls from the flight tests performed in 2024. This will be denoted as '2016-2024' dataset. The second dataset marked as '2016' contains only the already mentioned quasi-steady stalls from 2016. The last dataset, called 'Asymmetric' contains all stalls from the '2016-2024' dataset and a few more asymmetric quasi-steady stalls collected by Van Wezel et al. [12]. It is believed that asymmetric quasi-steady stalls will help with identification of C_{m_q} by decoupling the pitch rate and the angle-of-attack.

In addition to this, the effects of implementing the JT15D-4 3D look-up table from Chapter 7 were also investigated. It was expected that by removing the engine moment offset from the measured C_m data, the C_{m_0} value would improve. The new engine model was applied on the '2016' and the '2016-2024' stall maneuver datasets.

During the identification procedure, the SNLS method implemented by Herbold was applied [14], with 80% of the dataset allocated to identification and the remaining 20% reserved for validation. The results of this process are show in Table 8.1, Table 8.2 and Table 8.3. In addition, the same re-identification was done for the **M1** model by Van Ingen et. al. [10] and can be found in Appendix B.

Table 8.1: The effect of flight test dataset and engine model selection on Herbold's (M2) model [14] using SNLS [14].

Herbold's Model (M2)	JT15D-1 (old)			JT15D-4 (new)	
	Original, 2016-2024 [14]	**2016**	**Asymmetric**	**2016**	**2016-2024**
C_{L_0}	0.2318	0.1566	0.2279	0.1591	0.2328
$C_{L_{\alpha,ss}}$	1.3851	1.7240	1.3869	1.7089	1.3489
$C_{L_{\alpha,w}}$	2.5961	2.8450	2.6176	2.8544	2.6366
C_{L_q}	8.0747	8.6696	8.3395	8.7998	8.3385
$C_{L_{\delta e}}$	-0.3403	-0.0895	-0.3345	-0.1034	-0.3430
C_{D_0}	0.0165	0.0185	0.0171	0.0180	0.0169
$C_{D_{C_T}}$	0.3917	0.3534	0.3827	0.1460	0.1915
$C_{D_{\delta e}}$	-0.1894	-0.2075	-0.1902	-0.1886	-0.1919
$C_{D_{C_L^2}}$	0.0258	0.0210	0.0264	0.0259	0.0286
$C_{D_{X_{ss}}}$	0.0555	0.0493	0.0571	0.0467	0.0541
$C_{D_{X_w}}$	0.2062	0.2278	0.2105	0.2130	0.2108
C_{m_0}	0.0659	0.0392	0.0587	0.0388	0.0656
$C_{m_{C_T}}$	0.0794	0.0875	0.0627	0.0700	0.0563
$C_{m_{q^*}}$	-1.7502	-2.3714	-1.8973	-2.6465	-1.7226
$C_{m_{\delta_e}}$	-0.7431	-0.6523	-0.7087	-0.6655	-0.7414
$C_{m_{c.g}}$	-0.9616	-0.2579	-0.0859	-0.4014	-0.9649
$C_{m_{K_0}}$	3.2316	0.7926	0.1616	1.2985	3.2447
$C_{m_{K_{1,ss}}}$	-0.0517	-0.0673	-0.0581	-0.0711	-0.0498
$C_{m_{K_{1,w}}}$	-0.0681	-0.0371	-0.0690	-0.0371	-0.0678
$C_{m_{X_{ss}\delta_e}}$	-0.2576	-0.2792	-0.2380	-0.2742	-0.2628
$\tau_{1,ss}$	0.4191	0.3232	0.3387	0.3543	0.3969
$\tau_{2,ss}$	0.3391	0.6045	0.3835	0.5094	0.3345
$a_{1,ss}$	70.2846	47.9769	65.2705	46.3590	68.4891
α^*_{ss}	0.1956	0.2007	0.1941	0.2018	0.1948
$a_{1,w}$	13.9276	11.1464	14.3723	10.3403	13.6099
α^*_w	0.3267	0.3444	0.3294	0.3349	0.3269

The Table 8.1 contains all of the **M2** model coefficient values for each dataset used in identification. The first noticeable difference is the decrease of $C_{m_{CT}}$ and $C_{D_{CT}}$ coefficient values with JT15D-4 engine model across both '2016' and '2016-2024' datasets (highlighted in green). While this decrease is a positive improvement, this did not reduce the C_{m_0} value.

Another significant observation is that the '2016' dataset reduces the C_{m_0} value by around 40%, which is highlighted with a dark blue color in Table 8.1. This difference could be caused by the dynamic stall data starting at a higher velocity and therefore the higher trim speed. By removing this data and keeping the quasi-steady stalls only, the elevator trim deflections increase with lower airspeed and therefore C_{m_0} reduces. However, despite this reduction, the resulting value of $C_{m_0} = 0.039$ remains more than twice the target value of 0.02 and is therefore still unacceptable. In addition to the C_{m_0} reduction, the '2016' dataset decreases the flow separation delay time constant $\tau_{1,ss}$ by 31,7% and increases the hysteresis time constant $\tau_{2,ss}$ to nearly twice the value. Regarding the $\tau_{2,ss}$, this is unusual, since the original **M1** model by Van Ingen et al. [10] contains a 33 times smaller value. This could be attributed to increased correlation between $\tau_{1,ss}$ and $\tau_{2,ss}$ due to missing dynamic stall data, however, performing SNLS on the **M1** model with its original dataset also causes $\tau_{2,ss}$ to increase from 0.018 to 0.567, see Appendix B. This analysis cannot explain this phenomena and further investigation is required.

The values highlighted in light blue color show a quite high variation between different measurement

datasets. These are the highly correlated $C_{m_{K_0}}$ and $C_{m_{c.g.}}$ parameters, which proportionally increase or decrease between the sets. In this case, both parameters decreased by 75% and 94% at the same time for the '2016' and 'Asymmetric' datasets respectively. Lastly, the 'Asymmetric' stall data had little effect on predicting the C_{m_q} value (highlighted in light orange) compared to the original case of the **M2** model.

Regarding the model fit data in Table 8.2 and Table 8.3, the **M2** model provides the best fit for dataset containing only the quasi-steady stalls. However, the relevance of this model would be limited, because this dataset does not contain dynamic stall effects. When it comes to fitting data to the 'Asymmetric' dataset or applying the new engine model, there is very little change to the accuracy of the fit.

Table 8.2: The M2 model fit to the flight test data of the training dataset.

Taining Data		**Herbold Model (M2)**				
	Engine Model:	JT15D-1 (original)			JT15D-4 (new)	
	Dataset:	2016	2016-2024 (original)	Asymmetric	2016	2016-2024
C_L	MSE	0.00250	0.00360	0.00340	0.00160	0.00360
	RMSE	0.04970	0.05960	0.05870	0.04040	0.05980
	R^2	0.89830	0.89160	0.89230	0.93270	0.89130
C_D	MSE	0.00010	0.00017	0.00016	0.00009	0.00017
	RMSE	0.01020	0.01300	0.01280	0.00950	0.01300
	R^2	0.84110	0.90910	0.90700	0.86050	0.89560
C_m	MSE	0.00010	0.00014	0.00018	0.00009	0.00014
	RMSE	0.01010	0.01200	0.01340	0.00960	0.01190
	R^2	0.75120	0.79160	0.75360	0.77500	0.78720

Table 8.3: The M2 model fit to the flight test data of the validation dataset.

Validation Data		**Herbold Model (M2)**				
	Engine Model:	JT15D-1 (original)			JT15D-4 (new)	
	Dataset:	2016	2016-2024 (original)	Asymmetric	2016	2016-2024
C_L	MSE	0.0017	0.0034	0.0034	0.0017	0.0034
	RMSE	0.0410	0.0581	0.0587	0.0411	0.0583
	R^2	0.9215	0.9056	0.8923	0.9211	0.9055
C_D	MSE	0.0001	0.00018	0.0002	0.0001	0.0002
	RMSE	0.0094	0.0132	0.0128	0.0096	0.0132
	R^2	0.8591	0.8611	0.9070	0.8579	0.8400
C_m	MSE	0.0001	0.00019	0.0002	0.0001	0.0002
	RMSE	0.0100	0.0137	0.0134	0.0101	0.0136
	R^2	0.7935	0.7120	0.7536	0.7834	0.7058

8.2. M2 Pitch Model Modifications

In addition to the stall database and engine model variations, a few alternative options of the **M2** pitch model were explored. One of the objectives was to assess if modifying the pitch model structure would reduce the C_{m_0} and C_{m_q} terms. The second motivation was to remove or replace the highly correlated C_L parameter terms nested under K_0, seen in Eq. (8.1), since, in simulated flight, these terms nearly cancel each other out. Lastly, in research by Singh and Jategaonkar [45], the flow separation parameters related to C_L were added to a C_m model which already had an existing $C_{m_\alpha}\alpha$ term. Therefore, the effect of adding this term to the baseline **M2** pitch model was also explored.

$$K_0: \quad C_{m_{K_0}}, \quad C_{m_{c.g.}} \frac{x_{c.g.}}{\bar{c}} \tag{8.1}$$

For the change of the C_L regressor, two promising C_m models were chosen: Cm-XXIX and Cm-LVIII. According to Herbold [14], these pitch models had one of the lowest mean squared error values out of all models excluding the terms from Eq.(8.1). Instead of these terms, the Cm-XXIX has flow separation regressors suggested by Singh and Jategaonkar [45], see Eq. (8.2). The second model Cm-LVIII has all components of the Cm-XXIX model and includes additional flow separation terms $C_{m_{X,ss_{\delta_e}}} X_{ss}\delta_e$ and $C_{m_{X,ww_{\delta_e}}} X_w\delta_e$ for the elevator effectiveness.

The resulting coefficient values are listed in Table 8.4, while the corresponding model fit is shown in Table 8.5. For this analysis, the original **M2** model identification dataset was used to fit the data, containing stall data from flights conducted in 2016 [10] and 2024 [14]. In addition, the original engine model of the JT15D-1 engine was retained. From table Table 8.4 it can be seen that almost no models showed any improvement for the C_{m_0} and C_{m_q} values. Only the fixed C_{m_0} model improved the C_{m_q} value from -1.7502 to -3.84, but it is nowhere as close as to known values of -8 and -22. In addition, the Cm-XXIX caused pitch damping value to become positive, which makes the aircraft unstable. The baseline **M2** model with a C_{m_α} addition has $C_{m_\alpha} > 0$, which can cause the aircraft to be unstable. Lastly, the Cm-LVIII model coefficients show no overall improvement.

$$C_m = C_{m_0} + C_{m_{CT}} C_T + C_{m_q} \frac{qc}{V} + C_{m_{\delta_e}} \delta_e + C_{m_{K_s,ss}} \frac{5(1-\sqrt{X_{ss}})^2 + 4\sqrt{X_{ss}}}{16} C_L + C_{m_{K_s,w}} \frac{5(1-\sqrt{X_w})^2 + 4\sqrt{X_w}}{16} C_L + C_{m_{ss}}(1-X_{ss}) + C_{m_w}(1-X_w) \tag{8.2}$$

The next modification was an addition of a $C_{m_\alpha}\alpha$ term to the original C_m equation ofthe **M2** model, resulting in Eq. (8.3). Lastly, an option to fix C_{m_0} to a known value of 0.02 was explored to see how it affects model fit and other coefficients such as pitch damping C_{m_q}.

$$C_m = C_{m_0} + C_{m_{C_T}} C_T + C_{m_{q^*}} \frac{q\bar{c}}{V} + C_{m_\alpha}\alpha - l_{c.p.} C_L + C^*_{m_{X\delta_e}} \delta_e \tag{8.3}$$

Table 8.4: Parameter estimates of different **M2** pitch model variations, using original engine model and 2016-2024 dataset.

Original Herbold Model (M2)	
Parameter	$\hat{\theta}$
C_{m_0}	0.0659
$C_{m_{C_T}}$	0.0794
$C_{m_{q^*}}$	-1.7502
$C_{m_{\delta_e}}$	-0.7431
$C_{m_{c.g}}$	-0.9616
$C_{m_{K_0}}$	3.2316
$C_{m_{K_{1,ss}}}$	-0.0517
$C_{m_{K_{1,w}}}$	-0.0681
$C_{m_{X_{ss}\delta_e}}$	-0.2576

$C_m + C_{m_\alpha}$	
Parameter	$\hat{\theta}$
C_{m_0}	0.073657209
$C_{m_{C_T}}$	0.077673973
$C_{m_{q^*}}$	-1.427565013
C_{m_α}	0.136257079
$C_{m_{\delta_e}}$	-0.752248264
$C_{m_{c.g}}$	-0.968930032
$C_{m_{K_0}}$	3.223596247
$C_{m_{K_{1,ss}}}$	-0.057949271
$C_{m_{K_{1,w}}}$	-0.094507917
$C_{m_{X_{ss}\delta_e}}$	-0.265136664

Cm-LVIII	
Parameter	$\hat{\theta}$
C_{m_0}	0.072716167
$C_{m_{C_T}}$	0.067805463
$C_{m_{q^*}}$	-0.972280199
$C_{m_{\delta_e}}$	-0.393284657
$C_{X_{Singh,1}}$	-0.037170217
$C_{X_{Singh,2}}$	-0.667181437
$C_{m_{X_1\delta_e}}$	-0.71842161

Cm-XXIX	
Parameter	$\hat{\theta}$
C_{m_0}	0.071558948
$C_{m_{C_T}}$	0.092671805
$C_{m_{q^*}}$	2.708792577
$C_{m_{\delta_e}}$	-0.36548727
$C_{X_{Singh,1}}$	-0.35796926
$C_{X_{Singh,2}}$	-0.14598875

Fixed C_{m_0}	
Parameter	$\hat{\theta}$
C_{m_0}	0.02
$C_{m_{C_T}}$	0.129637055
$C_{m_{q^*}}$	-3.843038663
$C_{m_{\delta_e}}$	-0.747458292
$C_{m_{c.g}}$	-0.604608378
$C_{m_{K_0}}$	2.049718497
$C_{m_{K_{1,ss}}}$	-0.087718219
$C_{m_{K_{1,w}}}$	-0.076569801
$C_{m_{X_{ss}\delta_e}}$	-0.06753063

The pitch model modification fit to the flight test data results, displayed in Table 8.5, show that the baseline model with a C_{m_α} term is the best performing model, outperforming the original **M2** model by Herbold both in training and validation datasets. However, the positive C_{m_α} value causing possible instabilities negates this result. While the fixed C_{m_0} model has the second best performance from all modified models, it performs rather poorly in fitting the validation set. The overall worst performance is by model Cm-XXIX. All modified pitch models performed worse or had marginal improvements and thus it was decided to keep exploring the original **M2** model for the experiments in the SRS.

Table 8.5: Model fit of alternative **M2** pitch model variations, using original engine model and 2016-2024 dataset.

		Herbold's Model (M2) Modifications				
		Original	$C_m + C_{m_\alpha}$	**Cm-LVIII**	**Cm-XXIX**	Fixed C_{m_0}
Training	MSE	0.00014	0.00014	0.00022	0.00046	0.00019
C_m	RMSE	0.0120	0.01200	0.0149	0.0215	0.0138
	R^2	0.7916	0.7918	0.6780	0.3310	0.7225
Validation	MSE	0.000187	0.000186	0.0003	0.0005	0.0006
C_m	RMSE	0.0137	0.0136	0.0164	0.0221	0.0238
	R^2	0.7120	0.7136	0.5851	0.2502	0.1304

9

DUECA Implementation

The experiment was implemented and controlled by using the DUECA framework. For this, an already existing project used by Bootsma et al. [13] was modified. The main modification to the project was adding two modules: a second aircraft dynamic module CitationModelM2 and a model selector module, which can be seen in Figure 9.1. CitationModelM2 and CitationModelM1 are run in parallel at the same time with the same pilot inputs, however, based on the selected setting, the model selector passes only one output signal to the simulation.

The general procedure is as follows. First, the simulation settings are selected through a user interface. This includes the experiment mode, the autopilot setting, the angle of attack indicator mode, simulator motion setting, simulation time and the aircraft model version. These inputs go to ECI block, which acts as a middle ground between the input interface and the simulation logic. The ECI also stores the initial condition, trim data and mass of all model variants. Once the 'apply' button is pressed, the ECI module passes the data to the Staircase. The Staircase module is the 'computer' of the experiment. It contains the logic for different experiment modes and reacts to autopilot button presses from the pilot. If a button is pressed, Staircase starts the simulation and sends the parameter data to the Citation Model blocks and a command to the Conventional Display module to show a countdown. When the simulation is over, Staircase re-applies the data to be ready for the next button press. The CitationModel modules apply trim data and, if the simulation is running, take column deflection as an input and provide the output. The selected output then travels to the motion base, cockpit displays and signal checker - a graphing tool for the operator to observe some model states. In addition, the signal checker sends a selection of model parameters to re-confirm that the correct model is running.

The CitationModel modules went through large modifications. First, the SIMULINK models were adjusted such that no workspace parameters were recorded into the constant memory. This allows an easy change of parameters for any desired simulation scenario. Second, and most importantly, the initialization of the SIMULINK model class was changed. Before, the SIMULINK model was initialized by calling a class and running initialization script, after which model parameters were changed. This was not suitable for this experiment, since by running initialization script early, all initial state data is locked and cannot be modified. Instead, the order was reversed. First, a model class was called, then initial condition and parameter changes were applied, and lastly the class initialization script was run. This way, changes are set as initial parameters and allow for a smooth simulation start.

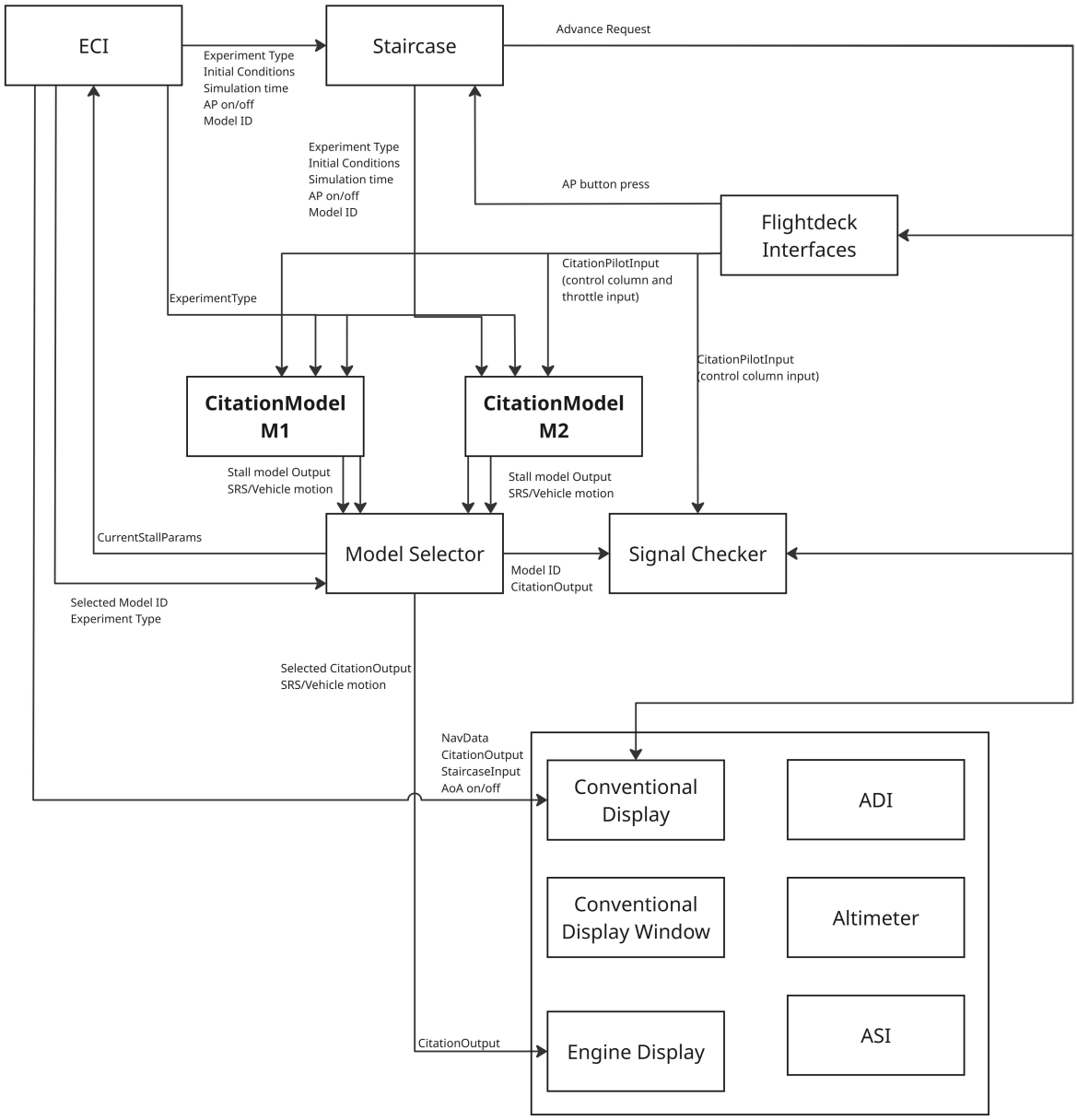

Figure 9.1: DUECA implementation flowchart.

Part IV

Closure

10

Conclusions & Recommendations

10.1. Conclusions

To conclude this report, the research objective and research questions are revisited. A short answer for each research question is provided here.

Research Objective

The research objective is to compare the two-state flow separation stall model **M2** [14] of the Cessna Citation II with the single-state flow separation stall model **M1** [10] by performing actively controlled quasi-steady stalls in SIMONA research simulator.

Research Question 1

To what extent is the measured data processing done in the stall model identification is performed robustly?

There were some inconsistencies in the current model identification and data reconstruction. The first spotted inconsistency was the approximated location of the AHRS1 sensor, which is used in the flight path reconstruction to account for rotational acceleration offsets. In this research, it was manually measured and updated. Since the distance difference and acceleration errors were rather small, the newly reconstructed data did not have any significant offsets compared to data reconstructed before the correction, meaning that the previous approximation was sufficiently robust.

Another inconsistency was spotted in the aerodynamic coefficient reconstruction, where mismatching data for the aircraft parameters, i.e., wingspan, MAC, and engine position, was found. Since these parameters are heavily involved in the measurement and identification equations, the measured aerodynamic coefficient data was offset up to 2-3%.

Lastly, some glitches were found in the engine fan speed N1 data, which directly translated to visible peaks in the measured C_m data. Since the current models contain a C_T regressor, these glitches had little to no effect on the model identification. On the other hand, if C_T regressor was omitted, then the identified model would lose its fidelity by fitting to the false pitching moments. Therefore the N1 data requires careful filtering to ensure robust stall model identification. Overall, the flight path reconstruction is quite robust to slight inaccuracies in aircraft parameter data, whereas the model identification is less robust to discrepancies in the measured data.

Research Question 2

What changes need to be applied to the original **M2** model to implement it in full flight simulation?

The original **M2** model implemented in the full flight simulation was nearly uncontrollable and required a few pitch coefficient parameter changes. This model displayed high pitch oscillations that exceeded

the simulator motion base limits and therefore an increase in pitch damping C_{m_q} had to be applied, equally how it was done by Bootsma et al. [13] for **M1**. Furthermore, the zero-lift pitch moment and pitch effectiveness coefficients were altered, however, these were rather 'cosmetic' implementations to match the trim conditions and increase control forces and not a must in order to have a working and useful model.

Research Question 3

How large are the differences between JT15D-1 and JT15D-4 engine models and how do they affect the flight path reconstruction and model identification?

The comparison of the engine options can be seen in Chapter 7. While the thrust difference between the engines at the maximum power is about 10%, it was discovered that the altitude correction was never applied in the stall identification procedure. This means that so far the engine contribution was over-estimated. By applying a simple altitude correction the thrust output reduces 45% . Additionally, a 3D look-up table was created in Chapter 7 based on the engine manual data and for corrected altitude. The 3D look-up table value was in between the original estimates and the simple altitude correction. In flight path reconstruction, the engine thrust mainly affects the measured aerodynamic force and moment coefficients. After applying the new engine model, the start and end on the maneuver had the most change, where the thrust is present. During the stall it self, virtually no difference was observed. When the models were re-identified, the $C_{m_{CT}}$ had reduced by 12-29%, while the $C_{D_{CT}}$ coefficient reduced by 50-61%. On the other hand, the C_{m_0} had no reduction. Unfortunately, due to uncertainties in the look-up table accuracy, and little desired effect on C_{m_0}, it was decided to leave the engine model as it stands. While the potential is there, the engine model needs to be visited in more detail later.

Research Question 4

What are the candidates for the **M2** stall model that have accurate pitch damping and trim characteristics?

Unfortunately, none of the proposed candidates in Chapter 8 resulted in acceptable C_{m_0} and C_{m_q} values. Since no large differences were observed, it would have been required to implement each model individually in DUECA and create more versions with manual modification, which would have prohibitively expanded the scope of this research. It was therefore decided to proceed to the experiment with the original **M2** model and manually change the values of pitch parameters.

Research Question 5

How accurately can the modified and re-identified aerodynamic models of **M2** capture the stall of the Cessna Citation II compared to measured data and offline simulation? To what extent does the **M2** model need to be modified to be applicable in piloted simulation?

As mentioned before, the re-identified models were not used in the experiment due to lack of improvements and reduced research scope. As for the **M2** model modification, the pitch coefficient C_{m_q} was increased to -22 and the C_{m_0} reduced to 0.02 to match the **M1** model at the start of simulation. This was used as a baseline model for which other modifications were applied on top for comparing the models.

Research Question 6

What is the difference in the quasi-steady stall between **M1** and **M2** models in full flight simulation?

There are a few differences that were observed during piloted simulation experiment and data analysis. First, the **M2** model contains more oscillations in stall onset than the **M1** model. This is due to elevator effectiveness reduction being coupled with the negative magnitude increase of $-l_{c.p.}C_L$ causing the aircraft to pitch down and recover more than the **M1** model and requiring to stall again. On the other hand, the

slight pitch down moment in stall onset of **M1** is only caused by elevator effectiveness reaching a minimum at 50% flow separation, after which no more oscillations were present. The second and most noticeable difference between **M2** and **M1** models is the stall recovery. Often times, the **M2** model lead to pilot induced oscillations, while the **M1** model enabled a stable recovery. The test pilot feedback indicated, that the stall onset of the **M2** model was more realistic, while the recovery of the **M1** model was preferred. The tables summarizing the pilot's response can be found in Appendix C.

In the end, it is difficult to draw any conclusions on the effect of *one-flow separation* state against *two-flow separation* states ***only***. The **M1** and **M2** models differ too much in the aerodynamic pitch equation, which is the most 'observed' and controlled dynamic by the pilot in the full flight simulation. Since the **M1** model pitch is a function of angle-of-attack, it does not contain pitch moment fluctuations due to $C_L(X_{ss}, X_w, ...)$ changes that the **M2** model has. In addition, these moments couple with other parameters linked to the flow separation, such as elevator effectiveness. Therefore, to truly isolate and assess the effect of flow separation variable amount is to re-identify models to contain similar dependencies in their aerodynamic functions.

Research Question 7

How can the buffet model be accurately applied when two flow separation parameters are present?

While re-identifying a new buffet threshold for the **M2** model was outside the scope of this research, some comments can be made about using a flow separation separation state X from the **M1** model. To have the buffet present in the full flight simulation experiments, an external flow separation state X was implemented to the **M2** model. It took the same inputs (α and $\dot{\alpha}$) as the flow separation state X_{ss}, however, it was not connected to any aerodynamic forces and moments. It was only used for the buffet model, which eventually was connected with the vertical body axis force. Initially, the X and X_{ss} values seemed close enough for buffet to be accurate, however, it was later discovered that this might have given the test pilot a wrong cue for leveling out in the recovery. Since X state had a smaller separation delay τ_2 than X_{ss}, this made the buffet shed off just as X_{ss} has started to initiate re-attachment. This meant the pilot initiated a pitch up input while the elevator effectiveness was changing rapidly, leading to some overshoots in the aircraft attitude and later PIO. It is therefore strongly advised to identify a new buffet model for X_{ss} flow separation state if the piloted simulation research involves stall recovery.

10.2. Recommendations

The first recommendation is to implement a reversible control feedback into the control column. During the piloted simulation experiments it was evident that the forces felt on the control column are one of the major deciding factors when choosing between the models for realism. By introducing these forces, it may alter the pilot input rate and magnitude and provide a more suitable input to currently identified models. For example, it could be that the original control effectiveness values may not affect the model excitation as much, since now the input magnitude from the pilot is limited by the forces acting against in the column. In addition, the lack of buffet cue on the control column was also identified as a fidelity flaw. On the other hand, this may introduce complexity in future experiment design, since it becomes a control variable that needs to be carefully tuned. In the end, the goal of the stall research group at Delft University of Technology is to help improve and better define stall training and control column force is one steps forward to improving it.

Another recommendation is to collect flight test data (with aerodynamic angle vane boom) for clean quasi-steady stalls such that there could be a direct comparison with the piloted simulation data for verification. While the stall database is large, most of the recorded maneuvers are done for model identification purposes, i.e., they contain control perturbations during the stall. In contrast, the maneuvers performed in the piloted experiment are clean quasi-steady stalls. Therefore it has been difficult to compare and rule out whether some reactions to elevator inputs are anomalies or not. Of course, even then the data will never be perfectly longitudinal, since each stall is different and often times contain roll corrections, but it will be more comparable than what is used in this research. In addition, if any flight-tests get planned for the control column force identifications, they could be combined with gathering verification data for piloted

simulation. Lastly, having a video recording of the flight test with the outside view and the cockpit might help as well, especially for future projects many years ahead to provide a better insight of what the stall was like (for example, Flight Gear reconstruction from flight-data is not ideal to observe buffet severity).

If gathering flight test data is not possible, some student practical flights could potentially be used if the there are no large β angles during the stall. According to Van Ingen et al. [10], the flight path reconstruction can predict the true angle-of-attack from student practical data quite well if there are no large lateral disturbances. On the other hand, the amount of data to analyze and refine is large and most of it involves irrelevant maneuvers. Therefore it is recommended to explore this data if nothing else is available.

Lastly, for projects that involve new model implementation to the SIMONA research simulator and DUECA, the recommendation is to test these models in the simulator as soon as possible. This can help with early model issue diagnosis and allow a faster start in the iterative process of troubleshooting and updating the model. An example of such process would be: implement the model, test it with stall autopilot, test it with joystick inputs in DUECA, then perform a piloted simulation and re-tune the autopilot to match the new simulator data. This also brings the benefit of completing the initial and time-consuming DUECA set-up early in the project, after which, if done correctly, the new changes and solutions are fairly easy to implement. Currently nearly every parameter that is imported to SIMULINK through MATLAB workspace (such as gains, mass model, initial condition, aerodynamic parameters) can be changed in DUECA during the simulation, however, changing the aerodynamic equations of the model may require separate stand-alone models.

References

[1] U.S. Customs and Border Protection. *CBP: Air and Marine Operations no (Photo 15)*. https://www.cbp.gov/newsroom/photo-gallery/photo-library/cbp-air-and-marine-operations-no-photo-15. Public domain image. Source: U.S. Customs and Border Protection. 2024.

[2] Boeing Commercial Airplanes. *Statistical Summary of Commercial Jet Airplane Accidents Worldwide Operations 1959–2023*. Tech. rep. Boeing, Aug. 2024. URL: https://www.boeing.com/content/dam/boeing/boeingdotcom/company/about_bca/pdf/statsum.pdf.

[3] International Air Transport Association. *Loss of Control In-Flight Accident Analysis Report, 2019 edition*. Guidance Material and Best Practices. Montreal-Geneva: IATA, 2019. URL: https://www.iata.org/contentassets/b6eb2adc248c484192101edd1ed36015/loc-i_2019.pdf.

[4] Airbus. *A Statistical Analysis of Commercial Aviation Accidents 1958 - 2024*. Tech. rep. Airbus, 2025. URL: https://accidentstats.airbus.com/wp-content/uploads/2025/02/20241325_A-Statistical-analysis-of-commercial-aviation-accidents-2025-links.pdf.

[5] S. K. Advani et al. "What Really Can Be Done in Simulation to Improve Upset Training?" In: *AIAA Modeling and Simulation Technologies Conference*. American Institute of Aeronautics and Astronautics Inc. (AIAA), June 2012. DOI: 10.2514/6.2010-7791.

[6] S. Jacobson. "Aircraft Loss of Control Causal Factors and Mitigation Challenges". In: *AIAA Guidance, Navigation, and Control Conference*. Toronto, Ontario, Canada, Aug. 2010. DOI: 10.2514/6.2010-8007.

[7] S. K. Advani et al. "Global Implementation of Upset Prevention & Recovery Training". In: *AIAA Modeling and Simulation Technologies Conference*. American Institute of Aeronautics and Astronautics Inc. (AIAA), Jan. 2016. DOI: 10.2514/6.2016-1430.

[8] A. J. Schroeder et al. "An Evaluation of Several Stall Models for Commercial Transport Training". In: *AIAA Modeling and Simulation Technologies Conference*. American Institute of Aeronautics and Astronautics Inc. (AIAA), Jan. 2014. DOI: 10.2514/6.2014-1002.

[9] P. R. Grant et al. "Post-stall Flight Model Fidelity Effects on Full Stall Recovery Training". In: *AIAA Modeling and Simulation Technologies Conference*. American Institute of Aeronautics and Astronautics Inc. (AIAA), June 2018. DOI: 10.2514/6.2018-2937.

[10] J. B. van Ingen et al. "Stall Model Identification of a Cessna Citation II from Flight Test Data Using Orthogonal Model Structure Selection". In: *AIAA SCITECH 2021 Forum*. American Institute of Aeronautics and Astronautics Inc. (AIAA), Jan. 2021, pp. 11–15 & 19–21. DOI: 10.2514/6.2021-1725.

[11] P. A. R. Brill et al. "Improved Kirchhoff Stall Model Parameter Estimation Accuracy Through Optimal Data Slicing". In: *AIAA SCITECH 2025 Forum*. American Institute of Aeronautics and Astronautics Inc. (AIAA), Jan. 2025. DOI: 10.2514/6.2025-1248.

[12] C. van Wezel et al. "Identifying Dynamic Stall Effects on the Pitching Moment From Cessna Citation II Flight Test Data". In: *AIAA SCITECH 2025 Forum*. American Institute of Aeronautics and Astronautics Inc. (AIAA), Jan. 2025. DOI: 10.2514/6.2025-1252.

[13] S. Bootsma et al. "Comparing Active and Passive Just Noticeable Difference Thresholds for Stall Abruptness in Symmetric Stall". In: *AIAA SCITECH 2025 Forum*. American Institute of Aeronautics and Astronautics Inc. (AIAA), Jan. 2025. DOI: 10.2514/6.2025-0975.

[14] J. A. Herbold. "Improved Longitudinal Stall Modeling with Separable Nonlinear Least Squares and Dynamic Stall Maneuvers". MA thesis. Delft, Zuid-Holland, 2629HS, the Netherlands: Delft University of Technology, Jan. 2025.

[15] P. Deligios. “Modeling Flow Separation from Quantified Tuft Motions”. MA thesis. Delft, Zuid-Holland, 2629HS, the Netherlands: Delft University of Technology, Nov. 2025.

[16] Jr. Anderson John D. *Fundamentals of Aerodynamics*. 6th. New York, NY: McGraw-Hill Education, 2017.

[17] E. Obert. *Aerodynamic Design of Transport Aircraft*. Amsterdam, The Netherlands: IOS Press, 2009. URL: http://ebookcentral.proquest.com/lib/delft/detail.action?docID=448784.

[18] W. J. McCroskey. *The Phenomenon of Dynamic Stall*. Tech. rep. NASA-TM-81264. Publicly available NASA Technical Memorandum. Moffett Field, CA, United States: NASA Ames Research Center, Mar. 1981. URL: https://ntrs.nasa.gov/citations/19810011501.

[19] A. Choudhry et al. “An insight into the dynamic stall lift characteristics”. In: *Experimental Thermal and Fluid Science* 58 (Oct. 2014), pp. 188–208. DOI: 10.1016/j.expthermflusci.2014.07.006. URL: https://doi.org/10.1016/j.expthermflusci.2014.07.006.

[20] M. A. Bromfield et al. “Loss of Control In Flight – time to re-define?” In: *AIAA Aviation 2019 Forum*. American Institute of Aeronautics and Astronautics Inc. (AIAA), June 2019. DOI: 10.2514/6.2019-3612.

[21] R. Newman. “Thirty Years of Airline Loss-of-Control Mishaps”. In: *AIAA Modeling and Simulation Technologies Conference*. American Institute of Aeronautics and Astronautics Inc. (AIAA), Aug. 2012. DOI: 10.2514/6.2012-4495.

[22] C. Dennis. “Accident Lessons for Stall Upset Recovery Training”. In: *AIAA Guidance, Navigation, and Control Conference*. American Institute of Aeronautics and Astronautics Inc. (AIAA), Aug. 2012. DOI: 10.2514/6.2010-8003.

[23] Bureau d’Enquêtes et d’Analyses pour la sécurité de l’aviation civile. *Final Report on the accident on 1st June 2009 to the Airbus A330-203 registered F-GZCP operated by Air France flight AF 447 Rio de Janeiro - Paris*. Tech. rep. BEA, July 2012. URL: https://www.faa.gov/sites/faa.gov/files/AirFrance447_BEA.pdf.

[24] C.C. de Visser et al. “Stalls and Splines: Current Trends in Flight Testing and Aerodynamic Model Identification”. In: *Journal of Aircraft: devoted to aeronautical science and technology* 60.5 (Sept. 2023). DOI: 10.2514/1.C037283.

[25] L. van Horssen et al. “Aerodynamic Stall and Buffet Modeling for the Cessna Citation II Based on Flight Test Data”. In: *2018 AIAA Modeling and Simulation Technologies Conference*. American Institute of Aeronautics and Astronautics, Jan. 2018. DOI: 10.2514/6.2018-1167.

[26] D. de Fuijk et al. “Asymmetric Cessna Citation II Stall Model Identification using a Roll Moment-based Kirchhoff Method”. In: *Proceedings of the 2024 CEAS EuroGNC Conference*. Bristol, UK, June 2024. DOI: 10.82124/CEAS-GNC-2024-026.

[27] A. Delfosse et al. “Asymmetric Stall Modeling of the Cessna Citation II Aircraft”. In: *Proceedings of the 2022 CEAS EuroGNC Conference*. CEAS-GNC-2022-011. Berlin, Germany, May 2022.

[28] S.C.E. Smets et al. “Subjective Noticeability of Variations in Quasi-Steady Aerodynamic Stall Dynamics”. In: *AIAA SCITECH 2019 Forum*. American Institute of Aeronautics and Astronautics Inc. (AIAA), Jan. 2019. DOI: 10.2514/6.2019-1485.

[29] A. Imbrechts et al. “Just Noticeable Differences for Variations in Quasi-Steady Stall Buffet Model Parameters”. In: *AIAA SCITECH 2022 Forum*. American Institute of Aeronautics and Astronautics Inc. (AIAA), Jan. 2022. DOI: 10.2514/6.2022-0510.

[30] D. Fischenberg. “Identification of an unsteady aerodynamic stall model from flight test data”. In: *20th Atmospheric Flight Mechanics Conference*. American Institute of Aeronautics and Astronautics Inc. (AIAA), Aug. 1995. DOI: 10.2514/6.1995-3438.

[31] E. N. Jacobs et al. *Characteristics of the NACA 23012 Airfoil from Tests in the Full-Scale and Variable-Density Tunnels*. Tech. rep. NACA-TR-530. National Advisory Committee for Aeronautics (NACA), 1936. URL: https://ntrs.nasa.gov/citations/19930091603.

[32] European Aviation Safety Agency. *Certification Specifications for Aeroplane Flight Simulation Training Devices 'CS-FSTD(A)'*. May 2018.

[33] S. Advani et al. "Upset Prevention and Recovery Training in Flight Simulators". In: *AIAA Modeling and Simulation Technologies Conference*. 2012. DOI: 10.2514/6.2011-6698.

[34] K. Cunningham et al. "Pilot Sensitivity to Simulator Flight Dynamics Model Formulation for Stall Training". In: *AIAA Scitech 2019 Forum*. American Institute of Aeronautics and Astronautics Inc. (AIAA), Jan. 2019. DOI: 10.2514/6.2019-0717.

[35] W. J. Dixon et al. "A Method for Obtaining and Analyzing Sensitivity Data". In: *Journal of the American Statistical Association* 43.241 (1948), pp. 109–126. DOI: 10.1080/01621459.1948.10483254.

[36] T. N. Cornsweet. "The Staircase-Method in Psychophysics". In: *The American Journal of Psychology* 75.3 (1962), pp. 485–491. DOI: 10.2307/1419876.

[37] C. Kaernbach. "Simple adaptive testing with the weighted up-down method". In: *Perception & Psychophysics* 49 (1991), pp. 227–229.

[38] W. A. Simpson. "The method of constant stimuli is efficient". In: *Perception & Psychophysics* 44 (1988), pp. 433–436. DOI: 10.3758/BF03210427.

[39] W. Berkouwer et al. "Measuring the Performance of the SIMONA Research Simulator's Motion System". In: *AIAA Modeling and Simulation Technologies Conference and Exhibit*. San Francisco, California, Aug. 2005. DOI: 10.2514/6.2005-6504.

[40] L. D. Reid et al. *Flight Simulation Motion-Base Drive Algorithms: Part 1 - Developing and Testing the Equations*. UTIAS Report 296. University of Toronto Institute for Aerospace Studies (UTIAS), Dec. 1985.

[41] O. Stroosma et al. "Using the SIMONA Research Simulator for Human-Machine Interaction Research". In: *AIAA Modeling and Simulation Technologies Conference and Exhibit*. Austin, Texas, Aug. 2003. DOI: 10.2514/6.2003-5525.

[42] H. J. Damveld et al. "Motion Filter Design for Driver Observation in Hexapod Car Simulators". In: *2010 IEEE International Conference on Systems, Man and Cybernetics*. IEEE, Oct. 2010. DOI: 10.1109/ICSMC.2010.5642447.

[43] B. Gouverneur et al. "Optimisation of the SIMONA Research Simulator's Motion Filter Settings for Handling Qualities Experiments". In: *AIAA Modeling and Simulation Technologies Conference and Exhibit*. Austin, Texas, Aug. 2003. DOI: 10.2514/6.2003-5679.

[44] *JT15D Series Commercial Turbofan Engine Installation Handbook*. Technical Handbook. Pratt & Whitney of Canada LTD. Box 10, Longueuil, Quebec J4K 4X9, 1975.

[45] J. Singh et al. "Flight determination of configurational effects on aircraft stall behavior". In: *21st Atmospheric Flight Mechanics Conference*. AIAA. San Diego, CA, 1996, pp. 657–665. DOI: 10.2514/6.1996-3441.

A

Pratt and Whitney Engine Manual Tables

The tables are obtained from commercial turbofan engine installation handbook, Pratt and Whitney Canada[44]

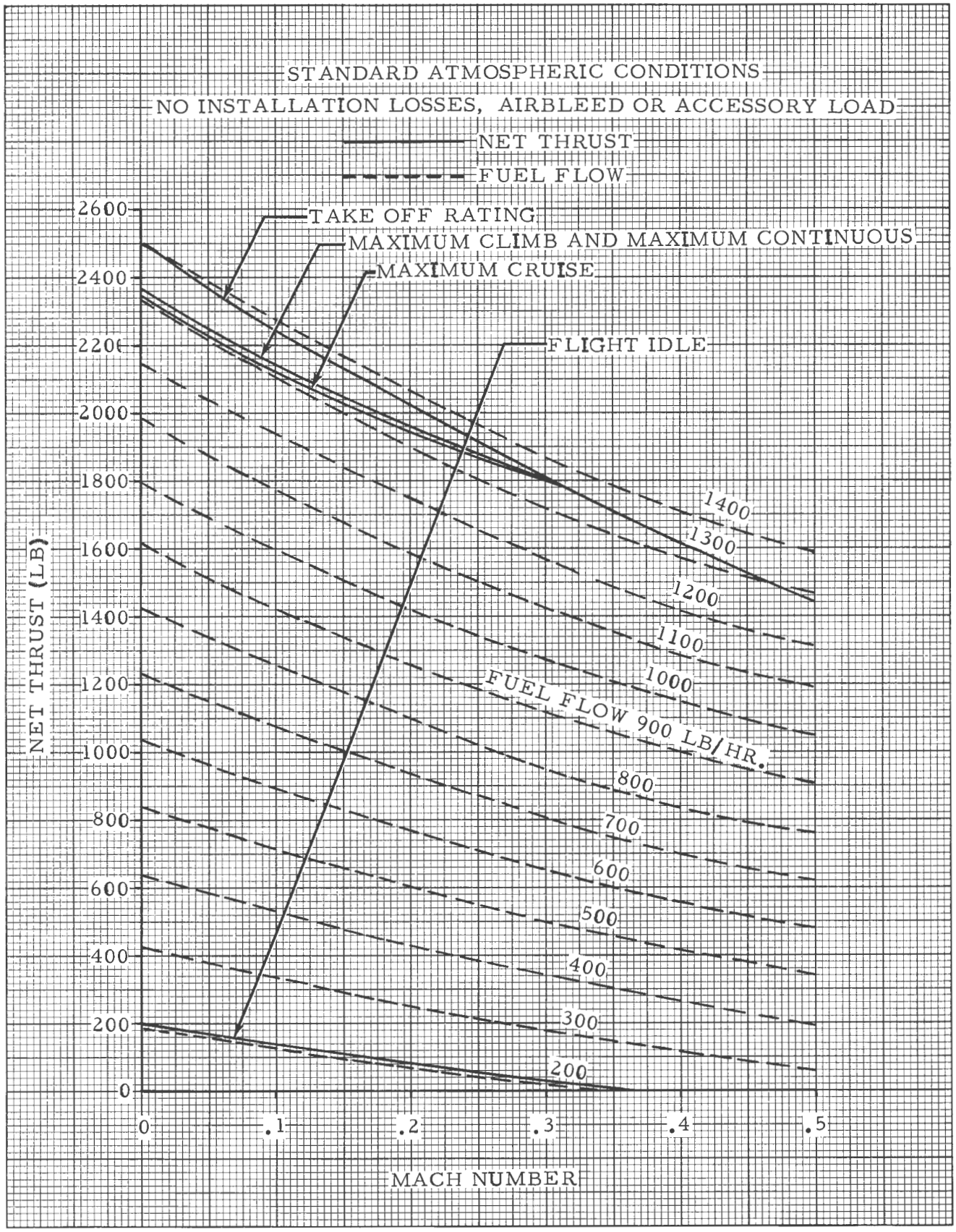

Figure 3-7 Estimated Net Thrust and Fuel Flow at Sea Level - JT15D-4 Engine

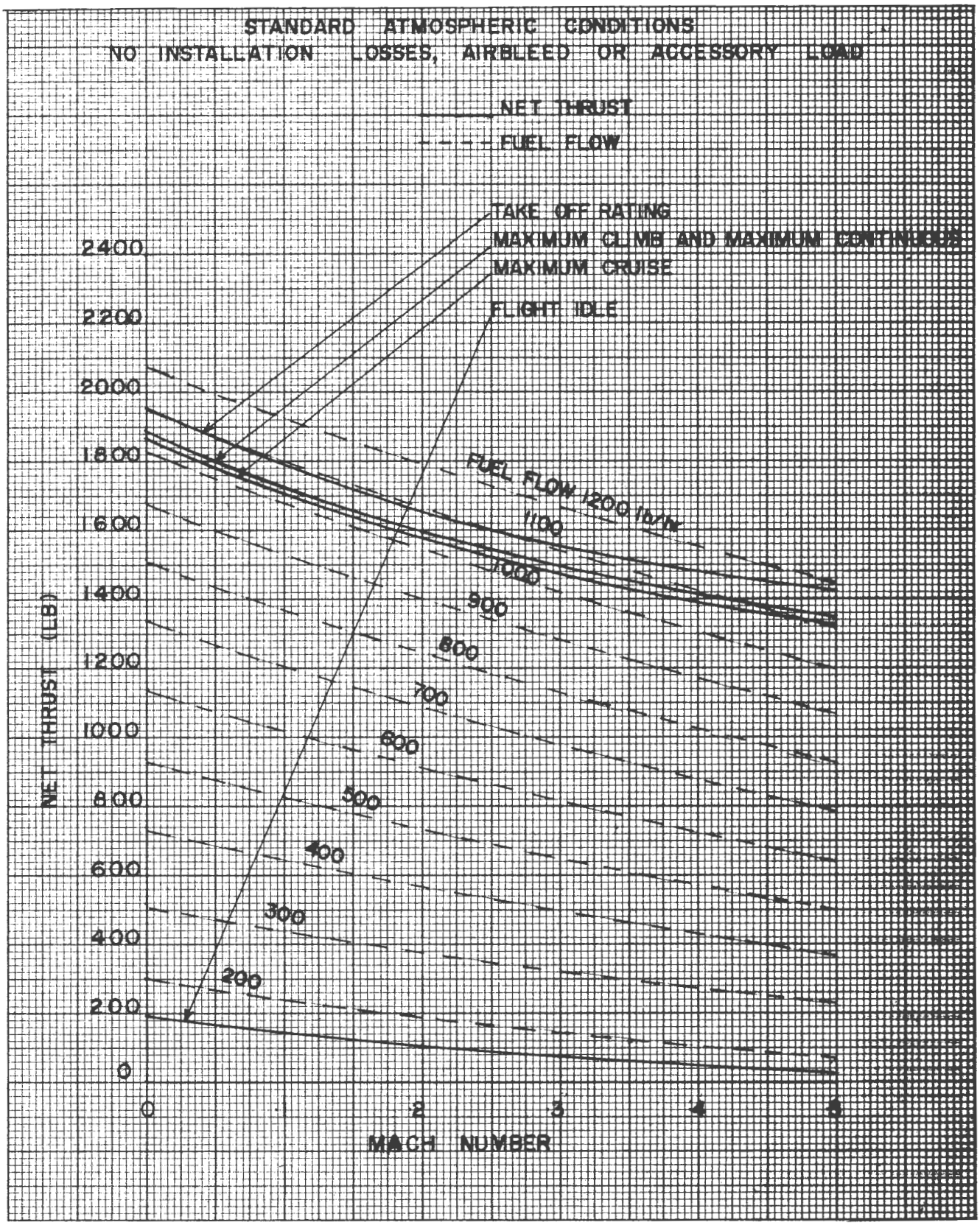

Figure 3-8 Estimated Net Thrust and Fuel Flow at 10,000 ft. Pressure Altitude - JT15D-4 Engine

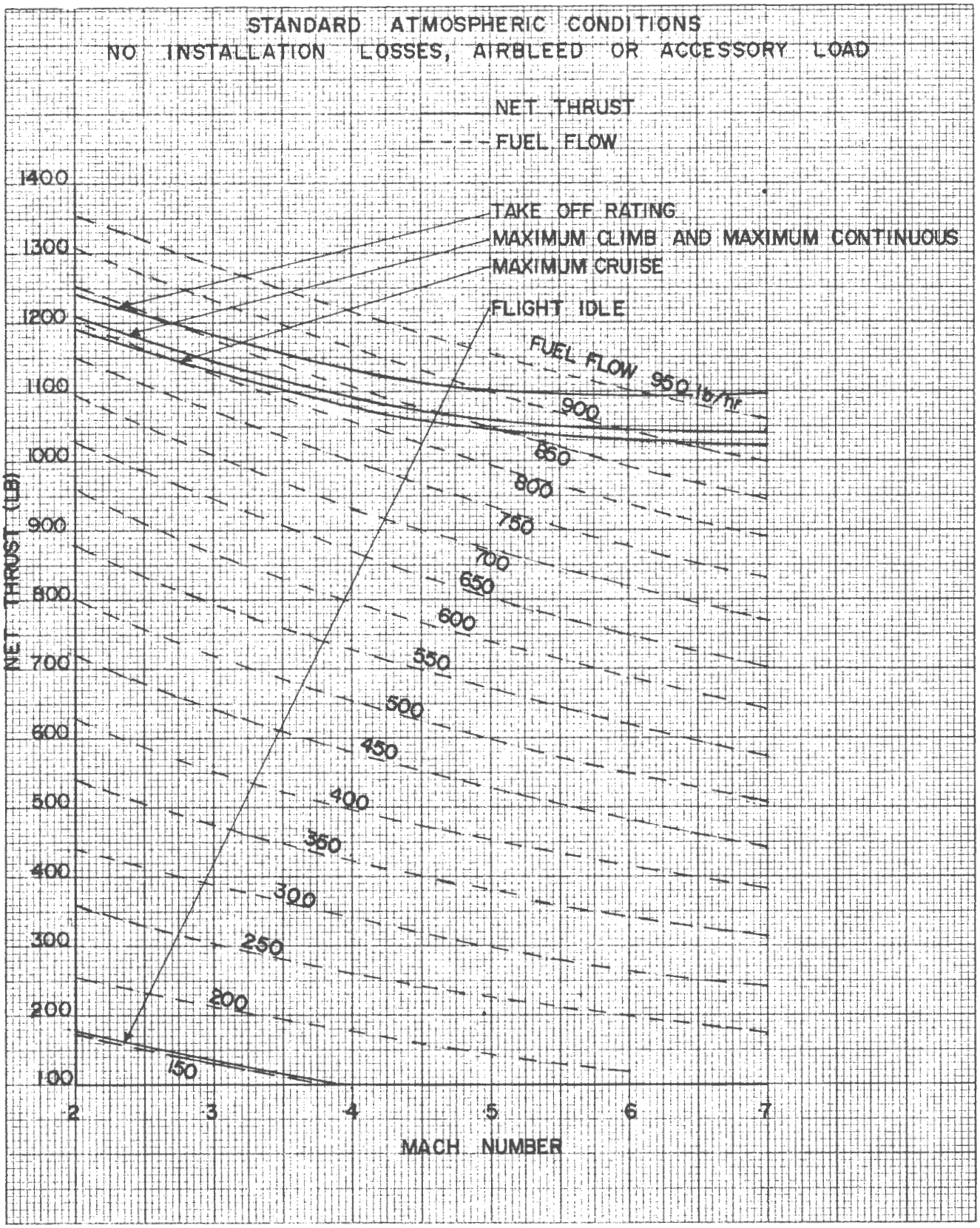

Figure 3-9 Estimated Net Thrust and Fuel Flow at 20,000 ft. Pressure Altitude - JT15D-4 Engine

B

Model Identification Result Tables

In Table B.1, the coefficient values of the **M1** model by Van Ingen et al [10] are displayed. The column called 'original' shows the baseline values obtained in research by Van Ingen et al. [10], while the 're-identified' contains the same module structure and the dataset, except re-identified using an SNLS method introduced by Herbold [14]. All other models were also identified using SNLS.

Table B.1: The effect of flight test data set and engine model selection on Van Ingen's model (M1) [10] using SNLS [14].

Van Ingen's model (M1)	JT15D-1 (original)				JT15D-4 (new)	
	Original	**re-identified**	**2016-2024**	**Asymmetric**	**2016**	**2016-2024**
C_{L_0}	0.176	0.210	0.214	0.210	0.213	0.214
C_{L_α}	4.661	4.102	4.388	4.403	4.097	4.414
$C_{L_{\alpha^2}}$	10.775	11.517	5.933	6.579	11.471	5.909
C_{D_0}	0.005	0.015	0.026	0.026	0.011	0.025
C_{D_α}	0.237	0.121	-0.050	-0.029	0.174	-0.031
$C_{D_{\delta e}}$	-0.186	-0.251	-0.230	-0.224	-0.235	-0.231
C_{D_X}	0.073	0.085	0.166	0.156	0.080	0.165
$C_{D_{C_T}}$	0.379	0.345	0.400	0.386	0.134	0.200
C_{m_0}	0.018	0.021	0.018	0.020	0.020	0.018
C_{m_α}	-0.568	-0.513	-0.513	-0.517	-0.508	-0.511
$C_{m_{\delta_e X}}$	-1.023	-0.870	-0.958	-0.954	-0.873	-0.965
$C_{m_{CT}}$	0.144	0.093	0.078	0.074	0.082	0.057
τ_1	0.255	0.053	0.036	0.036	0.052	0.036
τ_2	0.018	0.567	0.683	0.704	0.570	0.688
a_1	27.671	30.377	15.217	15.998	30.206	14.840
α^*	0.208	0.215	0.225	0.221	0.215	0.225

Interestingly, when the **M1** model is re-identified using SNLS on the same dataset, the τ_1 and especially τ_2 values increase. This effect also continues over the other datasets, for which the values are highlighted in orange. As seen from the scientific article in Part II, such increase in τ_2 can completely alter stall characteristics in piloted simulation. It is not exactly clear what causes this difference and requires further investigation. It can also be seen that introduction of dynamic stalls (2024 dataset) reduces the a_1 parameter by half, highlighted in yellow. The third difference, highlighted in blue, shows that the the drag component depending on angle-of-attack C_{D_α} negatively contributes to drag, i.e. reduces it, when the datasets contain dynamic stalls. This is counterintuitive, since lift induced drag should increase with AoA. Lastly, the reduction in the thrust related drag and pitch moment terms reduces with the new engine model, similarly as seen for the **M2** model in Chapter 7 and Chapter 8.

In Table B.2 and Table B.3, the data fit for the **M1** model increases in quality with SNLS method. However, it significantly reduces with introduction of dynamic stalls in '2016-2024' and 'asymmetric' datasets. This could mean that the current structure of **M1** is not suitable to capture the effects of dynamic stalls.

Table B.2: The M1 model (described in Table B.1) fit to the flight test data results on the training data set.

Training Data		**Van Ingen Model (M1)**					
	Engine model:	JT15D-1 (original)				JT15D-4 (new)	
	Dataset:	Original	Re-identified	2016-2024	Asymmetric	2016	2016-2024
C_L	MSE	0.0053	0.0024	0.0043	0.0042	0.0025	0.0043
	RMSE	-	0.0494	0.0043	0.0646	0.0497	0.0654
	R2	-	0.8999	0.8699	0.8695	0.8983	0.8699
C_D	MSE	0.0002	0.0001	0.0002	0.0002	0.0001	0.0002
	RMSE	-	0.0100	0.0137	0.0136	0.0102	0.0138
	R2	-	0.8394	0.8988	0.8949	0.8411	0.8832
C_m	MSE	0.0001	0.0001	0.0002	0.0002	0.0001	0.0002
	RMSE	-	0.0101	0.0132	0.0140	0.0101	0.0132
	R2	-	0.7660	0.7480	0.7295	0.7512	0.7406

Table B.3: The M1 model (described in Table B.1) fit to the flight test data results on the validation data set.

Validation Data		**Van Ingen Model (M1)**					
	Engine model:	JT15D-1 (original)				JT15D-4 (new)	
	Dataset:	Original	Re-identified	2016-2024	Asymmetric	2016.0000	2016-2024
C_L	MSE	0.0041	0.0021	0.0037	0.0036	0.0021	0.0037
	RMSE	-	0.0462	0.0607	0.0604	0.0463	0.0609
	R^2	-	0.9003	0.8970	0.8947	0.8997	0.8970
C_D	MSE	0.0002	0.0001	0.0002	0.0002	0.0001	0.0002
	RMSE	-	0.0096	0.0129	0.0126	0.0098	0.0129
	R^2	-	0.8517	0.8685	0.8700	0.8528	0.8461
C_m	MSE	0.0003	0.0001	0.0002	0.0003	0.0001	0.0002
	RMSE	-	0.0110	0.0157	0.0159	0.0110	0.0157
	R^2	-	0.7522	0.6212	0.6314	0.7433	0.6117

C

Subjective Pilot Feedback Results from the Comparison Test

Table C.1: A summary of test pilot's answers for each comparison in the pilot-in-the-loop test.

			Comparison Number:			
Comparison Type:			**1**	**2**	**3**	**4**
A	**M1-M1**	**Answer:**	yes/unsure	no	maybe no	maybe no
		Choice:	1st	-	2nd	2nd
B	**M2-M2**	**Answer:**	yes	yes	maybe no	no
		Choice:	1st	1st	2nd	-
C	**M1-M2**	**Answer:**	yes	yes, close	yes	yes
		Choice:	no preference	2nd, M2	2nd, M2	2nd M2
D	**M2-M1**	**Answer:**	yes	yes	yes	yes
		Choice:	2nd, M1	1st, M2	combination	combination

Table C.2: A score of how often a model was chosen during each comparison type.

	A M1 vs M1	**B** M2 vs M2	**C** M1 vs M2	**D** M2 vs M1
No. Comparisons	4	4	4	4
Difference observed (strict)	3	3	4	4
Difference observed (relaxed)	1	**2**	4	4
1st Better	1	2	0 (M1)	**1 (M2)**
2nd Better	2	1	**3 (M2)**	1 (M1)
Combined	0	0	1	2

Table C.3: A summary of reasons given for choosing a preferred model during each comparison.

	Deciding Choice Reasonings:
M2 vs M2	Balanced, Stable Recovey Longer Stall Onset Higher Stick forces
M1 vs M1	Longer Stall Onset Stable Recovery
M2 vs M1	(More) Stall Onset Oscilations Heavier Dip on Stall Approach Stable Recovery